Supramolecular modification of baclofen in the solid state

By

Ramokone Junia Malapile

214306038

Thesis submitted in fulfilment of the requirements for the degree

Masters of Applied Sciences: Chemistry

in the faculty of Applied Sciences

at the Cape Peninsula University of Technology

Supervisor: AProf NB Báthori (CPUT)

Co-Supervisor: Prof LR Nassimbeni (UCT)

Bellville Campus

February 2020

The financial assistance of the National Research Foundation and CPUT towards this research is acknowledged. Opinions expressed in this thesis and the conclusions arrived at, are those of the author.

DECLARATION

I, RAMOKONE JUNIA MALAPILE, declare that the contents of this thesis represent my own unaided work, and that the thesis has not previously been submitted for academic examination towards any qualification. Furthermore, it represents my own opinions and not necessarily those of the Cape Peninsula University of Technology.

Signature

05 May 2020

Date

Abstract

Baclofen (BAC, (R/S)-4-amino-3-(4-chlorophenyl)butanoic acid), a γ-amino acid, was used to form multicomponent crystals (MCCs) with coformers (CFs) of different acidic strength and molecular size. Crystallisation of BAC with oxalic acid (OXA), salicylic acid (SAL), phenoxyacetic acid (POA), 2,4-dichlorophenoxyacetic acid (2,4ClPOA), 4-picoline (4PIC) and 3,4-lutidine (3,4LUT) yielded seven MCCs, $[BAC^+][OXA^-]\cdot w$, BAC·SAL·w, $[BAC^+][POA^-]$, $[BAC^+][2,4ClPOA^-]$, $[BAC^+][2,4ClPOA^-]\cdot w$, 2BAC(4PIC)·w and 2BAC(3,4 LUT)·w, respectively.

The bulk materials were analysed by thermoanalytical methods (thermogravimetry and differential scanning calorimetry), powder X-ray analysis and Fourier transform infrared spectrometry. Liquid assisted grinding (LAG), as a green chemistry method, was also applied to form the MCCs.

X-ray analysis of the single crystal structures revealed that BAC exists in zwitterionic or cationic form in these crystals, and the MCCs represent a large variety of crystal classes, such as salts, salt solvates, cocrystal salt solvates or solvates with different stoichiometry. It was noted that BAC appeared in many different conformations in the MCCs and the crystal $[BAC^+][2,4ClPOA^-]$ represents a new conformer of BAC found in the solid state.

Comparative crystal packing analysis revealed similarities in the packing arrangement of the MCCs, with the exception of the oxalate salt, where the hydrogen bonded layers formed by the polar functional groups of the BAC and the CFs alternating with the hydrophobic aromatic layers. Contrarily, the polar layers show great variety in their hydrogen bonding pattern.

In conclusion, BAC is a good candidate to form MCCs with the selected CFs, but the predictability of the nature of interactions formed between the BAC moieties or between the BAC and CF molecules are poor and this makes BAC a challenging target when crystal engineering techniques are used.

Acknowledgements

Special thanks go to:

- My supervisor, Prof Nikoletta B. Báthori from who I have learnt much more than chemistry.
- My co-supervisor Prof Nassimbeni for all the lessons on the basics.
- Kudzanai Nyamayaro for initiating the project.
- My loving family and friends for their constant support.
- Glory be to God.

Dedication

To Dikolobe le Ditlou

Conferences

'Multicomponent crystal formation of baclofen with acids and bases', Poster presentation at the 32nd European Crystallographic Meeting, Vienna, Austria (18-23 August 2019). Ramokone J. Malapile, Luigi R. Nassimbeni and Nikoletta B. Báthori.

'Multicomponent crystal formation of baclofen with acids and bases', oral presentation at the 32nd European Crystallographic Meeting- Young Crystallographers session, Vienna, Austria (18-23 August 2019). Ramokone J. Malapile, Luigi R. Nassimbeni and Nikoletta B. Báthori.

Table of contents

List of figures

Appendix figures

List of tables

Key terms

Coformer	The compound that will interact with the active pharmaceutical ingredient during crystallisation to form a multicomponent crystal.
Conformation	The spatial arrangement/s which atoms in a molecule may take or convert to for example by rotation
Crystal engineering	Crystal engineering is a tool which can be used for the alteration of the physical properties of an already existing drug with the intention of improving properties such as solubility, bioavailability and tabletability
Hydrate	The result of a product that has water included in its crystal structure
Onset temperature	The temperature at which the solid material begins to melt
Solubility	The ability of the solid material to be dissolved in a liquid at a given temperature and pressure.
Supramolecular chemistry	The study involving the orientation of complex assemblies and molecular recognition through non-covalent bonding
Synthon	Synthons are units that portray the essential features of the crystal structure, more specifically how the units are assembled according to the intermolecular interactions which are involved

List of symbols

a, b, c	unit cell axes (Å)
α	designates angle between unit cell *b* and *c* axes (°)
β	designates angle between unit cell *a* and *c* axes (°)
γ	designates angle between unit cell *a* and *b* axes (°)
τ	torsion angle (°)
ε	Dielectric constant
2,4ClPOA	2,4-dichlorophenoxyacetic acid
4PIC	4-picoline
3,4LUT	3,4-lutidine
API	Active pharmaceutical ingredient
ASU	Asymmetric unit
BCS	Biopharmaceutics Classification System
CSD	Cambridge Structural Database
DSC	Differential Scanning Calorimetry
FTIR	Fourier transform infrared
GDP	Gross domestic product
GRAS	Generally regarded as safe
LAG	Liquid assisted grinding
MCC	Multicomponent crystal
OXA	Oxalic acid
pK_a	Acid dissociation constant
POA	Phenoxyacetic acid
PSE	Process system engineering
PXRD	Powder X-ray diffraction
SAHPRA	South African Health Product Regulatory Authority
SAL	Salicylic acid
SEC	Slow evaporation crystallisation
SCXRD	Single crystal X-ray diffraction
T_{onset}	Onset temperature (°C)
T_{peak}	Peak temperature (°C)
TGA	Thermal gravimetric analysis
V	Unit cell volume ($Å^3$)
W	Water
WHO	World Health Organization
Z	Number of formula units per unit cell

Atom colour code

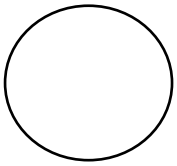

Hydrogen

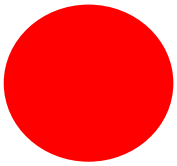

Oxygen

Chlorine

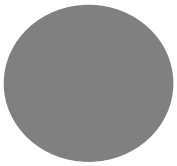

Carbon

Nitrogen

Chapter 1

Introduction

1.1 New drug development

The cost of placing a new drug on the market is close to $1.15 billion and the duration for this is approximately 12.5 years (Fig. 1.). This estimate also varies according to the drug company and the treatment used; for example, HIV/AIDS drugs have higher clinical costs and are therefore more expensive[1].

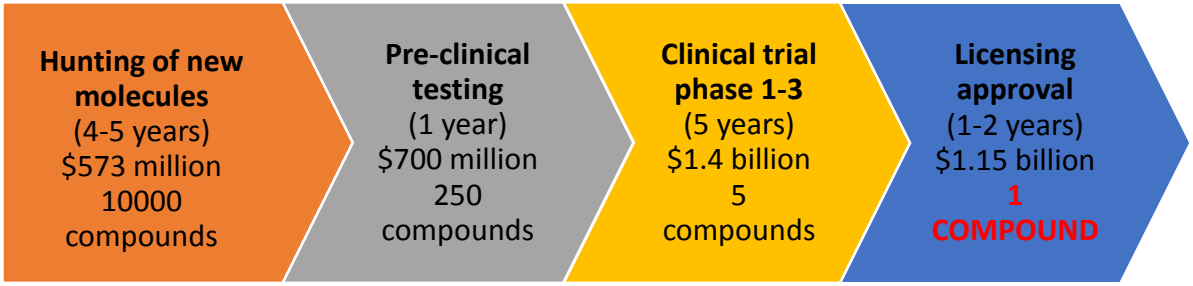

Figure 1.1 The schematics of the drug discovery process

The first two stages of the drug discovery process are the drug hunting and the pre-clinical testing stages. The aim of the first stage is to synthesize new molecules. The said molecules are tested in assays and animal models for chemical or biological activity in stage two. This is normally investigated in a university research laboratory or the research and development (R&D) department of a pharmaceutical company or research institute[2]. In the pre-clinical testing stage, the potential pharmacological effects of the proposed drug on biological processes is investigated. The pharmacokinetic effects of the compound, looking specifically at toxicology, single and repeat-dose toxicity testing and special toxicity testing (carcinogenic and reproductive toxicity tests) are also studied[3]. If the results are unsatisfactory, the compound will be withdrawn.

The third stage in the drug discovery process is the clinical trial stage which has three phases. In phase I, the drug is tested on a small group of healthy volunteers to determine safe doses and information on the absorption, distribution, metabolic effects, excretion and toxicity, so called ADMET properties of the compound. However, there have been ethical arguments raised about giving volunteers doses that are below the therapeutic dose as the usefulness of the information that is collected from this study can be argued[4]. Phase II has a

larger volunteer group, normally over a hundred individuals participate. The aim of this phase is to give the drug to volunteers who have the targeted disease or condition to confirm the biological activity against the disease and the safety of the drug from the phase I results[5]. In phase III, an even larger group of volunteers coming from several hospitals, clinics or research facilities are involved. The purpose of this phase is to design trials that show the rigid efficacy of the drug candidate and to investigate side effects that may occur. This is possible as the volunteer pool in phase III is over a thousand individuals. The final stage of drug discovery is the licensing approval; this is done after collecting all the safety and efficacy results of the drug candidate and including data in the application to the appropriate regulatory authorities for licensing and marketing approval. In South Africa, this application is sent to the South African Health Product Regulatory Authority (SAHPRA)[2].

There are notable disadvantages to the drug development process, the most concerning being expenditure. The cost expenditure in the pharmaceutical industry has over the past few years grown at a much faster rate than other divisions within the health care system. The drug development process cost has a big influence on drug prices, regulatory policies and the possibility of whether generic forms will be formulated[1]. The decisions made in the drug development phase have a direct influence on the return of R&D investments. There is also a lot of pressure on pharmaceutical companies for newly developed drugs which are on shelves to be successful as the sales and revenue of said drugs determine the innovative route the company will take for future projects. This process of drug development should therefore be fast and cost effective. However, SAHPRA has a backlog dating back to the 1990s, therefore registering a new drug to the market in South Africa is a lengthy process[2].

1.2 Crystal engineering

The cost of developing drugs has been a longstanding topic of interest, particularly with regards to the cost containment pressures in the marketplace[2]. The cost of drug development has risen tremendously over the past thirty years; it is becoming increasingly unaffordable to develop drugs for companies and subsequently consumers. From a holistic point of view, there is a need for access to medication as well as a need for innovative and cost effective methods of drug development in South Africa and Africa as a whole.

Of the ca 10 000 compounds formulated in the above-mentioned first stage of drug development, only one drug will make it to the shelf. However, it is necessary to recoup the loss of the 9 999 molecules which did not meet the requirements due to inefficacy and/or safety findings. The challenge one has to tackle is the avenues available for cost-saving, bearing in mind that the annual sales of a drug have to be ca $500 million in order for a company to regain its cost on investment. One of the avenues, which is the foundation of this research, is applying crystal engineering for the control of the physicochemical properties of drugs[3].

Crystal engineering is a tool which can be used for the alteration of the physicochemical properties of an already existing drug with the intention of improving properties such as solubility[6], bioavailability[7] and tabletability[8]. This is done without altering the pharmacological activity of the active pharmaceutical ingredient (API). Richard Feynman postulated that *"when we have some control of the arrangement of things on a small scale we will get an enormously greater range of possible properties that substances can have, and of different things that we can do"*[9]. This proposed planning of atoms and the related properties became the genesis of crystal engineering.

This method of drug design has gained attention in the last 50 years and it is where chemistry and crystallography merge. Crystal engineering, as defined by Gautam Desiraju, is "*the understanding of intermolecular interactions in the context of crystal packing and the utilization of such understanding in design of new solids with desired physical and chemical properties".* In crystal engineering, the molecules are the building blocks of crystals, however the crystal structure is not related exclusively to the molecular structure [10].

This process of forming crystals can be quite complex as there are many pathways crystal growth can take place. The crystal growth will follow a particular pathway, as seen in Scheme 1, unless the crystallisation pathway does not yield good crystals. For example, clusters may form, but redissolve before forming a sufficiently large nucleus [10].

Scheme 1.1 The Aufbau crystal growth process[11]

The chemistry involved in crystal growth is referred to as supramolecular chemistry, which is the study involving the orientation of complex assemblies and molecular recognition through non-covalent bonding [12]. It has also been defined by Jean-Marie Lehn as "*chemistry beyond the molecule"* and by Desiraju as the "*chemistry of molecular assemblies and of the intermolecular bond*" [13,14]. Initially, the term supramolecular chemistry was used to define areas of chemistry including crown ether chemistry, host-guest chemistry and the chemistry of molecular recognition. Over the years, the concepts of supramolecular chemistry have been used to improve and develop fields such as material and pharmaceutical science[15,16]. In supramolecular chemistry, we are particularly interested in the size, shape and geometry of molecules to see how molecules can combine to become unique chemical species that express new physical and chemical properties[17].

Both physical and chemical properties of compounds can be modified via crystallisation but our efforts will focus on the physical modification of the selected API, baclofen. The physical modification of the crystalline API may aim to increase the surface area and improve the solubility and stability of the API. There are implications for the modification of physical properties such as a change in solubility[6], melting point[18], hardness, novel electrical and optical properties of the crystal[19]. For an already existing drug, it is important to note that no chemical modifications, such as the addition of a functional group, can be carried out as this would result in a new chemical entity altogether and eventually the need for clinical trials. Thus the physical properties of an already approved drug should be tailored without changing the chemical structure of the API. One of the typical and accepted ways to modify properties of APIs is multicomponent crystal (MCC) formation[20].

MCCs are defined as crystals which constitute more than one chemical entity, independent of their physical state. Fundamentally, there is no difference between mono- constituent crystals and MCCs as the laws of crystal packing; the intermolecular interactions involved

and the route in which interactions combine with each other in the stable crystal packing are the same in both mono and multicomponent arrangements[16, 21].

The most important difference between single component and MCC systems is with respect to crystal growth. In the case of MCC formation, there are at least two chemical compounds involved and one has to consider their relative solubilities, vapour pressures or their intrinsic chemical nature. It is thus important to study a phase diagram of the system because MCCs can only be obtained within certain compositional ranges[10].

1.3 The eight stages of drug development using crystal engineering

1.3.1 Design and coformer selection

The pharmaceutical MCCs consist of an API, coformer and, where necessary, a solvent [16]. The coformer is normally a chemical from the generally regarded as safe (GRAS) list[22].

According to Margaret Etter, prior to cocrystallising two compounds, it is important to understand the interactions that sustain and direct crystal packing. The interactions that will be focused on are the non-covalent interactions, more specifically hydrogen bonding, which is the strongest secondary bond. Hydrogen bonding is defined as *an attractive interaction between a hydrogen atom from a molecule or a molecular fragment, X-H···A in which X is more electronegative than H, and an atom or group of atoms in the same or different molecule, in which there is evidence of bond formation. A is the proton acceptor.* Hydrogen bonding is important in crystal engineering particularly as it firstly pertains to the geometrical criteria that is used to characterize an *D-H···A*[10,23]. The most typical non-covalent interactions that may be seen in MCCs besides hydrogen bonding are van der Waals forces, halogen-halogen and π···π stacking interactions[24]. The contributors to the MCC are the API and coformers which normally have carboxylic acid and amine functional groups.

The intermolecular interaction between the API and coformer form synthons which are units that portray the essential features of the crystal structure, more specifically how the units are assembled[10]. The assembly or pattern is due to the directional interactions that take place in solution because crystallization is a kinetic phenomenon. There are two types of supramolecular synthons for crystal formation: homosynthon and heterosynthon.

Homosynthons are formed amongst the same complementary functional groups [Figure 1.2(a)] and heterosynthons are formed between dissimilar but complementary functional groups [Figure 1.2(b)].

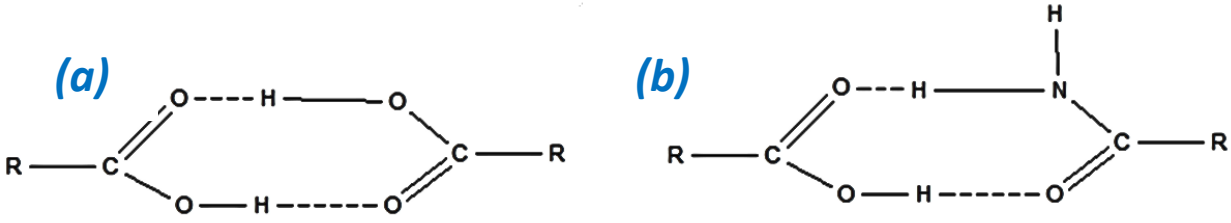

Figure 1.2 Depiction of homo-and heterosynthons[65]

A challenge in MCC formation is to create a hierarchy of preferred functional groups although there are rules given by Etter that guide the probability of hydrogen bonding to occur, i.e the best proton donor will hydrogen bond to the best hydrogen acceptor[23]. For example, when terephtalic acid is cocrystallised with 2-(2-pyridin-4-yl-vinyl)benzimidazole a salt is formed by a heterosynthon but when 2,5-bis-(4-t-butylphenoxy)-3-6-dihydroxyterephthalic acid, however substituted, is cocrystallised with ethanoic acid, a carboxylic acid dimer is formed as seen in Figure 1.3[25,26].

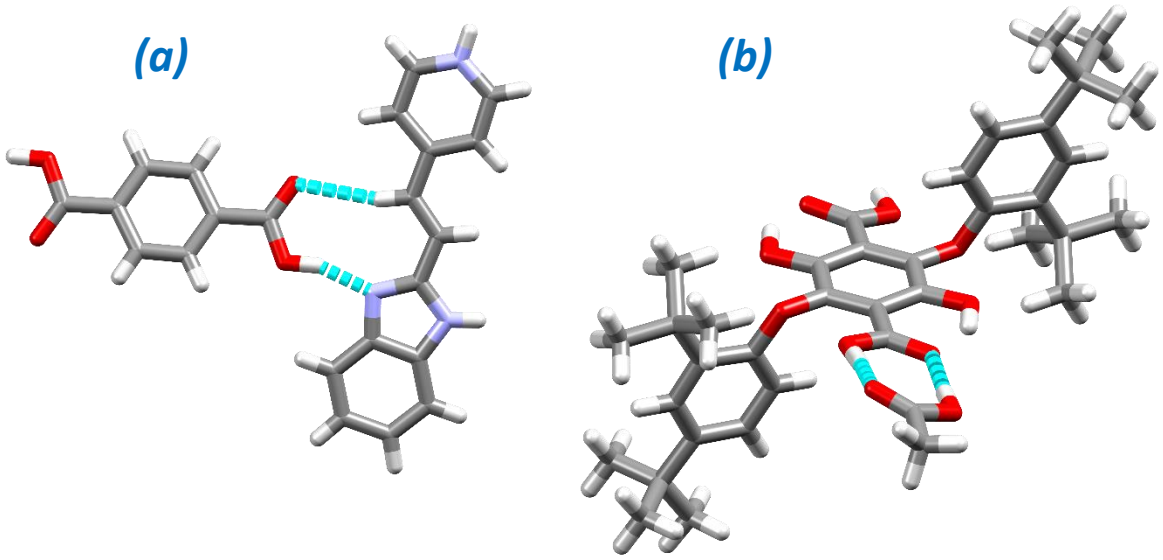

Figure 1. 3 Terephthalic acid cocrystallised with 2-(2-pyridin-4-yl-vinyl)benzimidazole (a) and 2,5-bis-(4-t-butylphenoxy)-3-6-dihydroxyterephthalic acid with ethanoic acid (b)

For successful crystallisation, there are certain factors to consider when cocrystallising an API with a coformer, such as the pK_a of each contributor (in case the API has acidic or basic

functional groups), polarity of the solvents used and supramolecular compatibility, which in general terms is the process of self-assembly of the smaller subunits, which have complementary functionalities and thereby interact to form complex structures[27].

The pK_a is an indication of the propensity of an acid to donate a proton. It is expected that when the ΔpK_a of two cocrystallised compounds is greater than 2 or 3, a salt will be formed[28]. If the ΔpK_a is negative then cocrystals will be formed[29]. When the ΔpK_a is between 0 and 3, which is known as the salt-cocrystal continuum, it is difficult to tell whether a salt or a cocrystal will be formed[30]. It is however important to note that the ΔpK_a is influenced by the crystallisation solvent used and thus the polarity has an influence, as the pK_a value is related to the equilibrium behaviour in solution[31,32]. This is supported by Cruz-Cabeza's 'quantitative pK_a rule'. It was noted that in zone 1 where the ΔpK_a is less than -1, cocrystal formation has an occurrence of 99.1%. In zone 3, where the ΔpK_a is greater than 4, salt formation is observed. For zone 2, the salt-cocrystal continuum, it is impossible to predict whether a salt or cocrystal will form. However, it can be noted that in zone 2 when ΔpK_a is decreasing, the more likely a cocrystal will form. It is interesting to note that only simple molecules were used in this study, such as aliphatic carboxylic acids and pyridine bases, and by single proton transfer (the first ionisation constant) was evaluated[33].

1.3.2 Crystal growth methods

There are different methods used to grow MCCs. These methods include solvent evaporation crystallisation (SEC), mechanochemical methods of neat or liquid-assisted grinding (LAG) and sonic slurry. There are also computer programmes that can be used for screening to determine whether MCCs can be prepared experimentally[34] such as machine learning algorithms that can assist in predicting whether crystal growth will take place. This is done by building data bases or libraries from previous successful and unsuccessful cocrystallisations so that it is much easier to predict which solvents or coformers (and from which family) will most likely crystallize with the API[35].

1.3.3. Classification of MCCs

The classification of crystals has always been an interesting topic with many views. Initially, there was a disagreement between the FDA and the academic community on whether salts and cocrystals should be classified differently. The argument is that there are times when it

is difficult to distinguish salts and cocrystals. Such a case is when the movement of the proton is around or less than 1 Å. A classification system by Aitipamula *et al* [36] suggested three classes of crystalline multicomponent crystals; salts, cocrystals and hydrates/solvates and their polymorphs but this classification does not cater for MCCs with complex stoichiometry. This classification has been broadened by de Gelder *et al* and includes subclasses where the main overlap. (Figure 1.4 and Table 1.1)[21].

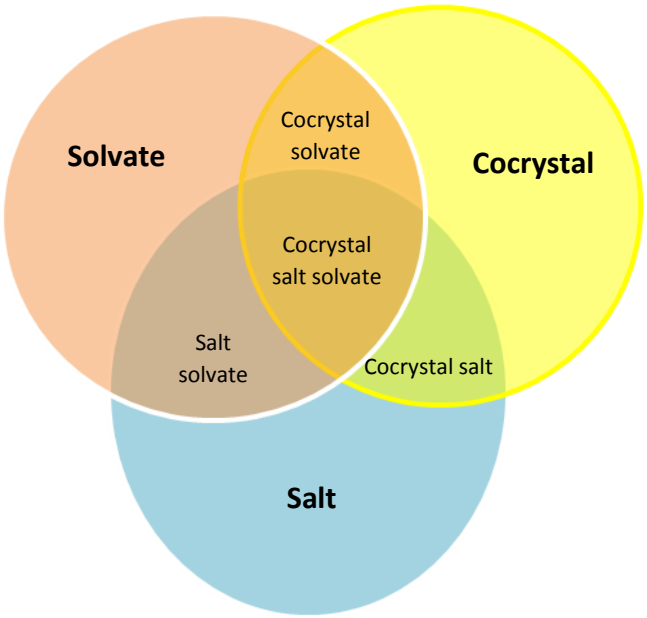

Figure 1.4 Main and sub-classes of multicomponent crystals

Table 1.1 Seven subclasses of multicomponent crystals based on Grothe et al

Class	*Definition*
True salt	Salts are crystals composing of at least two ions.
True solvate	One coformer and one or more solvents incorporated in the crystal.
True cocrystal	Cocrystals are multicomponent crystals where all pure components at ambient conditions are solids. One or more coformers, but no ions or solvents which are solids at room temperature. There is no proton transfer involved in this formation.
Salt solvate	A crystal which consists of one or more solvents and two or more ions.
Cocrystal solvate	A crystal with more than two coformers and one or more solvents.
Cocrystal salt	A crystal with one or more coformers and two or more ions.
Cocrystal salt solvate	A combination of one or more solvents, two or more ions and one or more coformers in a crystal structure.

1.3.4 Properties

Once the MCCs have been formed the property studies may commence to see if the study has been successful. Below is a brief discussion on some of the property issues faced by pharmaceutical companies and crystal engineering may be used to remedy these issues.

- Aqueous solubility of drugs

The solubility of a drug in water is very important although, unfortunately, more than 50% of novel drugs are insoluble in water[37]. Good solubility in water is important for APIs as they need to be taken up in the body's aqueous intestinal fluid that allows the API to enter the epithelial cell membrane by passive diffusion [38].

Whether a drug will enter the epithelial cell membrane depends on two factors, which are solubility and permeability. APIs have been classified under the Biopharmaceutics Classification System (BCS) according to their solubility and permeability. Good solubility is defined as having a compound that is soluble in 250 ml of water over a pH range of 1-7.5 at 37°C [38,39].

Table 1.2 Biopharmaceutics Classification System[39]

Class I	**Class II**
High solubility	Low solubility
High permeability	High permeability
Class III	**Class IV**
High solubility	Low solubility
Low permeability	Low permeability

- Stability

Stability tests are carried out on MCCs to determine whether it can withstand relative humidity stress, thermal stress, or to investigate the chemical stability of the MCC. The relative humidity stress test is used to determine the best storing conditions. This is especially important for MCCs containing water, because the water can compromise the quality of the product. The thermal and chemical stability tests are not regularly performed but more extensive stability tests, which are typically done, include temperature-varying tests, such as freeze-thaw or dark room tests[40].

The factors which determine the shelf life of a drug, are the chemical stability of the API in the dosage of the drug; if there is a presence of degradation products that could be hazardous to the patient. The stability factors may deter the API from optimal potency, loss of activity and the API may be released at a slow rate to the gastrointestinal tract[41].

- Melting point

The melting point of a solid is the temperature where the solid and liquid phases are in equilibrium. The melting point is an important physical property, especially for the stability studies of drugs that are in the solid phase. It is also important because it gives information on the ability of the MCC to be processed because the melting point is an indicator of the API's solubility[40]. According to a study by Mao *et al*, APIs with a melting point greater than 250°C are likely to have poor drug properties and will not pass the drug approval stage[42].

1.3.5 Pharmacokinetics

Before a pharmaceutical drug is manufactured in bulk, it is important to understand the pharmacokinetics of the drug which is the process that dictates the pathway a drug takes through the body and the concentration of the drug in different body compartments[43]. The pharmacokinetics study of the drug in this research was not conducted as no bulk batches were manufactured, but this would be necessary in the pharmaceutical industry.

1.3.6 Formulation

In industrial manufacturing the drugs are packaged in different forms dependent on how they will be administered, such as in tablet, gels or transdermal patches. The MCCs in this study are in solid form and will be in the preferred tablet form[44]. The tablet formulation of the MCC is an important step in drug synthesis and it is focused on the characteristics of the drug that will overcome mishaps, such as solubility. The formulation process is also focused on bioavailability studies with respect to the rate and extent the API reaches the gut[45].

1.3.7 Process and scale-up

In terms of industrial scale ups, there are quality systems that should be in place such as good manufacturing practice. It is important to use the correct coformer at the correct dose ratio as this affects the solubility and thus the biopharmaceutical capability of the drug [45]. However, it is quite challenging to scale up crystallisations as it is more likely than not to

change the crystal size distribution, purity and morphology of the crystals. This is due to the interaction between two factors that scale differently: hydrodynamics and crystallisation kinetics. Fortunately, there are applications which can be used to overcome and understand this issue such as computational fluid dynamics and process system engineering softwares[46].

1.3.8 Regulatory approval

The MCC is a new drug, it has unique physical properties different from the original drug and thus is novel. The pharmaceutical company may apply for intellectual property protection. To receive a patent, there are three criteria which need to be met: novelty, inventiveness and utility[22,45]. The condition for novelty for MCCs is that the new form has not been publicly disclosed. The inventiveness or non-obviousness criteria for pharmaceutical patents specifically MCCs is with regards to the composition of matter. The MCCs have a new formulation and the manufacturing process is different. Finally, the criteria for utility are all useful processes, machines, manufacturing or composition of matter and including all useful improvements to the above-mentioned criteria. MCCs can be regarded as an improvement of the original formulation[47,48].

1.4 The advantages of crystal engineering

Crystal engineering is an innovative and cost effective method that could be used for drug discovery. It has led to pharmaceutical companies, research institutes and the academic community growing their data storage tools in the form of molecular libraries and drug banks. The molecules in the molecular libraries and drug banks have become the building blocks for new drugs. These molecular libraries and drug banks store all the molecules which were successful or unsuccessful in previous studies. There are also drugs that have been discontinued as new and better formulations replaced them. This is extremely beneficial because, as previously stated, it is quite difficult to develop a novel drug[49]. An example of the usefulness of molecular libraries and drug banks is seen in the recent newspaper article published by The Washington Post which revealed a team of researchers from Pfizer who discovered that the rheumatoid arthritis drug, Enbrel, could potentially reduce the risk of Alzheimer's disease by 64% [50]. Therefore, molecular libraries provide an opportunity to look for potential drugs for non-targeted diseases.

Furthermore, when the opportunity arises to improve already existing drugs or molecules available, it could possibly cut the drug discovery process by 4-5 years and a cost saving of ca $400 million that could be used more effectively elsewhere in the business[1,2]. Moreover, crystal formation methods are affordable. There are also regulatory advantages in South Africa, however, as previously stated; the SAHPRA has a large backlog of applications. By using crystal engineering, it is not necessary to apply for regulatory approval of a new drug as the pharmacological activity has not been changed but rather the opportunity of intellectual property rights, a patent, of the new drug is available [16].

1.5 How can crystal engineering improve the efficacy of drugs?

There are cases where crystal engineering was used to improve drug efficacy. Itraconazole is an antifungal agent that is extremely insoluble in water and has been cocrystallised with several CFs such as seen in Figure 1.5 with succinic acid as a CF. However in order to achieve maximum bioavailability, the formulation was developed with HP-β-cyclodextrin which absorbs the API well and is currently sold in the market in this form[51,52].

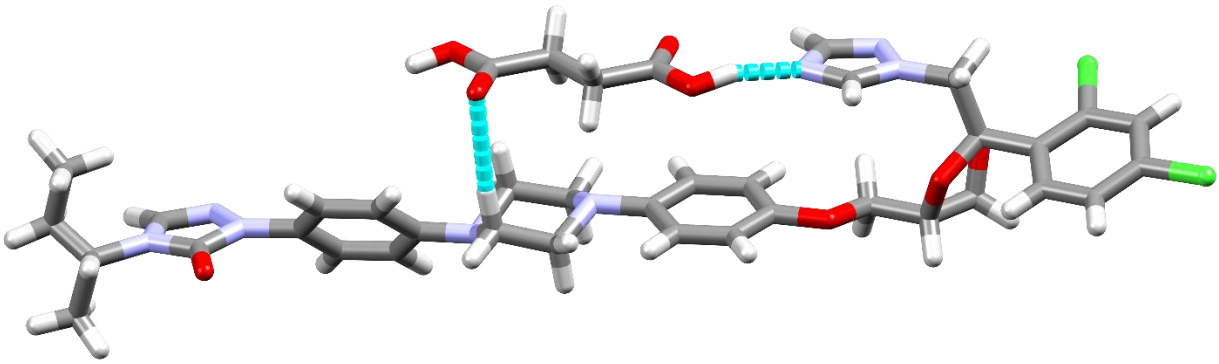

Figure 1.5 MCC of Itraconazole with succinic acid CF

Crystal engineering has also been used to improve the low aqueous solubility of danazol, a drug used in the treatment of endometriosis. Danazol was cocrystallised with vanillin to form a MCC (Figure 1.6). The MCC showed an improved solubility as compared to the drug alone. It is also interesting to note that the MCC performed even better when it was formulated with D-α-tocopheryl polyethyleneglycolsuccinate and Klucel LF pharma hydroxypropylcellulose[34,53].

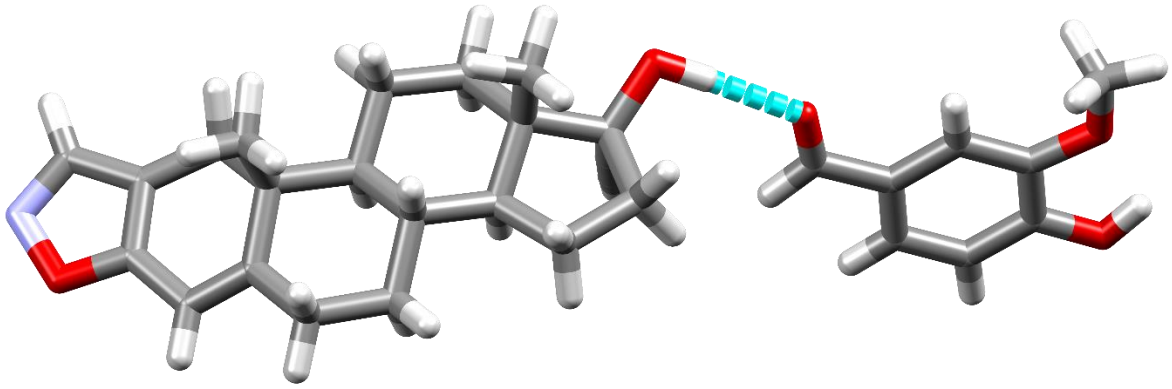

Figure 1.6 The MCC of danazol and vanillin

The drug Entresto™, which is used in the treatment of chronic heart failure, has been approved by the FDA as a pharmaceutical cocrystal. This particular drug is an example of a drug-drug cocrystal as seen in Figure 1.7. This drug is important as it has a mortality benefit and has a high potential market value which is advantageous for Novartis, the pharmaceutical company which formulated this drug[54].

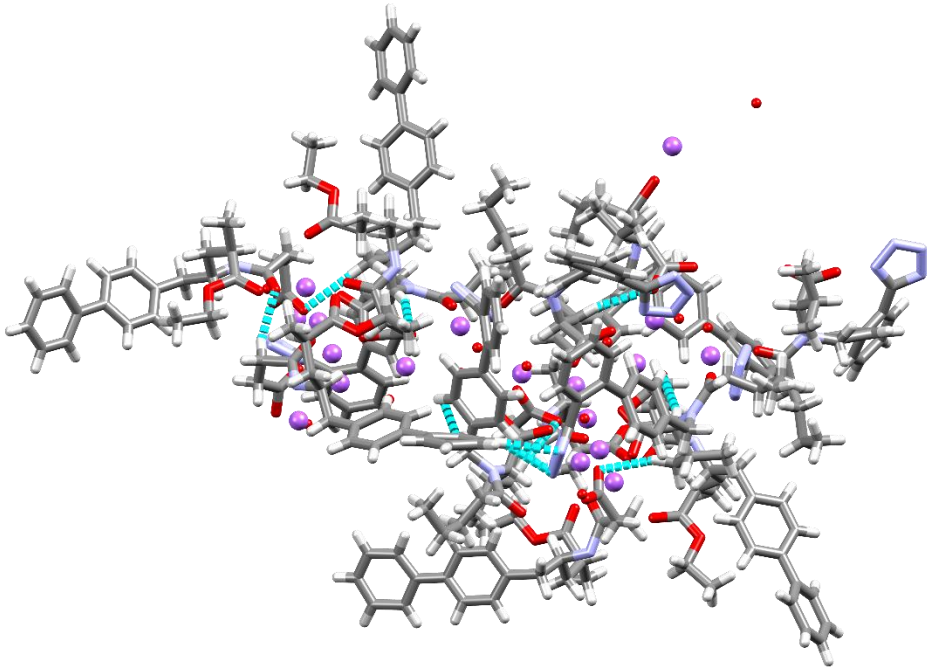

Figure 1.7 The crystal structure of pharmaceutical drug Entresto™

Enzalutamide is a drug used in the treatment of metastatic prostate cancer. Unfortunately, the active drug, S-enzalutamide, is easily contaminated with *O*-enzalutamide which is the substitution impurity of S-enzalutamide. To remedy this issue of contamination, S-

enzalutamide is cocrystallised in isopropyl alcohol to form a solvate which has a stability of 50 % or more[55]. The crystal structure of enzalutamide is seen in Figure 1.8.

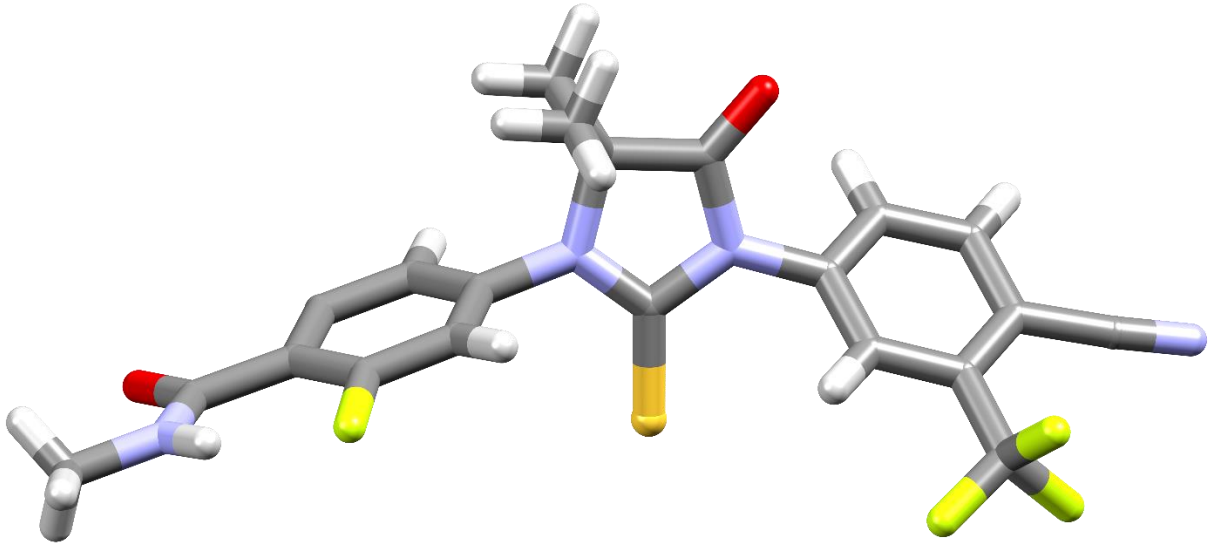

Figure 1.8 The crystal structure of enzalutamide

We can therefore postulate that cocrystallising baclofen with an appropriate coformer could lead to a MCC with improved solubility and in the appropriate stereochemistry, can present maximum efficacy.

1.6 Background of baclofen

Baclofen, as seen in Fig 1.9, is a γ-amino acid with low aqueous solubility of 0.712 mg ml^{-1} (see Table 1.3) and thus its efficacy is compromised. The formulation of baclofen manufactured is racemic but only the R enantiomer is active.

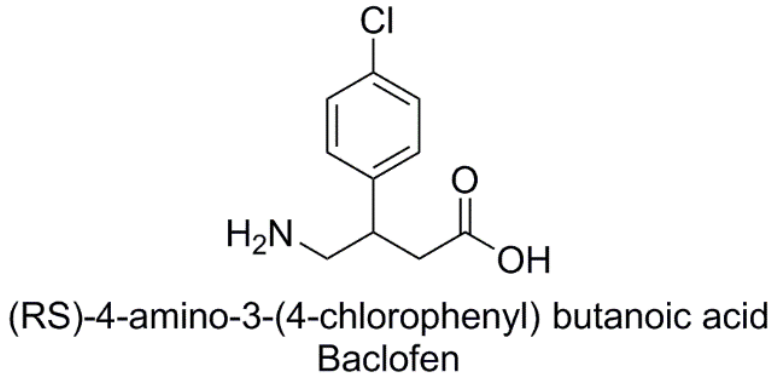

Figure 1.9 Baclofen molecular structure

Table 1.3 Properties of baclofen

COMMON NAME	**BACLOFEN**
IUPAC NAME	4-amino-3-(4-chlorophenyl) butanoic acid
CHEMICAL FORMULA	$C_{10}H_{12}ClNO_2$
MELTING POINT	207°C
AQUEOUS SOLUBILITY	0.712 mg ml^{-1} at 25°C

A study was done by Maniukiewicz *et al* on the structural characterization and Hirshfeld surface analysis of racemic baclofen. It was found that baclofen crystallizes in the orthorhombic *P*bca space group. The baclofen molecule exists in zwitterionic form and it has the same bond lengths as general amino acids. It was also found that the crystalline structure of baclofen can be represented in two forms, the unhydrated and the monohydrate forms [56].

The study also proved that due to reinforcement of charge assistance in the presence of the charged functional groups, hydrogen bonds are very strong between the ammonium and the carboxylate groups as compared to corresponding neutral groups. The Hirshfeld surface analysis showed that baclofen has different conformations which allow the interaction with positively and negatively charged molecules in biological systems [56].

An investigation by Báthori and Kilinkissa, entitled "*Are gamma amino acids promising tools for crystal engineering? - multicomponent crystals of baclofen*", resulted in the successful cocrystallisation of baclofen with acidic coformers (benzoic acid, p-toluic acid, 1-hydroxy-2-naphthoic acid, p-toluene sulfonic acid, oxalic acid and maleic acid). It was found that baclofen has four torsion angles which cause the conformational flexibility of the molecule. Close attention was also given to see if there is any correlation between the percentage of intermolecular reactions and the melting points of the MCCs obtained. There is, to some extent, a correlation between the % of the O···H intermolecular interaction and the melting point of some of the MCCs formed[57].

A crystal of baclofen and ferulic acid was formed in a study to determine the hierarchy of supramolecular synthons by Kavuru *et al*. The asymmetric unit showed two independent

baclofen zwitterions, two ferulic acid molecules and one molecule of water. It was found that the baclofen zwitterions interact through N-H···O hydrogen bonds to form quaternary subunits. One of the clusters formed was due to hydrogen bonding between a carboxylate moiety, ammonium moiety of two neighbouring baclofen molecules and a water molecule (O-H···O). The overall packing is a 3D H-bonded network[58].

Table 1.4 Summary of MCCs of baclofen from previous works

Báthori & Kilinkissa[57]	**Kavuru *et al***[58]
benzoic acid	Ferulic acid
p-toluic acid	
1-hydroxy-2-naphthoic acid	
oxalic acid	
maleic acid	
p-toluene sulfonic acid	

1.7 Statement of research problem

1.7.1 Alcoholism in South Africa

According to the 2018 global status report on alcohol and health by the World Health Organisation (WHO) South Africa has been ranked sixth place in nations of high drinkers. This is a prevalent issue in South Africa and Africa at large as alcoholism is responsible for 5.1 % of the global burden of disease. Furthermore, it is the leading factor in mortality and disability of individuals in the age group of 15-49 years. This value is unfortunately higher in disadvantaged populations where more deaths and hospitalizations have been recorded[59].

Besides the health implications of alcoholism, such as neuropsychiatric disorders, cirrhosis of the liver and various cancers, there is also a financial and social effect. In the broader financial context, alcoholism may lead to absenteeism, poor productivity, injuries in the workplace and damage to property. The financial burden in South Africa is estimated at R9 billion annually, which is equivalent to 1 % of the gross domestic product (GDP)[60]. This is alarming as the GDP, which is an indicator of the performance of the country's economy,

has a big influence on job creation, salaries and the health services provided to citizens of South Africa[61].

Drunkenness may also lead to behaviours of a violent and sexual nature, which may have secondary consequences, such as the transmission of sexually transmitted diseases, HIV or even death. Alcohol consumption during pregnancy may lead to foetal alcohol syndrome and may also lead to more psychological issues, such as child neglect with more long term consequences. Looking at the sustainable development goals, it is difficult to ignore the extent to which alcoholism can hinder the achievement of goals such as no poverty, zero hunger, decent work, economic growth as well sustainable cities and communities[60–62].

There is a need to look for treatments in aid to cure alcoholism; such an aid is baclofen, (R/S)-4-amino-3-(4-chlorophenyl) butanoic acid, which was initially only prescribed as a treatment for cerebral palsy, spinal injuries and opiate addictions and thereafter was extended to the treatment of alcoholism[57]. Baclofen is manufactured globally but in South Africa it is produced by Fine Chemical Corporation (Pty) Ltd[63-64]

As stated previously, the aqueous solubility of baclofen is low and this can be remedied by crystal engineering via forming new pharmaceutical crystalline forms.

1.8 Objective of the research

The objective is to evaluate whether baclofen can behave as an acid to protonate basic coformers.

This follows from previous work where we know that baclofen can form crystals with coformers of different acid strength and molecular size because of its flexibility. We could also deduce that baclofen is a good proton acceptor when it behaves as a base.

1.9 Research hypothesis

The proposed hypothesis is (1) that we can form MCCs of baclofen with carboxylic acid and amine bases and (2) that baclofen can behave as an acid or base depending on the coformer and environment.

1.10 References

1. Adams, C. P. and Van Brantner, V. Market watch : Estimating the cost of new drug development: Is it really $802 million? *Health Aff.* **25**, 420–428 (2006).

2. DiMasi, J. A., Hansen, R. W. and Grabowski, H. G. The price of innovation: New estimates of drug development costs. *J. Health Econ.* **22**, 151–185 (2003).

3. Rawlins, M. D. Cutting the cost of drug development? *Nat. Rev. Drug Discov.* **3**, 360–364 (2004).

4. Eisenhauer, E. A., O 'dwyer, P. J., Christian, M. and Humphrey, J. S. Phase I Clinical Trial Design in Cancer Drug Development. *J Clin Oncol*. **18**, 684–692 (2000).

5. Simon, R. Optimal two-stage designs for phase II clinical trials. *Control. Clin. Trials* **10**, 1–10 (1989).

6. Blagden, N., de Matas, M., Gavan, P. T. and York, P. Crystal engineering of active pharmaceutical ingredients to improve solubility and dissolution rates. *Adv. Drug Deliv. Rev.* **59**, 617–630 (2007).

7. McNamara, D. P., Childs, S.L., Giordano, J., Iarriccio, A., Cassidy, J., Shet, M. S., Mannion, R., O'Donnell, E. and Park, A . Use of a glutaric acid cocrystal to improve oral bioavailability of a low solubility API. *Pharm. Res.* **23**, 1888–1897 (2006).

8. Krishna, G. R., Shi, L., Bag, P. P., Sun, C. C. and Reddy, C. M. Correlation among crystal structure, mechanical behavior, and tabletability in the co-crystals of vanillin isomers. *Cryst. Growth Des.* **15**, 1827–1832 (2015).

9. Feynman, R. P. There's plenty of room at the bottom (Transcript of Talk Given on December 29, 1959, at the Annual Meeting of the American Physical Society). *Caltech Eng. Sci.* **23**, 22–36 (1960).

10. Desiraju, G. R. Crystal engineering: From molecule to crystal. *J. Am. Chem. Soc.* **135**, 9952–9967 (2013).

11. Ganguly, P. and Desiraju, G. R. Long-range synthon Aufbau modules (LSAM) in crystal structures: Systematic changes in C6H6-nFn ($0 \leq n \leq 6$) fluorobenzenes. *CrystEngComm* **12**,

817–833 (2010).

12. Huang, F. and Anslyn, E. V. Introduction: Supramolecular Chemistry. *Chem. Rev.* 6999–7000 (2015).

13. Lehn, J. M. Supramolecular chemistry- scope and perspectives molecules-supermolecules-molecular devices. 444–491 (1987).

14. Desiraju, G. R. Chemistry beyond the molecule. *Nature* **412**, 397–400 (2001).

15. Lehn, J. M. Supramolecular chemistry: Where from? Where to? *Chem. Soc. Rev.* **46**, 2378–2379 (2017).

16. Berry, D. J. and Steed, J. W. Pharmaceutical cocrystals, salts and multicomponent systems; intermolecular interactions and property based design. Adv. Drug Deliv. Rev (2017).

17. Soldatov, D. and Terekhova, I. . Supramolecular chemistry and crystal engineering. *J. Struct. Chem.* **46**, 1–8 (2005).

18. Batisai, E., Ayamine, A., Kilinkissa, O. E. Y. and Báthori, N. B. Melting point-solubility-structure correlations in multicomponent crystals containing fumaric or adipic acid. *CrystEngComm* **16**, 9992–9998 (2014).

19. Cyrac, P. A., Vimalan, M., Sagayaraj, P. and Madhavan, J. Thermal, optical, mechanical and electrical properties of a novel NLO active l-phenylalanine l-phenylalaninium perchlorate single crystals. *Phys. B Condens. Matter* **405**, 65–71 (2010).

20. Florence, A. T. and Attwood, D. *Physicochemical principles of pharmacy*. (Pharmaceutical Press, 2015).

21. Grothe, E., Meekes, H., Vlieg, E., Ter Horst, J. H. and De Gelder, R. Solvates, Salts, and Cocrystals: A Proposal for a Feasible Classification System. *Cryst. Growth Des.* **16**, 3237–3243 (2016).

22. Generally Recognized as Safe (GRAS) | FDA. Available at: https://www.fda.gov/food/food-ingredients-packaging/generally-recognized-safe-gras. (Accessed: 2nd September 2019)

23. Etter, M. C. Hydrogen bonds as design elements in organic chemistry. *J. Phys. Chem.*

95, 4601–4610 (1991).

24. Beran, G. J. O., Heit, Y. N. and Hartman, J. D. Noncovalent Interactions in Molecular Crystals. *Non-Covalent Interact. Quantum Chem. Phys.* 303–331 (2017).

25. Xia, C. K., Wei, C., Wu, Y.L., Wu, F., Yang, S. and Ma, J.L. Syntheses and characterization of three new compounds based on terephthalate and 2-(2-pyridin-4-yl-vinyl)benzimidazole ligands. *Zeitschrift fur Anorg. und Allg. Chemie* **641**, 896–902 (2015).

26. Benniston, A. C., Wingstnaley, T., Lemmetyinen, H., Tkachenko, N.V., Harrington, R.V. and Wills, C. Large stokes shift fluorescent dyes based on a highly substituted terephthalic acid core. *Org. Lett.* **14**, 1374–1377 (2012).

27. Savyasachi, A. J., Kotova, O., Shanmugaraju, S., Bradberry, S.J., Ó'Máille, G.M. and Gunnlaugsson, T. Supramolecular Chemistry: A Toolkit for Soft Functional Materials and Organic Particles. *Chem,* 764-811 (2017).

28. Guillory, J. K. Handbook of Pharmaceutical Salts: Properties, Selection, and Use Edited by P. Heinrich Stahl and Camile G. Wermuth. VHCA, Verlag Helvetica Chimica Acta, Zürich, Switzerland, and Wiley-VCH, Weinheim, Germany. 2002. ISBN 3-906. *J. Med. Chem.* **46**, 1277–1277 (2003).

29. Bhogala, B. R., Basavoju, S. and Nangia, A. Tape and layer structures in cocrystals of some di- and tricarboxylic acids with 4,4'-bipyridines and isonicotinamide. From binary to ternary cocrystals. *CrystEngComm* **7**, 551–562 (2005).

30. Ramon, G., Davies, K. and Nassimbeni, L. R. Structures of benzoic acids with substituted pyridines and quinolines: Salt versus co-crystal formation. *CrystEngComm* **16**, 5802–5810 (2014).

31. Cox, B. G. *Acids and Bases*. (Oxford, 2013).

32. Childs, S. L., Stahly, G. P. and Park, A. The salt-cocrystal continuum: The influence of crystal structure on ionization state. *Mol. Pharm.* **4**, 323–338 (2007).

33. Cruz-Cabeza, A. J. Acid-base crystalline complexes and the pK_a rule. *CrystEngComm* **14**, 6362–6365 (2012).

34. Duggirala, N. K., Perry, M. L., Almarsson, Ö. and Zaworotko, M. J. Pharmaceutical

cocrystals: Along the path to improved medicines. *Chem. Commun.* **52**, 640–655 (2016).

35. Pillong, M., Marx, C., Piechon, P., Wicker, J.G.P., Cooper, R.I. and Wagner,T. A publicly available crystallisation data set and its application in machine learning. *CrystEngComm* **19**, 3737–3745 (2017).

36. Aitipamula, S., Banerjee, R., Bansal, A. K., Biradha, K., Cheney, M.L., Choudhury, A. R., Desiraju, G. R., Dikundwar, A. G., Dubey, R., Duggirala, N., Ghogale, P. P., Ghosh, S., Goswami, P. K., Goud, N. R., Jetti, R. R. K. R., Karpinski, P., Kaushik, P., Kumar, D., Kumar, M. B., Mukherjee, A., Mukherjee, G., Myerson, A. S., Puri, V., Ramanan, A., Rajamannar, T., Reddy, C. M., Rodriguez-Hornedo, N., Rogers, R. D., Row, T, N, G., R., Sanphui, P., Shan, N., Shete, G., Singh, A., Sun, C. C., Swift, J. A., Thaimattam, R., Thakur, T. S., Kumar Thaper, Thomas, S. P., Tothadi, S., Vangala, V. R., Variankaval, N. R., Vishweshwar, P., Weyna, D. R. and Zaworotko, M. J. Polymorphs, salts, and cocrystals: What's in a name? *Cryst. Growth Des.* **12**, 2147–2152 (2012).

37. Vikas, Y., Sandeep, K., Braham, D., Manjusha, C. and Budhwar, V. Cyclodextrin complexes: An approach to improve the physicochemical properties of drugs and applications of cyclodextrin complexes. *Asian J. Pharm.* **12**, S394–S409 (2018).

38. Hart, M. L. Brief Overview of Various Approaches to Enhance Drug Solubility. *J. Dev. Drugs* **02**, 1–7 (2014).

39. Papich, M. G. and Martinez, M. N. Applying Biopharmaceutical Classification System (BCS) Criteria to Predict Oral Absorption of Drugs in Dogs: Challenges and Pitfalls. *AAPS J.* **17**, 948–964 (2015).

40. Kumar, S. and Nanda, A. Pharmaceutical cocrystals: An overview. *Indian J. Pharm. Sci.* **79**, 858–871 (2017).

41. Waterman, K. C. Understanding and Predicting Pharmaceutical Product Shelf-Life. in *Handbook of Stability Testing in Pharmaceutical Development* 115–135 (Springer New York, 2009).

42. Mao, F., Kong, Q., Ni, W., Xu, X., Ling, D., Lu, Z. and Li, J. Melting Point Distribution Analysis of Globally Approved and Discontinued Drugs: A Research for Improving the Chance of Success of Drug Design and Discovery. *ChemistryOpen* **5**, 357–368 (2016).

43. Negus, S. S. and Banks, M. L. Pharmacokinetic-Pharmacodynamic (PKPD) Analysis with Drug Discrimination. *Curr. Top. Behav. Neurosci.* **39**, 245–259 (2018).

44. Nunn, T. and Williams, J. Formulation of medicines for children. *Br. J. Clin. Pharmacol.* **59**, 674–676 (2005).

45. Gadade, D. D. and Pekamwar, S. S. Pharmaceutical cocrystals: Regulatory and strategic aspects, design and development. *Adv. Pharm. Bull.* **6**, 479–494 (2016).

46. Wei, H. Y. Computer-aided design and scale-up of crystallization processes: Integrating approaches and case studies. *Chem. Eng. Res. Des.* 1377-1380 (2010).

47. Trask, A. V. An overview of pharmaceutical cocrystals as intellectual property. *Mol. Pharm.* **4**, 301–309 (2007).

48. USPTO. 35 USC 101: Statutory Requirements and Four Categories of Invention. (2015).

49. Wassermann, A. M., Camargo, L. M. and Auld, D. S. Composition and applications of focus libraries to phenotypic assays. *Front. Pharmacol.* **5 JUN**, 1–12 (2014).

50. Christopher Rowland. Pfizer had clues its blockbuster drug could prevent Alzheimer's. Why didn't it tell the world? *The Washington Post* (2019). Available at: https://www.msn.com/en-za/health/medical/pfizer-had-clues-its-blockbuster-drug-could-prevent-alzheimers-why-didnt-it-tell-the-world/ar-AACpdRZ?li=BBqfP3n. (Accessed: 11th June 2019)

51. Shan, N. and Zaworotko, M. J. The role of cocrystals in pharmaceutical science. *Drug Discov. Today* **13**, 440–446 (2008).

52. Remenar, J. F., Morissette, S .L., Peterson, M. L., Moulton, B., MacPhee, J. M., Guzmán, J. M. and Almarsson, Ö. Crystal engineering of novel cocrystals of a triazole drug with 1,4-dicarboxylic acids. *J. Am. Chem. Soc.* **125**, 8456–8457 (2003).

53. Childs, S. L., Kandi, P. and Lingireddy, S. R. Formulation of a danazol cocrystal with controlled supersaturation plays an essential role in improving bioavailability. *Mol. Pharm.* **10**, 3112–3127 (2013).

54. Feng, L., Karpinski, P., Sutton, P., Liu, Y., Hook, D.F., Hu, B., Blacklock, T.J., Fanwick,

P.E., Prashad, M., Godtfredsen, S. and Ziltener, C. LCZ696: A dual-acting sodium supramolecular complex. *Tetrahedron Lett.* **53**, 275–276 (2012).

55. Maini, L., Braga, D., Farinella, F., Melotto, E., Verzini, M., Brescello, R., Michieletto, I. and Munari, R. Crystal Forms of Enzalutamide and a Crystal Engineering Route to Drug Purification. *Cryst. Growth Des.* **18**, 3774–3780 (2018).

56. Maniukiewicz, W., Oracz, M. and Sieroń, L. Structural characterization and Hirshfeld surface analysis of racemic baclofen. *J. Mol. Struct.* **1123**, 271–275 (2016).

57. Báthori, N. B. and Kilinkissa, O. E. Y. Are gamma amino acids promising tools of crystal engineering? - Multicomponent crystals of baclofen. *CrystEngComm* **17**, 8264–8272 (2015).

58. Kavuru, P., Aboarayes, D., Arora, K. K., Clarke, H. D., Kennedy, A., Marshall, L., Ong, T. T., Perman, J., Pujari, T., Wojtas, L. and Zaworotko, M. J. Hierarchy of supramolecular synthons: Persistent hydrogen bonds between carboxylates and weakly acidic hydroxyl moieties in cocrystals of zwitterions. *Cryst. Growth Des.* **10**, 3568–3584 (2010).

59. WHO-Regional Office for Africa. Alcohol | WHO | Regional Office for Africa. (2017). Available at: https://www.afro.who.int/health-topics/alcohol. (Accessed: 1st August 2019)

60. Medical Association of South Africa., J., Royal College of Obstetricians and Gynaecologists (Great Britain). South African Regional Council. & South African Society of Obstetricians and Gynecologists. *South African journal of obstetrics and gynaecology. : Suid-Afrikaanse tydskrif vir obstetrie en ginekologie. South African Medical Journal* **102**, (2012).

61. Statistics South Africa. What is GDP and its impact? | Statistics South Africa. Available at: http://www.statssa.gov.za/?p=1143. (Accessed: 29th August 2019)

62. World Health Organization. Harmful use of alcohol. Available at: https://www.who.int/health-topics/alcohol#tab=overview. (Accessed: 29th August 2019)

63. Dario, A. and Tomei, G. A benefit-risk assessment of baclofen in severe spinal spasticity. *Drug Saf.* **27**, 799–818 (2004).

64. Assadi, S. M., Radgoodarzi, R. and Ahmadi-Abhari, S. A. Baclofen for maintenance treatment of opioid dependence: A randomized double-blind placebo-controlled clinical trial

[ISRCTN32121581]. *BMC Psychiatry* **3**, (2003).

65. Adalder, T. K., Sankolli, R. and Dastidar, P. Homo- or heterosynthon? A crystallographic study on a series of new cocrystals derived from pyrazinecarboxamide and various carboxylic acids equipped with additional hydrogen bonding sites. *Cryst. Growth Des.* **12**, 2533–2542 (2012).

Chapter 2

Materials and methods

2.1 Materials

Baclofen is an active pharmaceutical ingredient, locally manufactured by Fine Chemicals Corporation (Pty) Ltd in Epping, South Africa[1] (Chart 1). Baclofen is a γ amino acid and thus has a carboxylic acid and an amine functional group. The pK_a values for these two functional groups in the BAC molecule are 3.89 and 9.79, respectively, and the possibility of a proton transfer is likely resulting in a zwitterion (Table 2.1[2]) Therefore it is logical to select coformers that are basic or acidic[3].

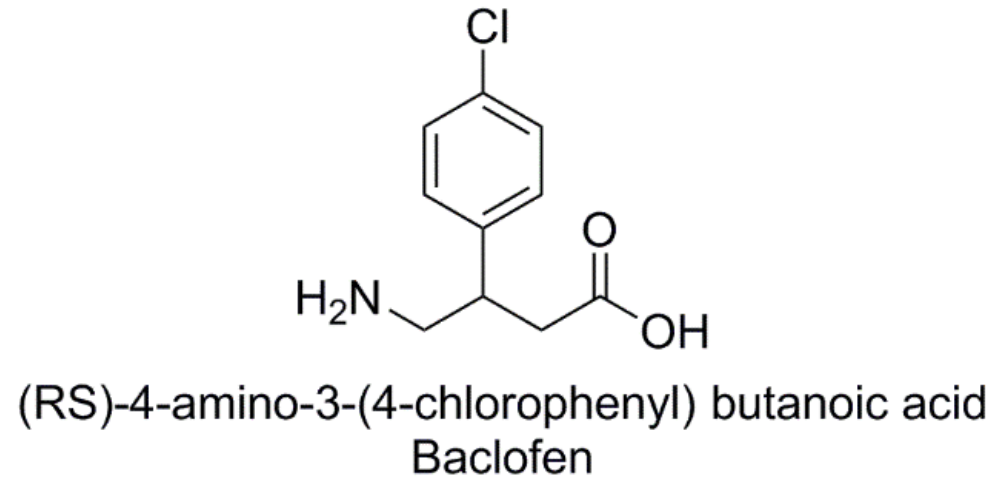

Chart 2.1 Line diagram of baclofen

Table 2.1 Properties of baclofen

Name	**baclofen**
Molecular formula	$C_{10}H_{12}ClNO_2$
Molar mass	213.66 $g.mol^{-1}$
Melting point	207.92°C
p*Ka1* (COOH)	3.89
p*Ka2* (NH_2)	9.79

2.1.1 Coformer selection

The coformers were selected on the criteria that they could hydrogen bond with baclofen as either good proton acceptors or donors. Our research focused on coformers with amine and carboxylic acid functional groups (Table 2.2 and 2.3). Highlighted in red are the coformers that resulted in successful cocrystallisation.

Table 2.2 List of attempted acidic coformers

Oxalic acid	Acetic acid	Formic acid	L-Glutamic acid
Succinic acid	L-(-)- tartaric acid	Propionic acid	Aspirin
Adipic acid	**Salicylic acid**	Butyric acid	Phenylaminoacetic acid
Suberic acid	Stearic acid	Hexanoic acid	Undecanoic acid
Malic acid	Myristic acid	Ethylhexanoic acid	Bromohexanoic acid
Maleic acid	Palmitic acid	Meso tartaric acid	DL proline
Tartaric acid	**Phenoxyacetic acid**	Heptanoic acid	O-O'-dibenzoyl-tartaric acid
Lactic acid	Phenylacetic acid	Octanoic acid	D- (-) -Quinic acid
Stearic acid	L-aspartic acid	Glycine	O-O'-di-p-toluoyl-tartaric acid
2,4-dichlorophenoxyacetic acid			

Table 2.3 List of attempted basic coformers

2-picoline	Isopropylamine	2,6-lutidine	Pyridine
3-picoline	Disec butylamine	**3,4-lutidine**	Sec-butylamine
4-picoline	Aniline	3,5-lutidine	3-chloropyridine
2,3-lutidine	Tertbutylamine	3-chloropyridine	Butylamine
2,4- lutidine			

The coformers that had positive outcomes are as follows:

Acidic coformers:

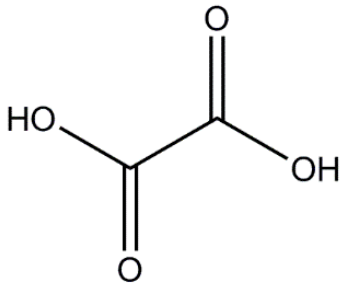

oxalic acid
OXA

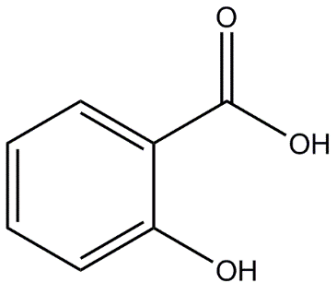

salicylic acid
SAL

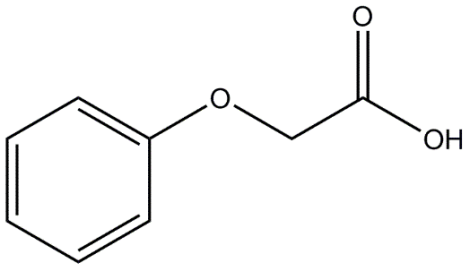

phenoxyacetic acid
POA

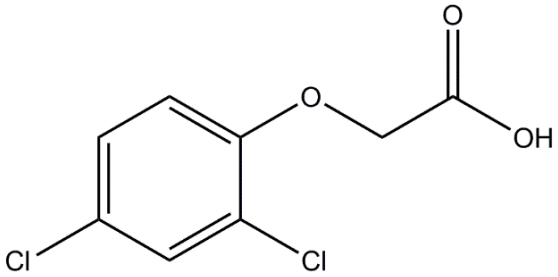

2,4-dichlorophenoxyacetic acid
2,4ClPOA

Basic coformers:

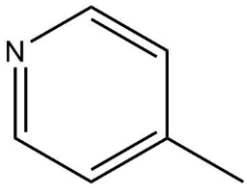

4-picoline
4PIC

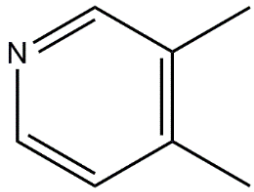

3,4-lutidine
3,4LUT

The coformers below were purchased from Sigma-Aldrich and Merck & Co.

Table 2.4 Properties of the coformers which successfully cocrystallised with baclofen

Name	Molecular formula	Molar mass (g/mol)	Melting point (°C)	pK_{a1} (COOH)	pK_{a2} (NH_2)
Oxalic acid	$C_2H_2O_4$	90.03	192.19	1.36 (4.11)	
Salicylic acid	$C_7H_6O_3$	138.12	158.53	2.97	
Phenoxyacetic acid	$C_8H_8O_3$	152.14	98.76	3.70	
2,4-dichlorophenoxyacetic acid	$C_8H_6Cl_2O_3$	220.04	140.95	2.81	
3,4-lutidine	C_7H_9N	107.15	-		6.33
4-picoline	C_6H_7N	93.13	-		5.85

The below solvents were purchased from KIMIX chemicals & Lab supplies

Table 2.5 Properties of solvents used

Solvent	Molecular formula	Polarity index	Solubility in water (%w/w)	Dielectric constant (ε)
Ethanol	C_2H_6O	5.20	100	24.50
Methanol	CH_4O	5.10	100	33.00
Tetrahydrofuran	C_4H_8O	4.00	100	7.58

Table 2.6 The solvents and melting points of the MCCs formed

Name	Molar ratio	Solvent used	Onset temperature (°C)
[BAC^+][OXA^-]·w	1:2	Ethanol	158.37
BAC·SAL·w	1:2	Ethanol	142.36
[BAC^+][POA^-]	1:1	Methanol	160.51
[BAC^+][2,4ClPOA$^-$]	1:1	50/50 isopropanol water	156.36
[BAC^+][2,4ClPOA$^-$]·w	1:2	50/50 isopropanol water	137.93
2BAC(4PIC)·w		Methanol/THF	104.39
2BAC(3,4 LUT)·w		Methanol/water	101.45

2.2 Methods of crystal growth

2.2.1 Screening of potential new materials

The solubility of baclofen with different solvents of varying polarity was evaluated. A spatula tip of baclofen was transferred to a watch glass, small amounts of solvent were added to the baclofen and the behaviour of baclofen was monitored to see if it dissolves in the solvent successfully.

The screening process was continued further by liquid assisted grinding (LAG) of baclofen and a coformer using a mortar and pestle for 10-15 minutes. Immediately after LAG was completed, the sample was run on the powder X-ray diffractometer to compare the powder pattern to that of the starting materials, baclofen and coformer.

Baclofen dissolved well when methanol and ethanol were used as solvents and it dissolved even better if the ethanol and methanol solvents were mixed with water. Therefore, it was noted that it is advantageous to use solvents in the polarity index range of methanol and ethanol.

2.2.2 Solvent evaporation crystallisation (SEC)

The drug and coformer were dissolved in a suitable solvent. The solution was allowed to evaporate at room temperature to produce a MCC. SEC takes place at room temperature because of the low boiling points of the organic solvents and this prevents thermal decomposition of the drug and coformer.

2.2.2.1 SEC with acidic coformers

Baclofen and the coformer were stoichiometrically measured and dissolved using a solvent. The mass of baclofen weighed between 0.01-0.015 g. The saturated solution was then heated at 60°C until a clear solution was obtained. If on heating the solution remained turbid, the solution was left to cool down to room temperature and was later filtered until a clear solution was achieved. The clear solution was left to crystallise at room temperature, to control the rate at which crystallisation takes place. Pierced parafilm was used to seal the vial.

2.2.2.2 SEC with basic coformers

0.01-0.015 g of baclofen and 2 ml of coformer were added to a vial. The saturated solution was heated at 60°C with the intention of achieving a clear solution. If on heating the solution remained turbid, the solution was left to cool down to room temperature and was later filtered until a clear solution was achieved. The clear solution was left to crystallise at room temperature, to control the rate at which crystallisation takes place. Pierced parafilm was used to seal the vial.

2.2.3 Liquid assisted grinding (LAG)

2.2.3.1 LAG with acidic coformers

For coformers which are in solid state at room temperature, 1-2 g of baclofen and the stoichiometric ratio of the coformer were added to the mortar and was ground using a pestle for 10-15 minutes. Droplets of the same solvent used in the SEC was added until a paste like texture is achieved. Once the paste was dry, the sample was ground further until a soft powder formed. The powder pattern of the new material was compared to that of the starting materials and generated powder pattern of the crystal structure to confirm whether the same material or the crystallisation was unsuccessful and the starting material remains.

2.2.3.2. LAG with liquid coformers

For the liquid basic coformers, the baclofen was ground with a mortar and pestle whilst adding small amounts of the coformer until a paste is formed. The powder pattern of the new material is compared to that of baclofen and generated powder pattern of the crystal structure from the SEC method for confirmation.

2. 3 Analytical tools

2.3.1 Thermal analysis

These instruments are used as tools to determine the physical properties of materials. The thermal instruments used in this study are as follows: differential scanning calorimetry and thermogravimetric analyser.

2.3.1.1 Differential scanning calorimetry (DSC)

DSC is a thermal technique involving the heating or cooling of a material. The DSC gives information such as the enthalpy associated with certain phase changes such as melting. The difference between the sample and reference sample heat flow rate are measured under a controlled temperature program[4].

DSC is useful as it is relatively easy to use, allows for a fast analysis period and requires a sample size of 3-5 mg[5]. DSC can be used to determine the purity of a material[6].

The fundamental equation of DSC is[7],

Signal (W/g) = Heat capacity (J/K) x scanning rate (K/s)

$$\frac{dH}{dt} = \frac{dH}{dT} \times \frac{dT}{dt} \qquad \text{Eq. 1}$$

There are two types of DSC,

- Heat flux DSC

Heat flux DSC has one furnace. The heat flows to the sample and reference pan through an electrically heated thermoelectric disk[8].

- Power compensation DSC

There are two furnaces, one for the sample pan and the other for the reference pan. The temperatures of both systems are different. The power compensation DSC is set that the heat from both furnaces is configured to ensure that the pans are exposed to the same temperature at a set time. The heat flow is plotted against temperature[8].

In this study, the DSC is used to compare the thermal behaviour of the MCC to the starting materials to see if a new product has been made.

2.3.1.3 Thermogravimetric analysis (TGA)

TGA is used to monitor the physical behaviour, specifically the mass of a material when it is exposed to a controlled temperature program in a set environment. TGA can be used to quantify water or solvent loss. It is also an effective confirmatory tool for transitions such as

volatilizations and decomposition[9,10]. The particular interest in this study is to observe the TGA for water or solvent loss and at which temperature this occurs.

The TA DSC 25 differential scanning calorimeter and TA Q500 thermogravimetric analyser with the Trios and TA universal analysis software were used. The dry sample in the 2-5 mg mass range was placed in the aluminium pan for DSC and the ceramic crucible for TGA. It was then exposed to a heating of 10 K min^{-1} until a desired temperature was obtained. The DSC and TGA are operated with a nitrogen flow rate of 60 ml min^{-1}.

2.3.2 Characterisation

There are chemical, experimental and computational methods that can be used for screening and predicting the conformation of a drug in solid state in three dimension. Below are the experimental and computational methods that were used to fully study the crystal structures.

2.3.2.1 Fourier transform infrared (FTIR)

FTIR is a technique used to view the functional groups present in a sample, whether in a liquid, gas or solid state. The functional groups are present at specific wavenumbers on the spectra. The theory is that molecules, more especially organics, absorb light in the infrared region which is converted to molecular vibrations and when some radiation is absorbed by a sample, a signal is detected in the form of a spectrum of the molecular fingerprint of the sample. The absorption of infrared radiation of the sample is measured against the wavelength, in wavenumbers. The universal attenuated total reflectance infrared spectrometer (ATR-FTIR) by Perkin Elmer® spectrum 2 was used to attain spectral data of the samples[11]. There are different types of MCCs, therefore FTIR helps to observe and confirm proton donation, accepting and sharing.

2.3.2.2 Diffraction methods

William Lawrence Bragg and William Henry Bragg continued the work of Max Laue who postulated that crystals can be thought of as three-dimensional grating and are therefore able to diffract X-rays. From the previous work of Laue, the Braggs could prove that crystals are made up of repeating arrangements of an atom[12,13].

X-ray diffraction is a technique that is used to study crystal structures and atomic spacing. An X-ray diffraction pattern is achieved when X-rays, which are generated by a cathode ray tube, are directed towards a crystal. The diffraction takes place when there is constructive interference between the monochromatic X-rays and a crystalline sample. If the interaction of the incident rays and the sample produces constructive interference and a diffracted ray Bragg's law is satisfied the following applies:

$$n\lambda = 2d \sin \theta \qquad \text{Eq. 2}$$

where θ= angle of incidence

λ= wavelength of the X-rays

d= interplanar spacing generating the diffraction

n= an interger

Bragg's law relates the electromagnetic radiation to the angle of incidence and the lattice spacing in a crystalline sample[14].

2.3.2.2.1 Powder X-ray diffraction (PXRD)

PXRD measures the diffraction pattern, which can be considered a fingerprint of a crystalline material. Each diffraction pattern is unique to the API, salt, polymorph or cocrystal. In this manner, we have used PXRD to confirm new materials and for screening. The PXRD measurements were recorded on the Bruker® D8 Advance X-ray diffractometer using Cu Kα radiation (λ = 1.5406 Å)[15].

2.3.2.2.2 Single crystal x-ray diffraction (SCXRD)

X-ray diffraction allows us to determine crystal structures that are a pattern of atomic nuclei and a continuation of electron density. This is done by scattering X-rays by electrons to extract structure factors from reflection densities as well as their Fourier transform data to calculate electron density map. The single crystal structural analysis gives information on intermolecular interactions like the van der Waals radii, directionality and interatomic distances. This extends to the geometrical structure of molecules and molecular solids. The single crystal diffraction data were collected using the Bruker® DUO APEX II diffractometer with a graphite-monochromated Mo Kα radiation (λ= 0.71073 Å) at 173 K using Oxford Cryostream 700 [16,17].

2.3.2.3 Crystal structure determination

The crystal structures were solved using SHELXL-2016 which performs full-matrix, blocked full-matrix or conjugate-gradient least-squares refinement using a conventional structure-factor summation with complex scattering factors. SHELXL may be used for refining small molecule and inorganic structures[18]. SHELXL-2016 was run under a graphical user interface, X-Seed[19,20]. The space groups were determined by using the collected intensities and pre-determined cell parameters as inputs to program XPREP[21]. SHELXL-2016 was used to solve all crystal structures by direct methods and the refinement was also completed using SHELXL-2016 using full matrix least-squares against F^2 for unique reflection.

$$\sum w(F_0^2 - kF_c^2)^2 \qquad \text{Eq. 3}$$

The agreement between the observed structure factors (F_0) and the calculated structure factors (F_c) were monitored by assessing the residual index R. The residual index R_1 is the agreement between the observed and calculated structure factors based on F, while the residual index, R_2, is the agreement based in F^2.

$$R_1 = \frac{\sum||F_0| - |F_C||}{\sum|F_0|} \qquad \text{Eq. 4}$$

$$R_2 = \left[\frac{\sum w\left(F_0^2 - F_c^2\right)^2}{\sum w(F_0^2)^2}\right]^{1/2} \qquad \text{Eq. 5}$$

The weighing scheme w was used to yield a constant distribution in terms of a and b, and further refined in the final cycles of structure refinement

$$w = \frac{1}{\sigma^2\left(F_0^2\right) + (aP)^2 + bP} \qquad \text{Eq. 6}$$

Where:

$$P = \frac{\max\left(o, F_0^2\right) + 2F_c^2}{3} \qquad \text{Eq. 7}$$

SHELXL-2016 refines against F^2, which leads to greater deviation of the Goodness of fit (S) from unity than the refinement against F. The Goodness of fit expression is:

$$S = [\frac{\sum w(|F_0|^2 - |F_c|^2)^2}{\left(N - n_p\right)^2}]^{\frac{1}{2}} \quad \text{Eq. 8}$$

The hydrogen atoms bound to carbon atoms were placed at idealized positions and refined as riding atoms with U_{iso} (H) = 1.2 U_{eq} (Ar-H, CH_2) or 1.5 U_{eq} (CH_3) of the atom to which the H is bound. If it was possible, the H atoms bonded to carboxylic acids and amines were located in the difference electron density map and their coordinates refined freely but their isotropic displacement parameters were fixed (U_{iso} (H) = 1.2 U_{eq} (O) or U_{eq} (N) if it was necessary.

X-ray powder patterns were calculated using LAZY PULVERIX and compared to experimental powder patterns for crystallisation. All the crystal diagrams were generated with POV-RAY. The program LAYER was utilized to test systematic absences and space group symmetry. X-Seed was used as a graphical interface for SHELXL-2016, LAZY PUVERIX, POV-RAY and LAYER[22,23,24].

2.3.3. Computing components

ConQuest: the primary program for advanced searching and retrieving of information of structures in the Cambridge Structural Database (CSD)[25,26].

Siemens Area Detector Absorption Corrections (**SADABS**): an application in the APEX suite used to scale and correct data for absorption collected on a Bruker AXS area detector. The program is designed to exploit data redundancy, corrects for errors resulting from the variation in the volume of crystal, absorption by the crystal support and crystal decay during the measurement[27].

XPREP: This program is used for data analysis and modification. XPREP determines the space group, reads the raw data file (.raw) and the parameter file (.p4p) written by the diffractometer control program. It also writes the instruction file (.ins) and reflection data (hkl)[19,20].

Pov-Ray: program which generates high quality three dimensional graphics[23].

Mercury: Analysis software which provides options to aid the investigation and analysis of crystal structures. It can be used to import information such as chemical bond types, 2D connection tables and present them in 3D illustration. It generates packing diagrams, defines and visualises Millers planes and takes a slice through a crystal in any direction. It also displays space group symmetry elements, calculates voids based either on contact surface or solvent accessible surface and intermolecular potentials and performs basic gas phase calculation[25].

2.4 References

1. Fine Chemicals Corporation PTY ltd | Home. Available at: http://www.fcc.co.za/Product-FullList.aspx. (Accessed: 29th August 2019)

2. Goldenberg, M. Pharmaceutical approval update. *P T* **43**, 734–735 (2018).

3. Etter, M. C. Hydrogen bonds as design elements in organic chemistry. *J. Phys. Chem.* **95**, 4601–4610 (1991).

4. Höhne, G., Hemminger, W. and Flammersheim, H. . *Differential Scanning Calorimetry - - Google Books*. (Springer, 2003).

5. Abu Bakar, M., Nagy, Z. and Rielly, C. A combined approach of differential scanning calorimetry and hot-stage microscopy with image analysis in the investigation of sulfathiazole polymorphism. *J. Therm. Anal. Calorim.* **99**, 609–619 (2010).

6. PerkinElmer. Differential Scanning Calorimetry: A Beginner's Guide. 1–9 (2014).

7. Gabbott, P. *Principles and applications of thermal analysis*. (Blackwell Pub, 2008).

8. Clas, S., Dalton, C. R., Hancock, B. C., Dalton, C. R. and Hancock, B. C. Differential scanning calorimetry: applications in drug development. *Pharm. Sci. Technol. today* **2**, 311–320 (1999).

9. Vitez, I. M., Newman, A. W., Davidovich, M. and Kiesnowski, C. The evolution of hot-stage microscopy to aid solid-state characterizations of pharmaceutical solids. *Thermochim. Acta* **324**, 187–196 (1998).

10. Perkin Elmer. Thermogravimetric Analysis (TGA): A Beginner ' s Guide. *Perkin Elmer* (2004).

11. FTIR Basics | ALPHA II | Bruker. Available at: https://www.bruker.com/products/infrared-near-infrared-and-raman-spectroscopy/ft-ir-routine-spectrometers/alpha/ftir-basics.html. (Accessed: 6th September 2019)

12. Glazer, A. M. The first paper by W.L. Bragg-what and when? *Crystallogr. Rev.* **19**, 117–124 (2013).

13. Bragg, P. W. H. and Bragg, W. L. 428 Prof. W. H. Bragg and Mr. W. L. Bragg. [Apr. 7,. **17**, 428–438 (1913).

14. Bunaciu, A. A., Udriştioiu, E. G. and Aboul-Enein, H. Y. X-Ray Diffraction: Instrumentation and Applications. *Crit. Rev. Anal. Chem.* **45**, 289–299 (2015).

15. Ticehurst, M. and Swanson, J. T. Strategies for Improving the Reliability of Accelerated Predictive Stability (APS) Studies. in *Accelerated Predictive Stability* 175–206 (Academic Press, 2018).

16. Schneider, H. J. and Yatsimirsky, A. K. *Principles and methods in supramolecular chemistry*. (Wiley, 2000).

17. Batsanov, A. S. Small Molecule Applications of X-Ray Diffraction. *Encycl. Spectrosc. Spectrom.* 2550–2558 (2010).

18. Sheldrick, G. M. A short history of SHELX. *Acta Crystallogr. Sect. A Found. Crystallogr.* **64**, 112–122 (2008).

19. Sheldrick, G. M. Crystal structure refinement with SHELXL. *Acta Crystallogr. Sect. C Struct. Chem.* **71**, 3–8 (2015).

20. Barbour, L. J. X-Seed — A Software Tool for Supramolecular Crystallography. *J. Supramol. Chem.* **1**, 189–191 (2001).

21. Poleti, D., Balić-Žunić, T., Hope, H. and Karanović, L. A beginner's guide to the Bruker AXS pack and other noble time wasters. *BruKer-AXS* 106 (2003).

22. Yvon, K., Jeitschko, W. and Parthé, E. *LAZY PULVERIX* , a computer program, for calculating X-ray and neutron diffraction powder patterns. *J. Appl. Crystallogr.* **10**, 73–74 (1977).

23. POV-Ray - The Persistence of Vision Raytracer. Available at: http://www.povray.org/. (Accessed: 6th September 2019)

24. Barbour, L. J. LAYER - A computer program for the graphic display of intensity data as simulated precession photographs. *J. Appl. Crystallogr.* **32**, 351–352 (1999).

25. Bruno, I. J., Cole, J.C., Edgington, P.R., Kessler, M., Macrae, C.F., McCabe, P., Pearson,

J. and Taylor, R. New software for searching the Cambridge Structural Database and visualizing crystal structures. *Acta Crystallogr. Sect. B Struct. Sci.* **58**, 389–397 (2002).

26. Groom, C. R., Bruno, I. J., Lightfoot, M. P. and Ward, S. C. The Cambridge structural database. *Acta Crystallogr. Sect. B Struct. Sci. Cryst. Eng. Mater.* **72**, 171–179 (2016).

27. PHOTON III - Detector, Single Crystal X-ray Diffraction - Detectors - Single Crystal X-ray Diffraction | Bruker. Available at: https://www.bruker.com/products/x-ray-diffraction-and-elemental-analysis/single-crystal-x-ray-diffraction/sc-xrd-components/sc-xrd-components/overview/sc-xrd-components/detectors/photon-iii.html?gclid=Cj0KCQjwh8jrBRDQARIsAH7BsXckgx4tB2KCy1AaA6w7qPcK72VXku. (Accessed: 6th September 2019)

Chapter 3

Discussion of crystal structures

Introduction

In this chapter, the crystal structures of baclofen with acidic and basic coformers: oxalic acid (OXA), salicylic acid (SAL), phenoxyacetic acid (POA), 2,4-dichlorophenoxyacetic acid (2,4ClPOA), 4-picoline (4PIC) and 3,4-lutidine (3,4LUT) are presented. The cocrystallisations were carried out by the slow evaporation crystallisation (SEC) method. Racemic baclofen was used for the crystallisations and the asymmetric units were selected to contain the *R* enantiomer for easy comparison.

3.1 Multicomponent crystal formation of baclofen with oxalic acid: $[BAC^{+}][OXA^{-}]\cdot w$

Baclofen (BAC) was previously cocrystallised with oxalic acid (OXA)[1] from ethanol solvent. The asymmetric unit (ASU) contained one molecule of BAC and half a molecule of OXA, $[BAC^{+}][½OXA^{2-}]$ and the space group was $P2_1/c$ (No. 14). The crystal was defined as a salt as both of the carboxylic acid protons were transferred to the baclofen moiety.

The cocrystallisation was repeated for experimental training purposes under the same conditions but surprisingly, a different stoichiometric ratio of the constituents was obtained in the centrosymmetric space group $P\bar{1}$ (No. 2). In this case, BAC cocrystallised with two half oxalic acids, where one of the OXA is neutral and the other is dideprotonated $[OXA^{2-}]$ and the BAC is protonated [BAC]. Also, one molecule of water is included in the ASU. The crystal can be described as a cocrystal-salt solvate[2] (hydrate), $[BAC^{+}][½OXA^{2-}]\cdot ½OXA\cdot H_2O$. For simplicity, this crystal will be named as $[BAC^{+}][OXA^{-}]\cdot w$ from now onwards. The crystal data and hydrogen bonds are listed in Table 3.1 and 3.2. Visual comparison of the ASUs of $[BAC^{+}][½OXA^{2-}]$ and $[BAC^{+}][OXA^{-}]\cdot w$ are shown in Figure 3.1.

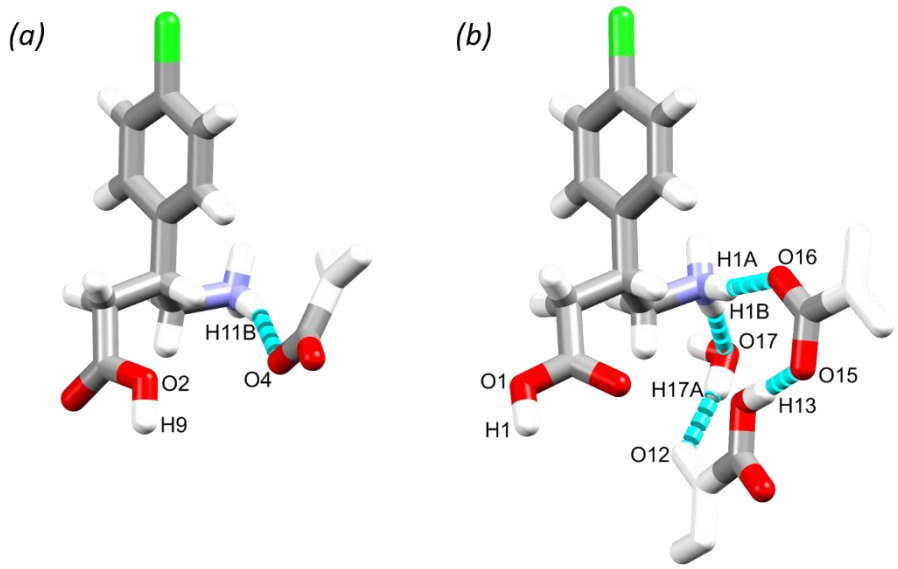

Figure 3. 1 The ASU of $[BAC^{+}][½OXA^{2-}]$ (a) and $[BAC^{+}][OXA^{-}]\cdot w$ (b) (part of the OXA that are not part of the ASU are faded for clarity).

Table 3.1 Crystallographic data of $[BAC^{+}][½OXA^{2-}]$ and $[BAC^{+}][OXA^{-}]\cdot w$

Compounds	$[BAC^{+}][½OXA^{2-}]$	$[BAC^{+}][OXA^{-}]\cdot w$
Molecular formula	$C_{11}H_{13}ClNO_4$	$C_{12}H_{16}ClNO_7$
Formula weight ($g.mol^{-1}$)	258.67	321.71
Crystal system	Monoclinic	Triclinic
Space group(No.)	$P2_1/c$ (No. 14)	$P\bar{1}$ (No. 2)
a (Å)	15.035(3)	7.0962(14)
b (Å)	7.2113(14)	9.6510(19)
c (Å)	11.025(2)	11.031(2)
α (°)	90.00	80.82
β (°)	106.86(3)	77.59
γ (°)	90.00	88.31
V (A^3)	1143.9(4)	728.4(3)
Z	4	2
ρ_{calc}($g.cm^{-3}$)	1.502	1.467
μ(MoKα) (mm^{-1})	0.336	0.295
F(000)	540	336
Crystal size(mm)	0.090×0.170×0.240	0.100x0.120x0.230
Temperature (K)	173(2)	173(2)
Radiation (Å)	MoKα, 0.71073	MoKα,0.71073
Theta min-max (°)	2.83, 27.48	1.914; 28.352
Dataset (±h; ±k; ±l)	-19:19; -9:9; -14:14	-9:9; -12:12; -14:14
Final R indices [I>2σ(I)]	R_1=0.0353; wR_2=0.0886	R_1=0.0507; wR_2= 0.1231
R indices [all data]	R_1=0.0508; wR_2=0.0979	R_1=0.0775; wR_2=0.1390
Tot., uniq. data, R (int)	2618; 2054; 0.0161	15206; 2515;0.0506
N_{ref}, N_{par}	2618; 171	3633; 218
S	1.046	1.057
Max. and av.shift/error	0.000/ 0.000	0.001/0.000
Min. and max. resd. Dens.($Å^3$)	0.214; -0.279	-0.500; 0.651

Table 3.2 Hydrogen bonds of [BAC$^+$][OXA$^-$]·w

D-H···A	d(D-H) (Å)	d(H···A) (Å)	d(D···A) (Å)	D-H···A (°)	Symmetry operators
O1-H1···O2	0.97	1.69	2.659(9)	178	[-x, -y, 1-z]
O13-H13···O15	0.93	1.54	2.464(2)	171	-x, 1- y, 1-z
N1-H1C···O15	0.93	2.34	2.996(7)	127	[1+x, y, z]
N1-H1C···O16	0.93	2.03	2.898(3)	153	[1-x, 1-y, -z]
N1-H1A···O16	0.87	1.98	2.836(7)	167	
N1-H1B···O17	0.84	1.96	2.790(7)	171	
O17-H17A···O12	0.88	1.91	2.782(7)	169	
O17-H17B···O12	0.76	2.13	2.862(4)	162	[1-x, 1-y, 1-z]
C8-H8B···O1	0.97	2.58	3.544(3)	171	[1-x, -y, 1-z]

The oxalic acids form hydrogen bonded chains in an alternating manner of OXA···[OXA^{2-}]···OXA via O13-H13···O15 (2.464(2) Å, 171°) in [001] direction (Fig. 3.2). The parallel acid chains are linked together via water molecules forming a $R_4^2(8)$ supramolecular synthon via the O17-H17A···O12 (2.782(7) Å, 169°) and O17-H17B···O12 (2.862(4) Å, 162°) hydrogen bonds (Fig. 3.2a, yellow). The amino groups of the BAC molecules are incorporated into this ionic layer and form hydrogen bonds with the neighbouring water (N1-H1B···O17, 2.790(7) Å, 171°) and two oxalic acid molecules (N1-H1A···O16, 2.836(7) Å, 167° and N1-H1C···O16, 2.898(3) Å, 153°) and the latter forms a $R_4^2(8)$ graph set (Fig. 3.2a, green). Two BAC molecules from adjacent ionic layers form carboxylic acid dimers by O1-H1···O2 (2.659(9) Å, 178°) hydrogen bonds and these BAC dimers interact with neighbouring dimers via C8-H8B···O1 (3.544(3) Å, 171°) hydrogen bonds. Both these interactions can be described by the $R_2^2(8)$ graph set and shown on Fig. 3.2b, with blue and purple, respectively. It is interesting to note that in the structure of [BAC$^+$][½OXA^{2-}] there are no carboxylic acid dimers between the BAC molecules but the BACs are interacting via carboxylic acid···amino interactions in a *head-to-tail* manner (defined the carboxylic acid group as the *head* and the amino group as the *tail*). The OXA molecules do hydrogen bond to each other but bridging between adjacent hydrogen bonded BAC chains. The resultant two hydrogen bonding motifs can be described with the $R_3^3(11)$ and the $R_4^4(22)$ graph sets (Fig. 3.3, blue and green, respectively).

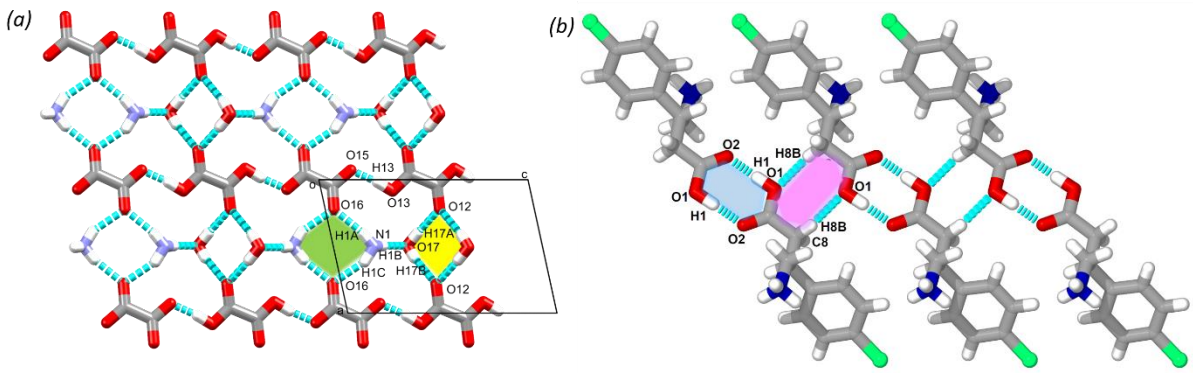

Figure 3. 2 The ionic layer formed by oxalic acid and water molecules with the amino groups that anchor BAC molecules (a) and interactions between the adjacent BAC molecules (b) in [BAC$^+$][OXA$^-$]·w.

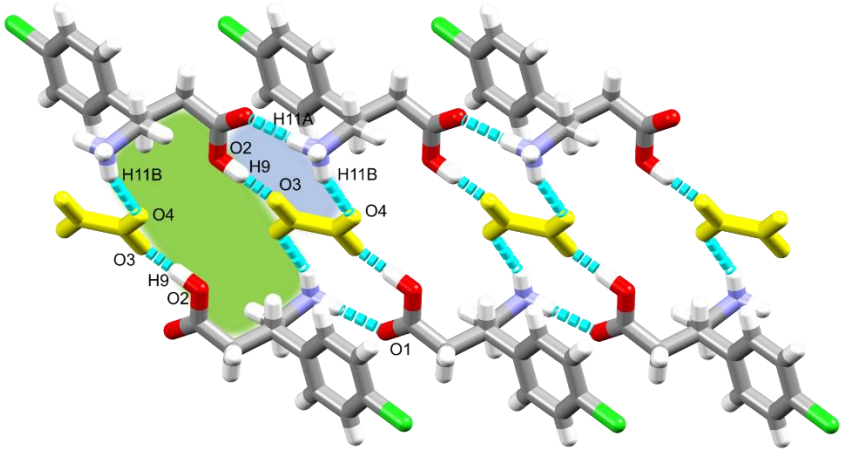

Figure 3. 3 Hydrogen bonds and the $R_3^3(11)$ and the $R_4^4(22)$ synthons (green and blue, respectively) in [BAC$^+$][½OXA^{2-}] (oxalic acid ions are yellow)

The other difference between the two oxalic acid MCCs is the conformation of the BAC molecules which are not similar. The crystal packing for both MCCs is layered. The packing for [BAC$^+$][½OXA^{2-}] has chlorine atoms of BAC which are facing each other and there is a tape formed by the oxalic acid coformers. For [BAC$^+$][OXA$^-$]·w, the chlorine atoms are facing the same direction. There is also a hydrophilic layer present (Fig. 3.4).

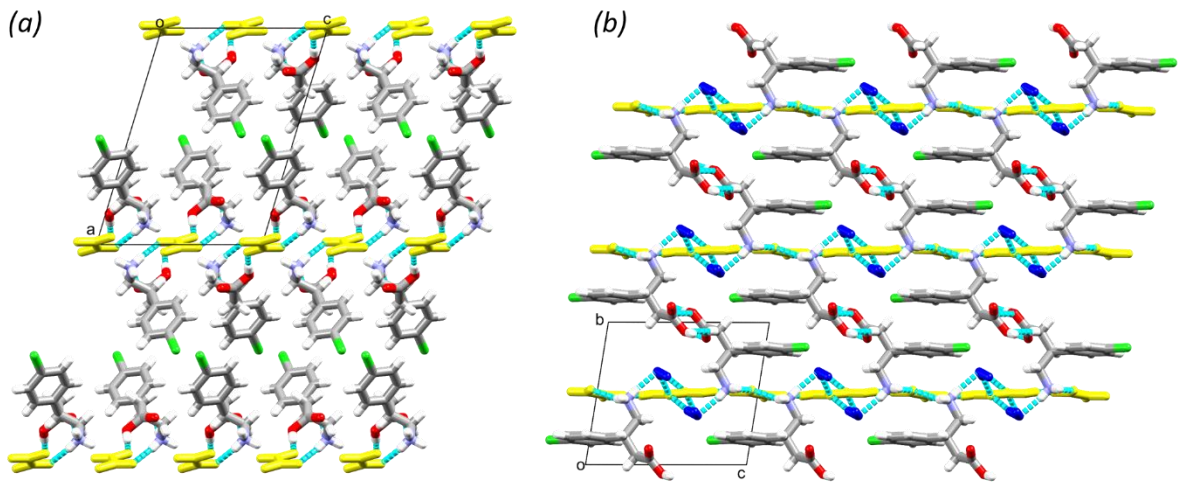

Figure 3. 4 Layered structure of [BAC$^+$][½OXA^{2-}] viewed down [010] direction (a) and [BAC$^+$][OXA$^-$]·w viewed down [100] direction (b) (OXAs are yellow, water molecules are blue).

3.2 Multicomponent crystal formation of baclofen with salicylic acid: BAC·SAL·w

Baclofen (BAC) was previously cocrystallised with benzoic acid (BA)[1] that is generally regarded as a safe (GRAS) substance in a 1:1 ratio. The crystal structure was solved in the monoclinic $P2_1/c$ (No. 14) space group and the asymmetric unit contained two molecules of BAC in zwitter ionic form and three molecules of neutral BA (BAC·BA).

The crystallisation of BAC with salicylic acid (SAL) was a logical extension of multidrug MCC formation with active pharmaceutical ingredients (APIs). BAC was cocrystallised with salicylic acid (SAL) in 1:1 ratio from ethanol solvent. The ASU contains a zwitter ionic BAC, a neutral SAL and a water molecule in 1:1:1 ratio (BAC·SAL·w), therefore the crystal can be classified as a cocrystal solvate (hydrate)[2] (Fig. 3.5a). The backbone of the BAC molecule is disordered in 90:10 ratio and the minor disorder shown with light blue wireframe representation of Figure 3.5a. A supramolecular unit, known as a tetramer, can be identified based on the hydrogen bonding between two BAC molecules of opposite chirality, two SAL and two water molecules and may be described with the $R_4^2(8)$ graph set (Fig. 3.5b, yellow). The crystal data and hydrogen bonds for BAC·SAL·w are shown in Table 3.3 and 3.4.

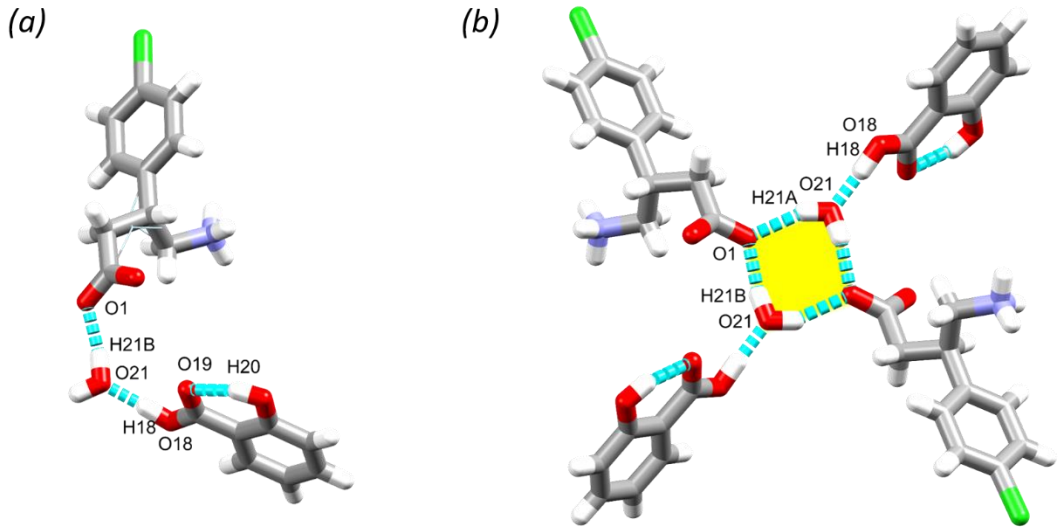

Figure 3. 5 ASU of BAC·SAL·w (minor disorder of the BAC moiety is shown with light blue wireframe representation) (a) and the tetramer formed (b) from two BAC, two SAL and two water molecules creating a hydrogen bonded ring (yellow)

Table 3.3 Crystallographic data of BAC·SAL·w

MCC	BAC·SAL·w
Molecular formula	$C_{17}H_{20}ClNO_6$
Formula weight (g.mol^{-1})	369.79
Crystal system	monoclinic
Space group(No.)	$P2_1/c$ (No. 14)
a (Å)	14.010(3)
b (Å)	17.797(4)
c (Å)	7.0663(14)
α(°)	90
β(°)	91.43
γ(°)	90
V(A^3)	1761.3(6)
Z	4
ρ_{calc}(g.cm^{-3})	1.395
μ(MoKα) (mm^{-1})	0.250
F(000)	776
Crystal size(mm)	0.060x0.230x0.330
Temperature (K)	173(2)
Radiation (Å)	MoKα,0.71073
Theta min-max (°)	1.454; 28.367
Dataset (±h; ±k; ±l)	-18:18; -23:23; -9:9
Final R indices [I>2σ(I)]	0.0451; 0.0946
R indices [all data]	0.0785; 0.1073
Tot., uniq. data, R (int)	22262; 3001; 0.0429
N_{ref}, N_{par}	4399; 273
S	1.031
Max. and av.shift/error	0.000/0.000
Min. and max. resd. Dens.(Å^3)	-0.230; 0.404

Table 3.4 Hydrogen bonds of BAC·SAL·w

D-H···A	d(D-H) (Å)	d(H···A) (Å)	d(D···A) (Å)	D-H···A (°)	Symmetry operators
N1-H1C···O2	0.93	1.92	2.826(3)	164	[x, y, -1+z]
N1-H1A···O19	0.94	2.11	2.917(9)	143	
N1-H1A···O21	0.94	2.39	2.941(2)	118	
N1-H1B···O2	0.94	1.84	2.774(7)	175	[x, ½-y, 1/2-+z]
O20-H20···O19	0.86	1.84	2.613(2)	150	
O21-H21A···O1	0.82	1.93	2.695(8)	156	[1-x, -y, 2-z]
O21-H21B···O1	0.89	1.81	2.681(5)	167	
O18-H18···O21	0.94	1.60	2.541(5)	175	

The tetramers interact via hydrogen bonds that are formed between neighbouring BAC units (N1-H1B···O2, 2.774(7) Å, 175° and C7-H7A···O2, 2.898(3) Å, 153°) and the SAL and adjacent BAC molecules (O18-H18···O21, 2.541(5) Å, 175° and 021-H21A···O1, 2.695(8) Å, 156°) (Fig. 3.6a). The crystal has a layered structure, built from alternating hydrophilic and aromatic regions (Fig. 3.6b, blue and green, respectively). There are Cl···π interactions in the aromatic layer that are formed between the BAC molecules and the adjacent aromatic rings of the SAL molecules (Cl1···C14, 3.44 Å, 163°, Fig. 3.6c).

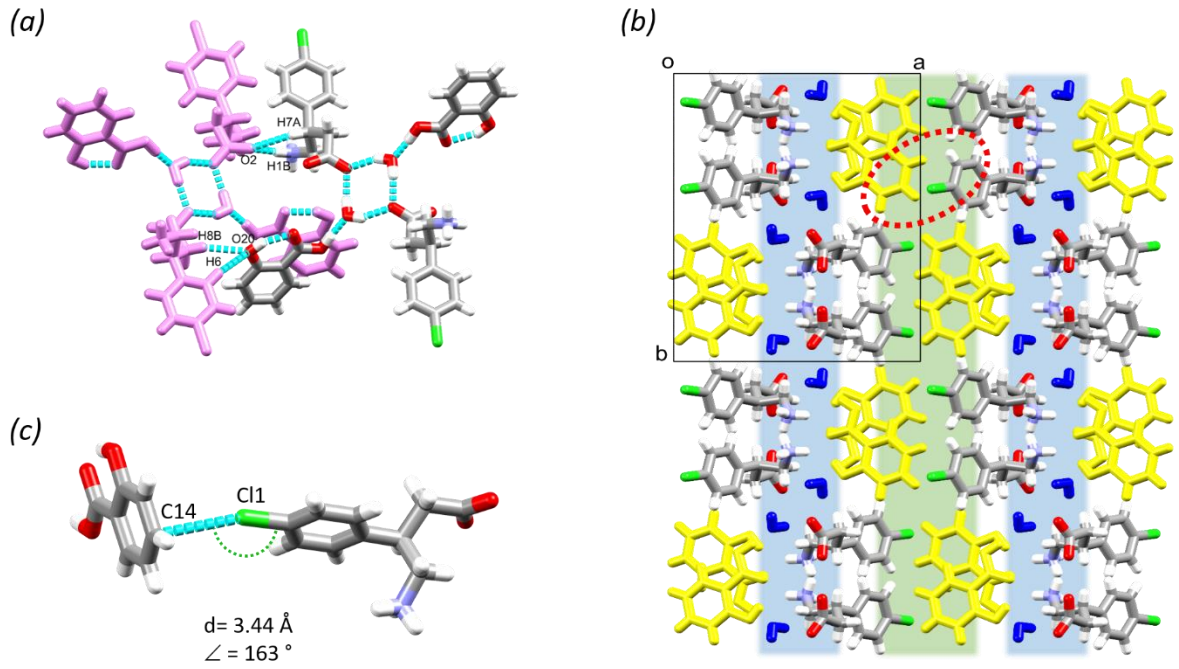

Figure 3. 6 The mode of interaction between adjacent tetramers in BAC·SAL·w (a) and the alternating hydrophilic and aromatic layers (blue and green, respectively) (b) and the observed Cl···π interaction in the aromatic layers (c).

3.3 Multicomponent crystal formation of baclofen with phenoxyacetic acid, [BAC$^+$][POA$^-$], and 2,4-dichlorophenoxyacetic acid: [BAC$^+$][2,4ClPOA$^-$] and [BAC$^+$][2,4ClPOA$^-$]·w

BAC was cocrystallised with phenoxyacetic acid (POA) and its halogenated form, 2,4-dichlorophenoxyacetic acid (2,4ClPOA). These compounds are plant growth retardants/herbicides, thus using them as coformer was reasoned based on structural considerations and not their chemical suitability. In previous studies by Báthori and Kilinkissa[1] and the BAC·SAL·w structure, it was speculated that increasing the number of chloro substituents on the aromatic ring of the coformer—that also have a carboxylic acid functional group—it will be possible to form Cl···Cl interactions in the aromatic layer, while the overall layered structure of the crystal can be maintained. Therefore these crystallisations would test crystal engineering principles, i.e. fine tuning the intermolecular interactions in the aromatic layer.

One MCC was obtained by crystallising BAC with POA, and two crystals were obtained from exposing BAC to 2,4ClPOA under different conditions. The crystal data and hydrogen bond information for these three MCCs are summarised in Table 3.5 and 3.6.

BAC was cocrystallised in 1:1 mole ratio with POA with methanol solvent. The crystal structure was solved and refined in $P\bar{1}$ (No. 2) and the ASU contains one molecule of BAC and one POA (Fig. 3.7a). The POA protonated the BAC and interacts via the charge assisted O1-H1···O4 (2.603(2) Å, 159°) hydrogen bond. The crystal is classified as a true salt[2], [BAC^+][POA^-]. A supramolecular unit can be described that forms from two BAC^+ and two POA^- and holds together by the O1-H1···O4 (2.603(2) Å, 159°, N1-H1A···O4 (2.742(7) Å, 151°), C10-H10A···O2 (3.462(7) Å, 168°) hydrogen bonds that refer to the $R_3^2(9)$ graph set (Fig. 3.7b, yellow) and their symmetry generated counterparts. The protonated amino group of the BAC hydrogen bonds to three POA ions that are parallel (Fig. 3.7c) and eventually causes the crystal packing to have hydrophilic and aromatic layers (Fig. 3.8a, blue and green, respectively), the former formed by the charge assisted hydrogen bonds between the carboxylic acid, carboxylate and amino functional groups, and the latter is created by the alternating aromatic rings of BAC and POA. There are Cl···Cl interactions in the aromatic layer that are formed between two BAC molecules (Cl1···Cl1, 3.57 Å, 155°, Fig. 3.8b).

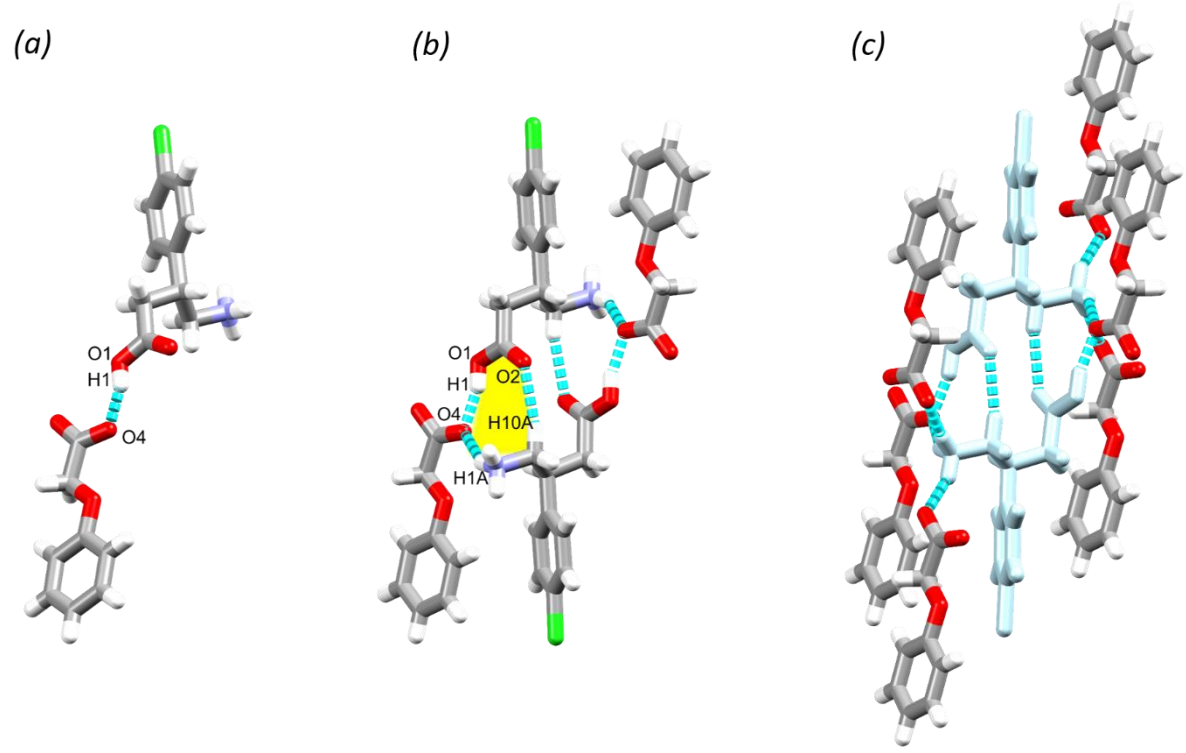

Figure 3. 7 ASU (a), supramolecular unit (b) and packing interactions that result in the layered structure (c) in [BAC^+][POA^-]

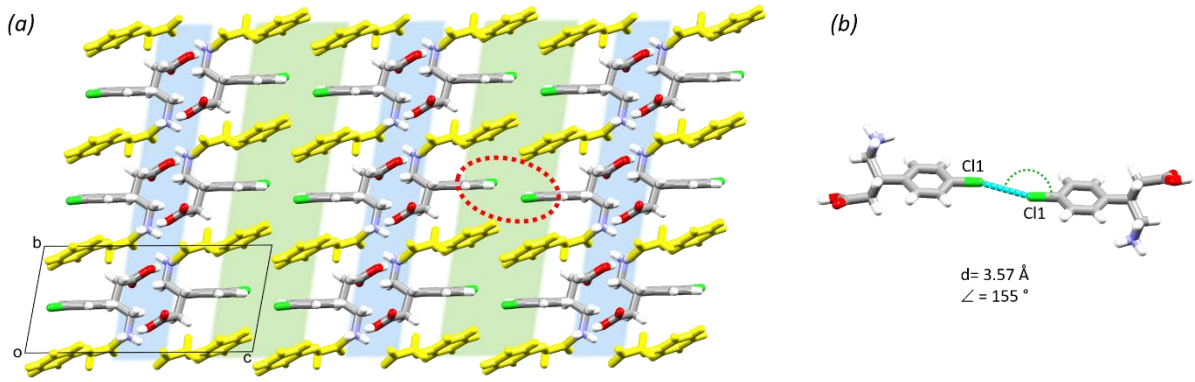

Figure 3. 8 Hydrophilic (blue) and aromatic layers (green) in [BAC$^+$][POA$^-$] (a) and Cl···Cl interactions in the aromatic layer(b).

Table 3.5 Crystallographic data of [BAC$^+$][POA$^-$], [BAC$^+$][2,4ClPOA$^-$] and [BAC$^+$][2,4ClPOA$^-$]·w

MCC	[BAC$^+$][POA$^-$]	[BAC$^+$][2,4ClPOA$^-$]	[BAC$^+$][2,4ClPOA$^-$]·w
Molecular formula	$C_{18}H_{20}ClNO_5$	$C_{18}H_{18}Cl_3NO_5$	$C_{26}H_{26}Cl_5NO_9$
Formula weight (g.mol^{-1})	365.80	434.68	673.73
Crystal system	Triclinic	monoclinic	Triclinic
Space group (No.)	$P\bar{1}$(2)	$P2_1/c$ (14)	$P\bar{1}$(2)
a (Å)	6.9834(14)	15.699(3)	7.4548(15)
b(Å)	7.8322(16)	8.7459(17)	13.856(3)
c(Å)	16.383(3)	14.834(3)	14.684(3)
α(°)	79.08	90	81.27
β(°)	86.83	106.08	81.44
γ(°)	83.81	90	80.50
V(A^3)	874.2(3)	1957.0(7)	1466.7(5)
Z	2	4	2
ρ_{calc}(g.cm^{-3})	1.390	1.475	1.526
μ(MoKα) (mm^{-1})	0.247	0.498	0.548
F(000)	384	896	692
Crystal size(mm)	0.100x0.140x0.250	0.200x0.260x0.360	0.100x0.110x0.120
Temperature (K)	173(2)	173(2)	173(2)
Radiation (Å)	MoKα,0.71073	MoKα,0.71073	MoKα,0.71073
Theta min-max (°)	2.534; 27.967	2.692; 28.351	1.414; 27.174
Dataset (±h; ±k; ±l)	-9:9; -10:10; -21:21	-20:20; -11:11; -19:19	-9:9; -17:17; -18:18
Final R indices [I>2σ(I)]	0.0413; 0.1011	0.0331; 0.0814	0.0374; 0.0806
R indices [all data]	0.0576; 0.1089	0.0416; 0.0863	0.0621; 0.0906
Tot., uniq. data, R (int)	15348;3222;0.0250	49316;4108; 0.0485	35463; 4732;0.0467
N_{ref}, N_{par}	4139; 230	4869;257	6522; 399
S	1.037	1.035	1.023
Max. and av.shift/error	0.001/0.000	0.001/0.000	0.001/0.000
Min. and max. resd. dens.(Å^3)	-0.281; 0.319	-0.480; 0.359	-0.432; 0.338

Table 3.6 Hydrogen bonds of [BAC$^+$][POA$^-$], [BAC$^+$][2,4ClPOA$^-$] and [BAC$^+$][2,4ClPOA$^-$]·w

MCC	D-H···A	d(D-H) (Å)	d(H···A) (Å)	d(D···A) (Å)	D-H···A (°)	Symmetry operators
[BAC$^+$][POA$^-$]						
	O1-H1···O4	0.88	1.76	2.603(2)	159	[1-x, 2-y, 1-z]
	N1-H1C···O5	0.92	1.98	2.840(5)	154	[-1+x, -1+y ,z]
	N1-H1A···O4	0.91	1.91	2.742(7)	151	[x, -1+y, z]
	N1-H1B···O5	0.92	1.95	2.872(1)	172	[1-x, 1-y, 1-z]
	C10-H10A-O2	0.97	2.51	3.462(7)	168	[1-x, 1-y, 1-z]
[BAC$^+$][2,4ClPOA$^-$]						
	O1-H1···O5	0.91	1.57	2.476(6)	171	[-x, -1/2+y, 1/2-z]
	N1-H1A···O4	0.89	2.02	2.847(2)	154	[-x+2, y-1/2, -z+3/2]
	N1-H1B···O4	0.92	2.00	2.830(2)	151	
	N1-H1C···O2	0.92	1.97	2.735(8)	140	
	C6-H6···O5	0.95	2.62	3.535(1)	161	
	C10-H10A···O5	0.99	2.36	3.267(4)	153	
	C8-H8B···O5	0.99	2.57	3.470(3)	152	[x, 3/2-y, 1/2+z]
[BAC$^+$][2,4ClPOA$^-$]·w						
	O1-H1···O8	0.82	1.83	2.648(1)	173	[-x, 1-y, 1-z]
	O9-H9B···O4	0.89	2.18	2.960(7)	147	
	O7-H7A···O5	1.04	1.40	2.447(2)	177	[-x, 1-y, -z]
	N1-H1A···O5	0.89	2.10	2.868(4)	145	[x, y, 1+z]
	N1-H1C···O2	0.89	2.06	2.902(3)	159	[-1+x, y, z]
	O9-H9A···O2	0.89	2.05	2.936(9)	170	[1-x, 1-y, 1-z]
	N1-H1B···O4	0.92	1.89	2.763(6)	158	[-x ,1-y, 1-z]
	C25-H25···O7	0.99	2.60	3.499(3)	151	[-x, 2-y, -z]

BAC was cocrystallised in 1:1 mole ratio with 2,4ClPOA using 50/50 isopropanol/ water solvent. The MCC crystallised in $P2_1/c$ (No. 14) space group with one molecule of BAC and one 2,4ClPOA in the ASU (Fig. 3.9a). Similar to [BAC$^+$][POA$^-$], the 2,4ClPOA protonated the BAC and interacts via the charge assisted O1-H1···O5 (2.476(6) Å, 171°) hydrogen bond. The crystal is classified as a true salt[2] and depicted as [BAC$^+$][2,4ClPOA$^-$]. A similar supramolecular unit that was discussed in [BAC$^+$][POA$^-$] can be described: two BAC$^+$ and two 2,4ClPOA$^-$ held together by the O1-H1···O5 (2.476(6) Å, 171°), N1-H1A···O4 (2.847(2) Å, 154°), N1-H1B···O4 (2.830(2) Å, 151°), N1-H1C···O2 (2.735(8) Å, 140°) hydrogen bonds. The motif can be described with the $R_5^4(14)$ graph set (Fig. 3.9b, yellow). These supramolecular units interact with adjacent ones via C6-H6···O5 (3.535(1) Å, 161°), C8-H8B···O5 (3.470(3) Å, 152°) and C10-H10A···O5 (3.267(4) Å, 153°) interactions (Fig. 3.9c). The crystal packing is also very similar to [BAC$^+$][POA$^-$] and resembles its layered structure with alternating hydrophilic and aromatic layers (Fig. 3.10a, blue and green, respectively). It is important to note that the crystallisation was successful from crystal engineering perspective too. The BAC interacted with the carboxylic moiety in similar manner as was observed in the POA and previous structures of BAC MCCs with aromatic carboxylic acids[1]. Thus the Cl substituent in the para-position of the aromatic ring of 2,4ClPOA was directed towards the aromatic layer

of the crystal, subsequently increasing the concentration of Cl substituents in that region of the crystal. Interestingly, there are only Cl···π interactions in the aromatic layer formed between BAC and 2,4ClPOA molecules (Cl1···C13, 3.38 Å, 139°, Fig. 3.10b). It may be concluded that the interaction between the BAC and aromatic carboxylic acids are conservative thus substitution of the aromatic ring of the coformer allows fine tuning the intermolecular interactions in the aromatic layer.

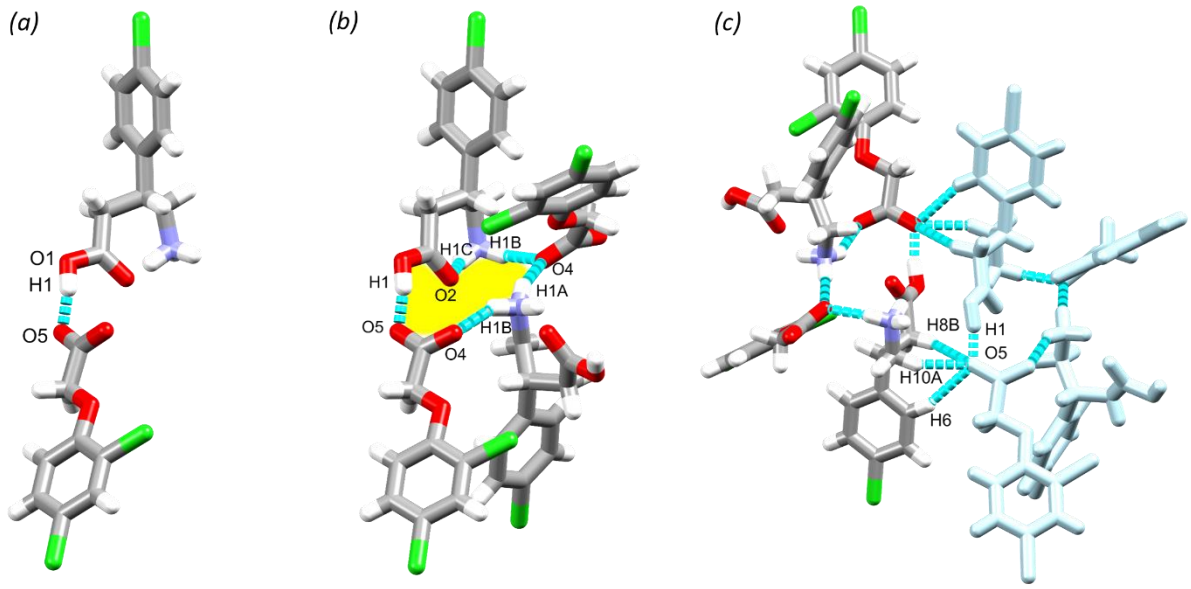

Figure 3. 9 ASU (a), supramolecular unit (b) and packing interactions that result in the layered structure (c) in [BAC$^+$][2,4POA$^-$]

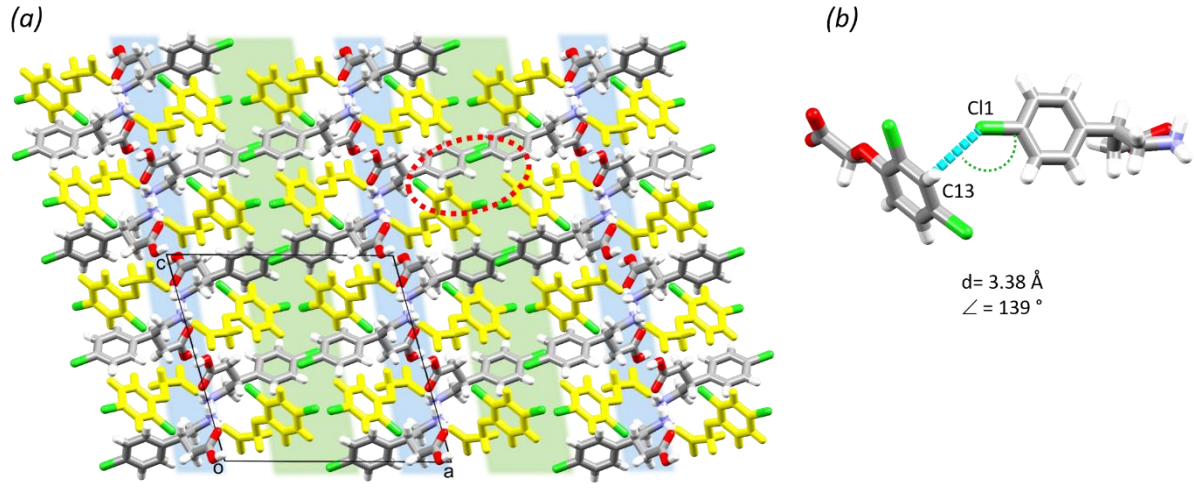

Figure 3. 10 Hydrophilic (blue) and aromatic layers (green) in [BAC$^+$][2,4POA$^-$] (a) and Cl···π interactions in the aromatic layer (b).

BAC was also cocrystallised in 1:2 mole ratio with 2,4ClPOA in 50/50 isopropanol/water solvent resulting in a crystal that was solved and refined in $P\bar{1}$ (No. 2) space group with one molecule of BAC, two molecules 2,4ClPOA and one water in the ASU (Fig. 3.11a). The BAC is protonated by one of the 2,4ClPOA, while the other 2,4ClPOA is neutral, thus the crystal may be depicted as [BAC^+][$2,4ClPOA^-$]·2,4ClPOA·w, a cocrystal salt solvate (hydrate)[2]. For simplicity, it will be referred to as [BAC^+][$2,4ClPOA^-$]·w. The BAC^+ forms a direct hydrogen bond with the neutral 2,4ClPOA (O1-H1···O8, 2.648(1) Å, 173°) and interacts with the deprotonated $2,4ClPOA^-$ via a bridging water (O9-H9A···O2, 2.936(9) Å, 170°and O9-H9B···O4, 2.960(7) Å, 147°). With their symmetry generated counterparts a larger supramolecular unit can be identified and described with the $R_8^8(28)$ graph set (Fig. 3.11b, yellow). These units interact with neighbouring ones by anchoring them via forming hydrogen bonds with the NH_3^+ groups (N1-H1A···O5 (2.868(4) Å, 145°), N1-H1B···O4 (2.763(6) Å, 158°) and N1-H1C···O2 (2.902(3) Å, 159°) Fig. 3.11c).

The crystal packing is very similar to the previously discussed layered structures, having alternating hydrophilic and aromatic layers (Fig. 3.12a, blue and green, respectively). It is interesting to note that although there are two symmetrically independent 2,4ClPOA moieties in the crystal that also differ in their protonation state, their structural role is very similar. The two 2,4ClPOA moieties form centrosymmetric tetramers via C25-H25A···O7 (3.499(3) Å, 151°) and O7-H7A···O5 (2.447(2) Å, 177°) hydrogen bonds and their symmetry related counterparts, in what their aromatic rings are in an offset face-to-face arrangement (ring distance is 3.59 Å and their angle is 2.28°, Fig. 3.12b and c). It is important to note that (1) despite the inclusion of the water and the different stoichiometry the nature of the crystal stayed layered and (2) despite the number of chlorine functional groups of the molecules, there are no interactions formed by these moieties that fulfil the geometrical requirements to be noted as any form of halogen interaction.

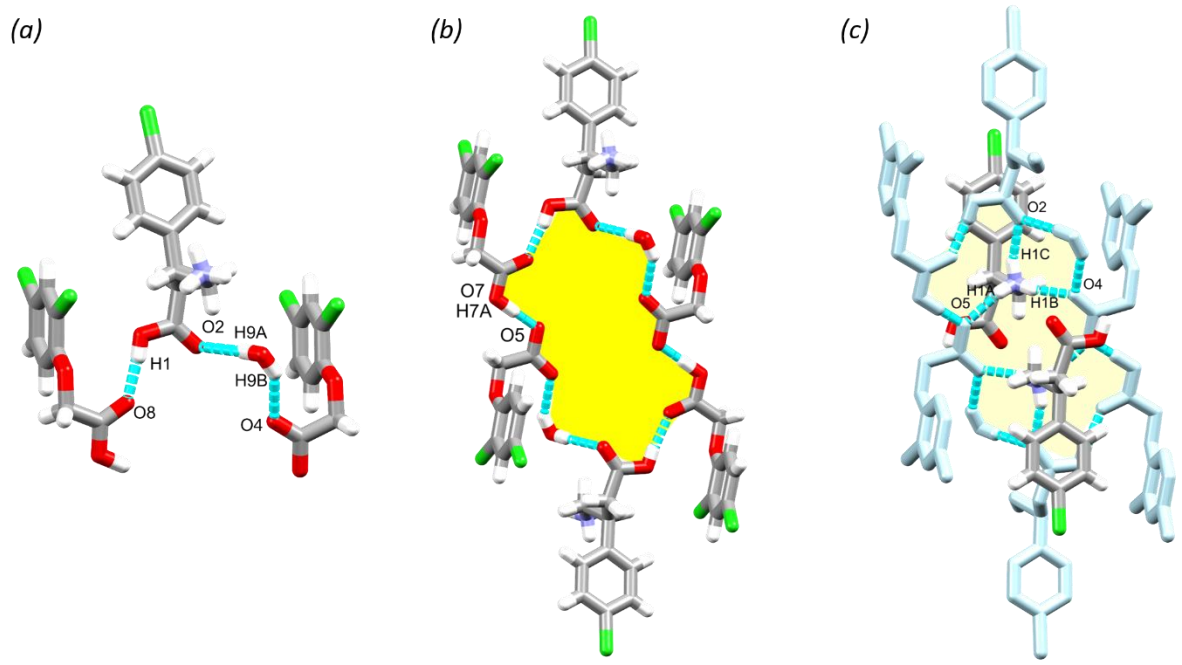

Figure 3. 11 ASU (a), supramolecular unit (b) and packing interactions that result in the layered structure (c) in [BAC$^+$][2,4ClPOA$^-$]·w

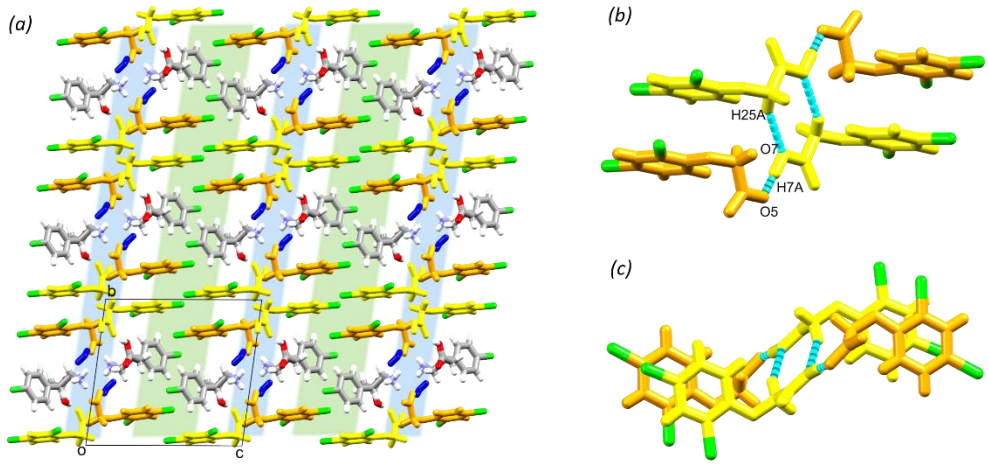

Figure 3. 12 Hydrophilic (blue) and aromatic layers (green) in [BAC$^+$][2,4ClPOA$^-$]·w (2,4ClPOA$^-$ orange, 2,4ClPOA yellow, water molecules are blue) (a) and the interactions between the acids (side view-b, top view-c)

3.4 Multicomponent crystal formation of baclofen with bases: 2BAC(4PIC)·w and 2BAC(3,4LUT)·w

Previously, on many occasions, Baclofen was successfully cocrystallised with acids thereby concluding that BAC is a good proton acceptor (base), however this raises the question of whether BAC can behave as an acid when cocrystallised with a basic coformer. In this section, the crystal structures formed from BAC and two basic N-heterocyclic coformers,

3,4-lutidine (3,4LUT) and 4-picoline (4PIC) are discussed. The two crystal structures are very similar, thus they will be discussed in parallel manner.

The ASU for the crystal obtained with 4PIC have two BAC, one 4PIC and one water molecule (2BAC(4PIC)·w) and was solved and refined in $P\bar{1}$ (No.2) space group (Fig. 3.13a). The ASU of 2BAC(3,4LUT)·w has the same stoichiometry and the same space group symmetry (Fig. 3.13b). In both MCCs, both BAC molecules are in zwitter ionic form and no protonation of the base was noted. The crystals can be classified as cocrystal solvates[2] (hydrates). Their crystal data and hydrogen bonds are listed in Table 3.7 and 3.8. To avoid repetitiveness, the discussion of the structures will focus on 2BAC(4PIC)·w but differences between the two crystal structures will be noted if necessary.

There is a notable difference between the conformations of the two BAC molecules in the ASU of 2BAC(4PIC)·w. The amino acid backbone is linear in Mol A but bent in Mol B (Fig. 3.13a). The two BAC molecules hydrogen bond in a head-to-tail manner (N1A-H1B···O1B, 2.728(3) Å, 178°) and the 4PIC molecule cleave between them through N1A-H1C···N11 (2.906(1) Å, 162°) and C16-H16···O2B (3.427(7) Å, 157°) hydrogen bonds. The water molecule is encaptured by BAC (Mol B) accepting C8B-H8D···O18 (3.443(4) Å, 160°) and N1B-H1D···O18 (2.824(2) Å, 155°) hydrogen bonds. The ASUs of 2BAC(4PIC)·w and 2BAC(3,4LUT)·w are isostructural (RMS= 0.0576 Å) (Fig. 3.13c) but there are minor differences noted in the position of the base (Fig. 3.13d). The main hydrogen bonds are from two supramolecular synthons that can be described by $R_2^2(12)$ and $R_6^4(24)$ graph sets (Fig. 3.14, blue and green, respectively). The water molecules are bridging between the parallel BAC chains.

The crystal packing is layered, similar to the previously discussed structures, having alternating hydrophilic and aromatic layers (Fig. 3.15a, blue and green, respectively). There are Cl···Cl interactions in the aromatic layer that are formed between two symmetrically independent BAC molecules, Mol A and Mol B (Cl1A···Cl1B, 3.42 Å, 163°, Fig. 3.15b). This interaction was observed in 2BAC(3,4LUT)·w too with slightly different descriptors (Cl1A···Cl1B, 3.46 Å, 141°).

It is interesting to note that although the ASUs of 2BAC(4PIC)·w and 2BAC(3,4LUT)·w are very similar, the subtle difference between the position of the bases lead to a more

pronounced difference between the crystal structures. The superimposition of the two structures reveals that there is a subtle shift between the adjacent aromatic layers in 2BAC(3,4LUT)·w compared to 2BAC(4PIC)·w (Fig. 3.16).

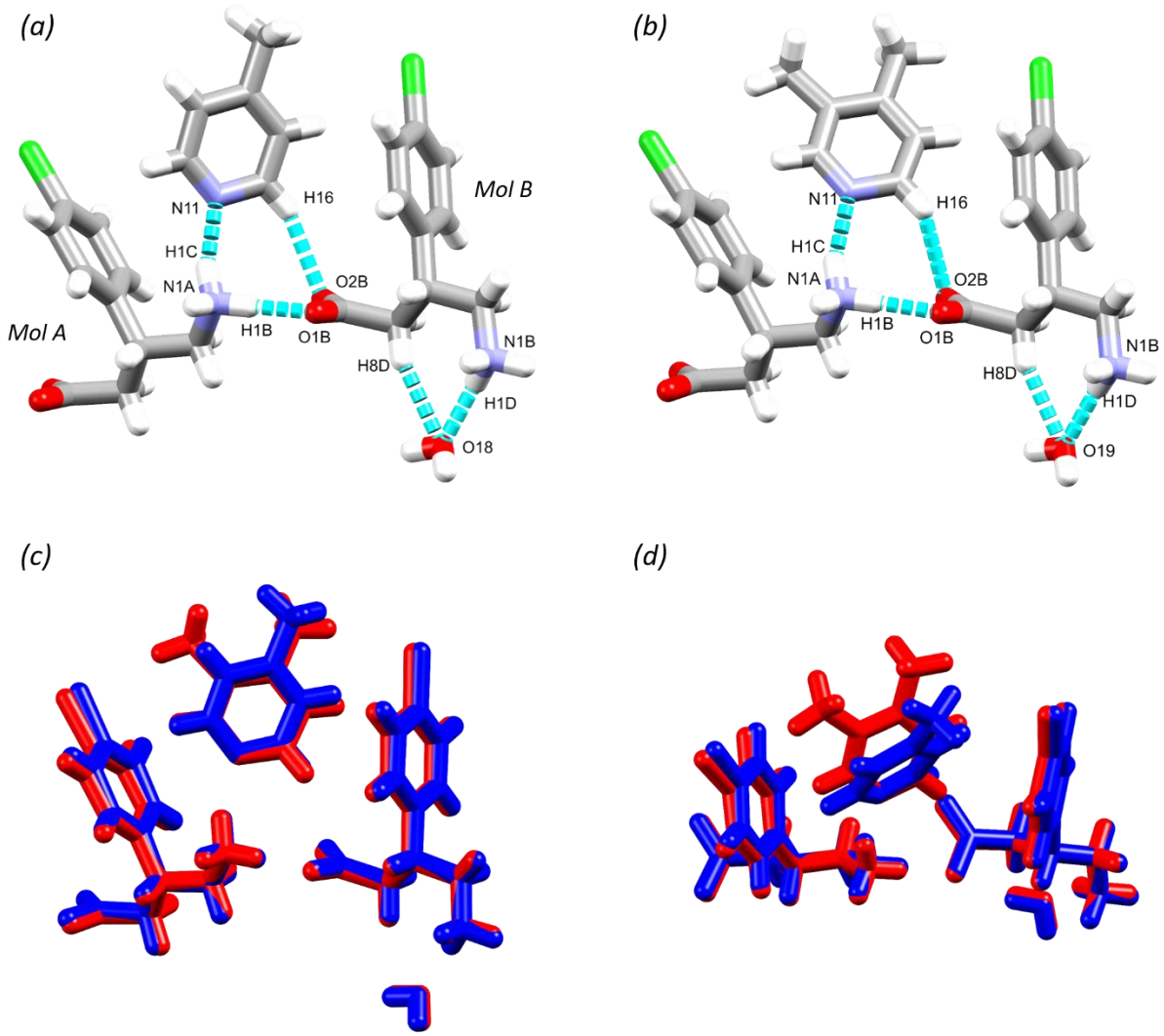

Figure 3. 13 ASUs of 2BAC(4PIC)·w (a) and 2BAC(3,4LUT)·w (b) and their superpositioned (c and d)

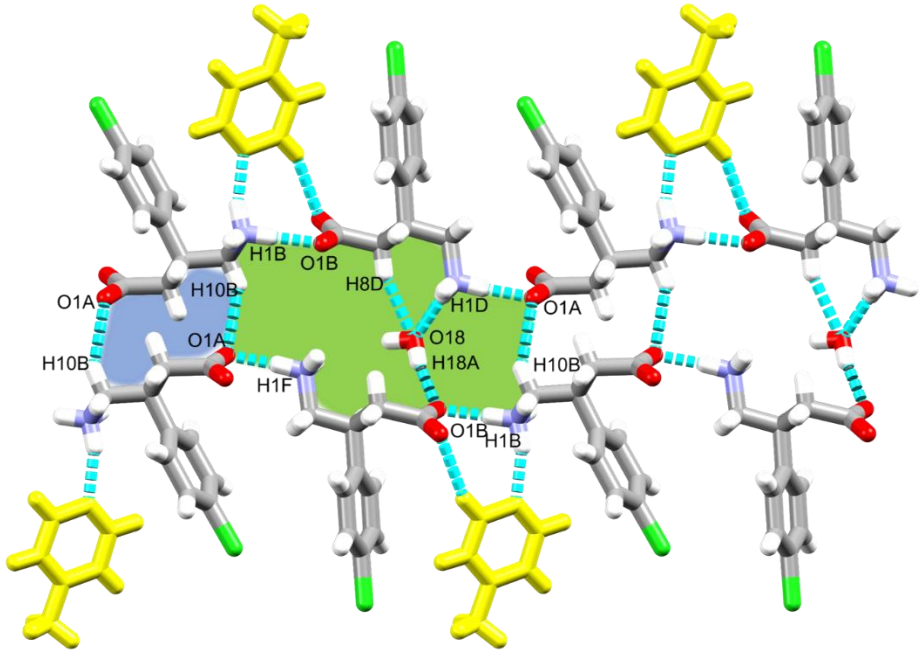

Figure 3. 14 Hydrogen bonds and synthons in 2BAC(4PIC)·w that can be described with the $R_2^2(12)$ and $R_6^4(24)$ graph sets (blue and green, respectively).

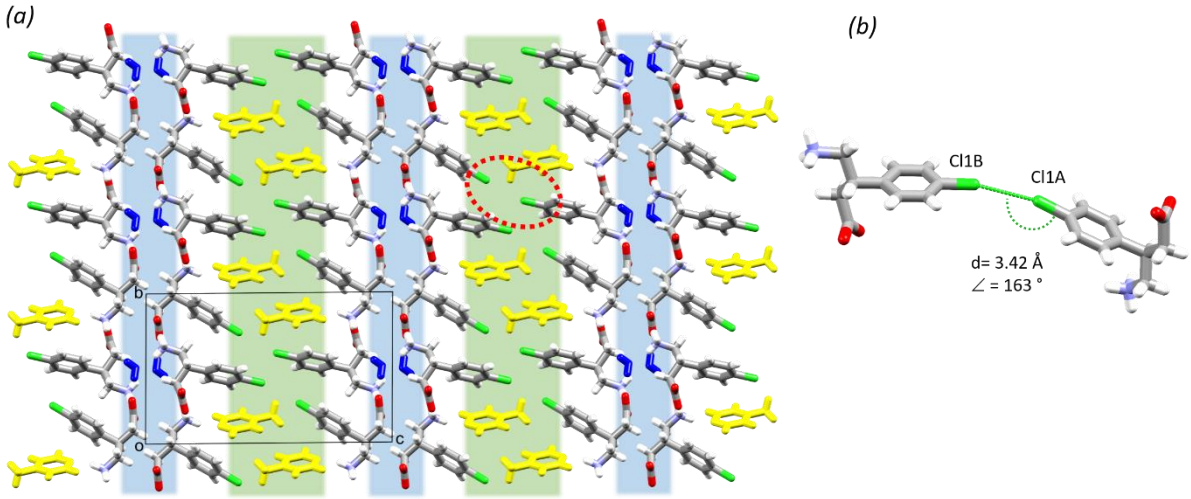

Figure 3. 15 Hydrophilic (blue) and aromatic layers (green) in 2BAC(4PIC)·w (water molecules are blue, 4PICs are yellow) (a) and the observed Cl···Cl interaction in the aromatic layers (b).

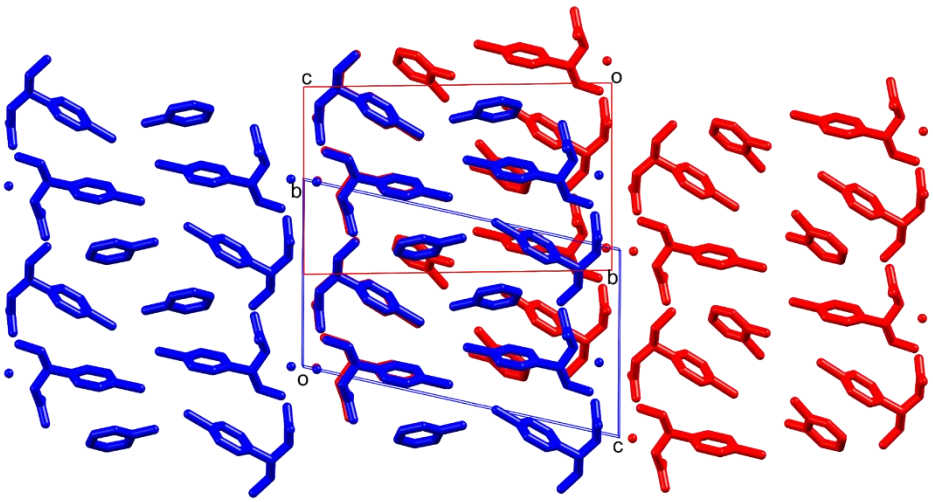

Figure 3. 16 Superimposed crystal structures of 2BAC(4PIC)·w (blue) and 2BAC(3,4LUT)·w (red) highlighting the shift between their adjacent aromatic layers.

Table 3.7 Crystallographic data of 2BAC(4PIC)·w and 2BAC(3,4LUT)·w

Compounds	2BAC(4PIC)·w	2BAC(3,4LUT)·w
Molecular formula	$C_{26}H_{33}Cl_2N_3O_5$	$C_{27}H_{35}Cl_2N_3O_5$
Formula weight ($g.mol^{-1}$)	538.45	552.48
Crystal system	triclinic	triclinic
Space group(No.)	$P\bar{1}(2)$	$P\bar{1}(2)$
a (Å)	5.9277(12)	5.9469(12)
b(Å)	12.150(2)	12.127(2)
c(Å)	19.491(4)	20.466(4)
α(°)	88.49	101.74
β(°)	86.58	92.00
γ(°)	77.10	101.56
V(A^3)	1365.8(5)	1411.3(5)
Z	2	2
ρ_{calc}($g.cm^{-3}$)	1.309	1.300
μ(MoKα) (mm^{-1})	0.278	0.271
F(000)	568	584
Crystal size(mm)	0.050x0.250x0.440	0.040x0.120x0.280
Temperature (K)	173(2)	173(2)
Radiation (Å)	MoKα,0.71073	MoKα,0.71073
Theta min-max (°)	1.720; 28.373	1.830; 27.914
Dataset (±h; ±k; ±l)	-7:7; -16:16; -25:26	-7:7; -15:15; -26:26
Final R indices [I>2σ(I)]	0.0431; 0.0946	0.0390; 0.0887
R indices [all data]	0.0674;0.1060	0.0582; 0.0981
Tot., uniq. data, R (int)	27666; 4855; 0.0479	31056,5143,0.0343
N_{ref}, N_{par}	6768,358	6727;368
S	1.025	1.033
Max. and av.shift/error	0.001/0.000	0.001/0.000
Min. and max. resd. Dens.($Å^3$)	-0.374; 0.285	-0.279; 0.289

Table 3.8 Hydrogen bonding of 2BAC(4PIC)·w and 2BAC(3,4LUT)·w

MCC	D-H···A	d(D-H) (Å)	d(H···A) (Å)	d(D···A) (Å)	D-H···A (°)	Symmetry operators
2BAC(4PIC)·w	N1B-H1F···O1A	0.97	1.76	2.724(5)	173	
	N1A-H1A···O2B	0.97	1.80	2.764(4)	175	[x, 1+y, z]
	N1A-H1B···O1B	0.95	1.78	2.728(3)	178	[1+x, 1+y, z]
	O18-H18B···O2A	0.87	1.88	2.753(8)	175	
	N1B-H1D···O18	0.90	1.98	2.824(2)	155	[1-x, 1-y, -z]
	O18-H18A···O1B	0.85	1.91	2.754(7)	170	[1+x, y, z]
	N1B-H1E···O2A	0.93	1.85	2.772(5)	175	[-1+x, y, z]
	N1A-H1C···N11	0.95	1.98	2.906(1)	162	[x, 1+y, z]
	C6B-H6B···O1B	0.95	2.53	3.468(7)	171	[1+x, y, z]
2BAC(3,4LUT)·w						
	N1B-H1E···O2A	0.93	1.85	2.772(2)	176	[1+x, y, z]
	N1A-H1B···O1B	0.91	1.82	2.728(3)	178	[-1+x, 1+y, z]
	N1B-H1D···O19	0.90	1.97	2.816(5)	156	[1-x, -y, -z]
	N1A-H1A···O2B	0.93	1.84	2.765(9)	176	[x, 1+y, z]
	N1A-H1C···N11	0.95	2.00	2.919(5)	161	[-1+x, y, z]
	O19-H19B···O2A	0.85	1.90	2.742(2)	176	
	O19-H19A···O1B	0.86	1.89	2.744(8)	169	[-1+x, y, z]
	C6B-H6B···O1B	0.95	2.51	3.437(3)	167	[-1+x, y, z]
	N1B-H1F···O1A	0.92	1.79	2.709(7)	176	

3.5 Comparative conformation analysis of the BAC moieties in the MCCs

The conformational variety of BAC was noted during the discussion of the MCC structures and a comparative analysis was carried out. BAC has four rotatable bonds and its conformational flexibility can be described by the following four torsion angles: τ1 indicates the rotation of the –COOH/–COO^- moiety, τ2 describes the rotation of the –CH_2–COOH/–CH_2–COO^- moiety, τ3 used to measure the movement of the –CH_2–NH_2/–CH_2–NH_3^+ group and the ring rotation relative to the amino acid functionality is defined by τ4 (Fig. 3.17a).

To understand which conformers of BAC are the most probable to form in the solid state, the CSD-Discovery - computer aided drug design software was used[3]. The knowledge-based conformer generation resulted in 24 lowest energy conformers (Fig. 3.17b) and their superimposition revealed that (1) the amine/amino moieties prefer two positions; (2) the carboxylic/carboxylate moieties cluster around three positions and (3) the aromatic ring can take up almost any position. Therefore not taking into account the aromatic ring rotation and focusing only on the amino-acid backbone, a careful analysis of the 23 conformers

revealed that there are 6 main conformers. These conformers can be labelled based on the shape of the backbone as linear, C-bend, N-bend, C,N-bend, C-tilt and C-tilt-N-bend (where C refers to –COOH/–COO^- moiety and N refers to –NH_2/–NH_3^+ group, Fig. 3.18). Out of the 23 lowest energy conformers, the linear and the C-bend occurred the most often (5 times each).

The identified torsion angles of the BAC moieties in the current MCCs were measured and summarized in Table 3.9. All structures crystallized in centrosymmetric space groups and the torsion angles were measured on the R enantiomers. In the case of deprotonated carboxylic acid groups, the carboxylate oxygen atoms are indistinguishable; therefore for the measurement of τ1, the smaller torsion angle was recorded. The 7 described MCCs contain 9 molecules of BAC in their ASU and they show conformational variety: 4 of them can be classified as C-bend conformer, 2 of the BAC moieties are N-bend, another 2 are linear, and 1 can be categorised as C,N-bend conformer.

This conformational variety reflects the observed conformations in the already known 13 BAC crystals (containing 16 BAC moieties) found in the CSD (Table 3.10): 7 of them can be classified as C-bend conformer, 8 of the BAC moieties are linear and finally 4 are N-bend. It is interesting to note that there is no C-bend conformer in the published crystal structures, therefore the crystal [BAC^+][2,4ClPOA$^-$] represents a new conformer of BAC found in the solid state.

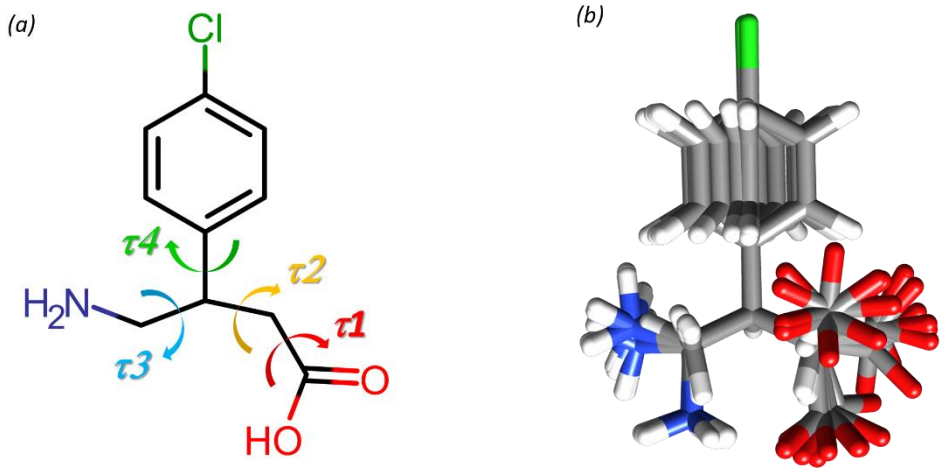

Figure 3.17 Graphical explanation of the torsion angles used to describe the four rotatable bonds of baclofen (a) and the superimposed baclofen molecules (23) of the generated lowest energy conformers (b).

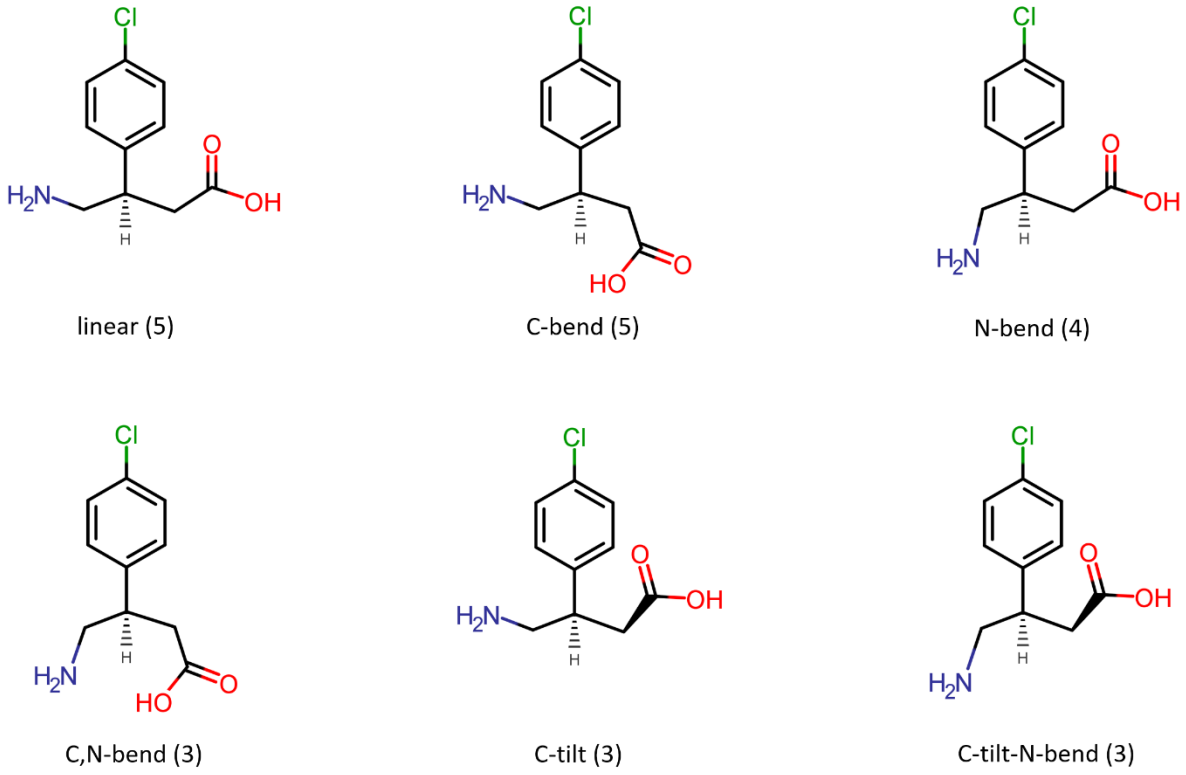

Figure 3.18 Main conformers and their occurrence out of the 23 generated lowest energy conformers

Table 3.9 Torsion angles of baclofen moieties reported in this study

MCC	τ1 (O*-C9-C8-C7)	τ2 (C9-C8-C7-C1)	τ3 (C1-C7-C10-N1)	τ4 (C2-C1-C7-C10)	Conformation
[BAC$^+$][OXA$^-$]·w	12.58	-157.43	-58.67	-118.15	*C-bend*
BAC·SAL·w	53.16	-173.75	63.62	-106.80	*C-bend*
[BAC$^+$][POA$^-$]	54.18	-172.91	62.18	-144.03	*C-bend*
[BAC$^+$][2,4ClPOA$^-$]	-22.29	-158.36	171.14	-123.72	*C,N-bend*
[BAC$^+$][2,4ClPOA$^-$]·w	62.49	-161.95	64.47	-120.48	*C-bend*
2BAC(4PIC)·w (Molecule A)	-55.54	-49.75	54.51	-114.02	*linear*
(Molecule B)	-55.72	-60.56	175.03	-114.18	*N-bend*
2BAC(3,4LUT)·w (Molecule A)	-55.52	-49.80	57.50	-110.98	*linear*
(Molecule B)	-52.74	-60.68	176.22	116.01	*N-bend*

Table 3.10 Torsion angles of baclofen moieties in the crystal structures in the CSD

CSD Refcode		τ1	τ2	τ3	τ4	Conformation
AQEKUE		41.20	-174.18	62.78	-112.49	*C-bend*
CRBMZC10*		16.57	-84.10	168.06	-110.99	*N-bend*
LUSXAA	**(Molecule A)** #	-16.61	-167.94	56.99	72.07	*C-bend*
	(Molecule B) #	-5.17	-163.96	56.57	73.76	*C-bend*
LUSXEE #		39.08	-166.84	60.60	36.67	*C-bend*
LUSXII #		-10.55	-68.50	64.31	57.29	*linear*
LUSXII01 #		-10.77	-69.00	64.53	58.80	*linear*
LUSXOO		58.51	-165.19	67.10	-127.38	*C-bend*
LUSXUU		19.92	-82.67	175.14	-86.52	*N-bend*
LUSYAB		-31.15	-63.55	74.82	-113.73	*linear*
RUWGOG	**(Molecule A)** #	-5.62	-72.30	167.97	43.07	*N-bend*
	(Molecule B) #	-34.00	-51.77	175.98	69.89	*N-bend*
WONSIE		-10.95	-68.63	64.16	-121.39	*linear*
WONSIE01		-10.90	-68.82	64.38	-121.27	*linear*
YIPLAN	**(Molecule A)**	57.98	-179.18	57.10	-129.10	*C-bend*
	(Molecule B)	53.67	-166.67	58.66	-124.66	*C-bend*

* An early work by Chang et al[4] presented S and R-baclofen hydrochloride without 3D coordinates (CSD refcodes CRBMZB and CRBMZC), and later, the same group published the 3D coordinates of the R enantiomer (CRBMZC10)[5]
#Angles were measured on the S enantiomer and converted for comparison.

3.6 Comparative crystal packing analysis of the MCCs

The packing arrangement of all the MCCs, with the exception of the oxalate salt, resembles the packing observed in pure hydrophobic α-amino acids[6], namely the hydrogen bonded layers formed by the polar functional groups of the BAC and the coformers alternating with the hydrophobic aromatic layers. Contrarily, the polar layers formed from the BAC moieties show great variety (Table 3.11).

The BAC moieties form centrosymmetric dimers in two crystals, $[BAC^+][OXA^-]\cdot w$ and $[BAC^+][POA^-]$ but in a different manner. In the $[BAC^+][OXA^-]\cdot w$ MCC the BAC moieties interact via forming the well-known carboxylic acid dimers (depicted as Ia) but in $[BAC^+][POA^-]$ the BAC molecules interact via –CH···carbonyl interactions (Ib). The BAC moieties hydrogen bonded to one another in a 'head-to-tail' manner and the coformer (CF) cleaves itself between the two neighbouring BAC molecules (II). This motif, head to tail chain, is noted in the crystals of 2BAC(4PIC)·w and 2BAC(3,4LUT)·w. A very similar motif is noted in $[BAC^+][2,4ClPOA^-]$ with the lack of interactions between the adjacent BAC moieties (III). In BAC·SAL·w and $[BAC^+][2,4ClPOA^-]\cdot w$ crystals, the head-to-tail arrangement of the neighbouring BAC molecules is based on hydrogen bonds and the coformers bridging

between the BAC molecules via forming direct hydrogen bonds and via bridging water molecules (IV).

In summary, BAC is a good candidate to form MCCs with the selected coformers, but the predictability of the nature of interactions between the BAC moieties or between the BAC and CF molecules are poor and this makes BAC a challenging target when crystal engineering techniques are used.

Table 3.11 Simplified interactions of the MCCs

MCCs	Motif	Symbol
[BAC$^+$][OXA$^-$]·w		**Ia**
[BAC$^+$][POA$^-$]	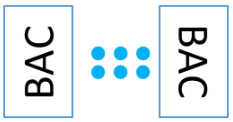	**Ib**
2BAC(4PIC)·w **2BAC(3,4LUT)·w**	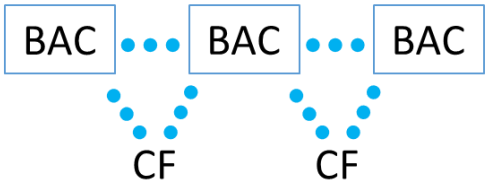	**II**
[BAC$^+$][2,4ClPOA$^-$]	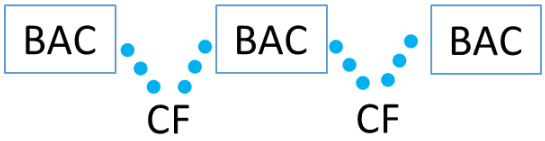	**III**
BAC·SAL·w **[BAC$^+$][2,4ClPOA$^-$]·w**	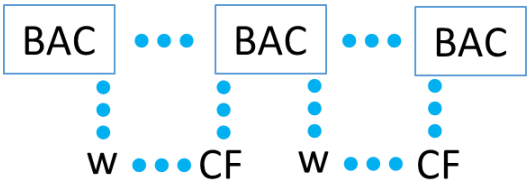	**IV**

3.7 References

1. Báthori, N. B. and Kilinkissa, O. E. Y. Are gamma amino acids promising tools of crystal engineering? - Multicomponent crystals of baclofen. *CrystEngComm* **17**, 8264–8272 (2015).

2. Grothe, E., Meekes, H., Vlieg, E., Ter Horst, J. H. and De Gelder, R. Solvates, Salts, and Cocrystals: A Proposal for a Feasible Classification System. *Cryst. Growth Des.* **16**, 3237–3243 (2016).

3. Cole, J. C., Korb, O., McCabe, P., Read, M. G. and Taylor, R. Knowledge-Based Conformer Generation Using the Cambridge Structural Database. *J. Chem. Inf. Model.* **58**, 615–629 (2018).

4. Chang, C. H. Yang, D.S.C., Yoo, C.S., Wang, B.C., Pletcher, J. and Sax, M. The crystal structures of (S) and (R) baclofen and carbamazepine . *Acta Crystallogr. Sect. A Found. Crystallogr.* **37**, C71–C71 (1981).

5. Chang, C. H., Yang, D. S. C., Yoo, C. S., Wang, B. C., Pletcher, J., Sax, M. and Terence, C. F. Structure and absolute configuration of (R)-baclofen monohydrochloride . *Acta Crystallogr. Sect. B Struct. Crystallogr. Cryst. Chem.* **38**, 2065–2067 (1982).

6. Görbitz, C. H., Vestli, K. and Orlando, R. A solution to the observed Z' = 2 preference in the crystal structures of hydrophobic amino acids. *Acta Crystallogr. Sect. B Struct. Sci.* **65**, 393–400 (2009).

Chapter 4

Bulk analysis of the multicomponent crystals of baclofen

The analysis of the bulk material of the MCCs will be discussed in this chapter with the focus on the thermoanalytical results (DSC and TGA), powder XRD and FTIR analysis. Original data are shown on individual figures and included in the Appendix.

4.1. Thermal analysis of the MCCs

Thermogravimetric analysis (TGA) and differential scanning calorimetry (DSC) were used to monitor the thermal behaviour of BAC MCCs. The TGA was useful in determining the presence of an included solvent and the DSC was applied to accurately determine the melting temperatures and enthalpies of the BAC crystals. The results for the bulk materials obtained via the solvent evaporation crystallisation (SEC) are summarised in Table 4.1, while the results for compounds synthesised by liquid assisted grinding (LAG) are shown in Table 4.2. The TGA and DSC curves for the multicomponent crystals are presented in the Appendix.

Table 4.1 Thermal data of MCCs (bulk) obtained by SEC

Compound	**TGA Decomposition**			**DSC Melting point**		
SEC (bulk)	Measured %	Theoretical %	Host: Guest ratio	Onset °C	Peak °C	ΔH J/mol
BAC	n/a	n/a	n/a	207.91	210.41	306.68
OXA	n/a	n/a	n/a	192.19	192.23	368.64
SAL	n/a	n/a	n/a	158.53	159.48	35.83
POA	n/a	n/a	n/a	98.75	99.85	939.75
2,4ClPOA	n/a	n/a	n/a	136.76	139.10	138.55
[BAC$^+$][OXA$^-$]·w	1. 5 2. 28	1. 6 2. 28	1. ~1:1 2. 1:1	158.37	164.49	15827.17
BAC·SAL·w	1. 98	1. 5 2. 38	n/a	142.36	142.86	9276.18
[BAC$^+$][POA$^-$]	1. 98	1. 42 2. 58	n/a	160.51	162.85	89887.60
[BAC$^+$][2,4ClPOA$^-$]	1. 83	1. 51 2. 49	n/a	156.36	157.16	106732.14
[BAC$^+$][2,4ClPOA$^-$]·w	1. 97	1. 3 2. 66	n/a	137.93	145.73	73949.81
2BAC(4PIC)·w	1. 20 2. 14	1. 21 2. 29	1. ~1:1	114.52	128.53	5177.65
2BAC(3,4LUT)·w	1. 22	1. 23	1. ~1:1	122.72	125.91	3714.70

The [BAC$^+$][OXA$^-$]·w has a three step decomposition. The first step (5 %) is due to dehydration, the second step is related to the loss of one oxalic acid (28 %) and the last step is the final decomposition of the crystal (Fig. A6). The material obtained via LAG shows similar behaviour (Fig. A7). Congruent melting occurs in BAC·SAL·w, [BAC$^+$][POA$^-$],

[BAC^+][2,4ClPOA$^-$] and [BAC^+][2,4ClPOA$^-$]·w where the decomposition of the MCC happens in one step[1] (Figures A11, A16, A19, A20, A23 and A24, respectively). It is interesting to note that the T_{onset} of [BAC^+][2,4ClPOA$^-$] and [BAC^+][2,4ClPOA$^-$]·w are very similar for the material obtained from the LAG. The reason could be that not enough solvent was used to make the paste or the solids were not ground sufficiently in the LAG experiment. The melting points for [BAC^+][OXA^-]·w and BAC·SAL·w obtained via LAG are lower than the melting point of the bulk crystals from SEC and this can be credited to impurities. LAG experiments often do not mean 100 % conversion of the starting materials to the final products and thus contamination by the starting materials lower the melting point of the product.

The crystals of 2BAC(4PIC)·w and 2BAC(3,4LUT)·w obtained via SEC show very similar thermal decomposition (Fig. A27 and A32, respectively). The first mass loss (20 % and 22 %) occurs due to the simultaneous release of one water and one 4PIC or 3,4LUT, and this is followed by the total decomposition. It is important to note that in the case of 4PIC and the 3,4LUT crystals, the LAG was unsuccessful. The TGA shows no sign of included solvent (Fig. A28 and A32) and this was supported by the PXRD and FTIR results, where the patterns of the LAG agreed with the pure BAC.

It is also interesting to note that the melting points of the [BAC^+][OXA^-]·w, [BAC^+][POA^-], [BAC^+][2,4ClPOA$^-$] and [BAC^+][2,4ClPOA$^-$]·w lie between the melting point of BAC and the respective solid coformer. However, for BAC·SAL·w the melting point of the MCC is less than starting materials. This could be as a result of weaker intermolecular interactions present in the MCC[2]. Generally, the T_{onset} for MCCs obtained by LAG is lower than the crystals obtained by SEC and this is an indication of impurities, which could be due to the presence of excess starting material. This is with the exception of [BAC^+][2,4ClPOA$^-$]·w which has a higher melting point for LAG, which is very close to the melting point of [BAC^+][2,4ClPOA$^-$] and indicates that they are very likely the same.

Table 4.2 Thermal data of MCCs obtained by LAG

Compound	TGA Decomposition			DSC Melting point		
LAG	Measured %	Theoretical %	Host: Guest ratio	Onset °C	Peak °C	ΔH J/mol
BAC	n/a	n/a	n/a	207.91	210.41	306.68
OXA	n/a	n/a	n/a	192.19	192.23	368.64
SAL	n/a	n/a	n/a	158.53	159.48	35.83
POA	n/a	n/a	n/a	98.75	99.85	939.75
2,4ClPOA	n/a	n/a	n/a	136.76	139.10	138.55
[BAC$^+$][OXA$^-$]·w	1. 6 2. 28	1. 6 2. 28	1. 1:1 2. 1:1	147.26	150.13	1727.29
BAC·SAL·w	1. 95	1. 5 2. 37	n/a	125.32	127.30	14628.89
[BAC$^+$][POA$^-$]	1. 95	1. 42 2. 58	n/a	159.92	162.35	76421.77
[BAC$^+$][2,4ClPOA$^-$]	1. 96	1. 51 2. 49	n/a	155.83	157.70	91812.99
[BAC$^+$][2,4ClPOA$^-$]·w	1. 97	1. 3 2. 66	n/a	155.28	156.64	58242.89
2BAC(4PIC)·w	1. 13 2. 85	1. 21 2. 79	n/a	115.31	116.37	2804.40
2BAC(3,4LUT)·w	1. 13 2. 84	1. 42 2. 58	n/a	207.10	210.86	150829.84

4.2 PXRD analysis of the MCCs

The PXRD analysis was used to confirm if the single crystal selected for analysis is a true representation of the bulk and whether the cocrystallisation was successful when repeated using LAG. This was true for only [BAC$^+$][OXA$^-$]·w and [BAC$^+$][POA$^-$], where the XRD patterns of the bulk material agree well with the generated pattern of the single crystal structure and also show good agreement with the XRD pattern of the LAG products (Fig. A8 and A17). It can be concluded that LAG can be used as an alternative method of cocrystallisation of BAC with OXA or POA.

The XRD pattern of the bulk material agrees with the generated pattern from the single crystal for compounds [BAC$^+$][2,4ClPOA$^-$], 2BAC(4PIC)·w and 2BAC(3,4LUT)·w (Figures A21, A29 and A33, respectively). Unfortunately, the patterns of the LAG products do not show similarity with the bulk and thus LAG is not suitable to prepare these compounds.

Based on the XRD analysis, the crystal selected for data collection and the bulk are significantly different for BAC·SAL·w and [BAC$^+$][2,4ClPOA$^-$]·w (Fig. A12 and A25, respectively). For BAC·SAL·w, the LAG product seems to be the same as the bulk material

and agrees well with the pattern of SAL, one of the starting materials. The same can be concluded for [BAC^+][2,4ClPOA$^-$]·w.

In summary, in case of hydrated crystals (BAC·SAL·w and [BAC^+][2,4ClPOA$^-$]·w) the analysis of bulk revealed that the crystals probably decomposed by the time of the analysis. In all the other cases the single crystal structure was a good representation of the bulk material. In some cases LAG was found to be a suitable method for cocrystallisation.

4.3 FTIR analysis of the MCCs

BAC is zwitterionic under the applied crystallisation conditions, thus has a COO^- and a NH_3^+ functional group. The expected bands for BAC are seen in Table 4.3 as well as the possible protonation stages of the molecule in Scheme 4.1. The coformer is expected to form hydrogen bonds with one of the two functional groups or neighbouring BAC molecules are expected to interact with each other via forming hydrogen bonds. Therefore the analysis focuses on the stretching frequencies of the C=O, C-O, O-H and N-H bonds. Infrared spectrometry was used to evaluate proton transfer[3] in the MCCs.

Table 4. 3 The peak regions of interest as expected from the IR

Functional groups of interest	Theoretical band regions, cm^{-1}
C=O	1710-1680(s)
N-H	3500-3200 (m,b)
O-H	3300-2400(s,b)
C-O	1250-1050(s)
COO^-	1550-1450

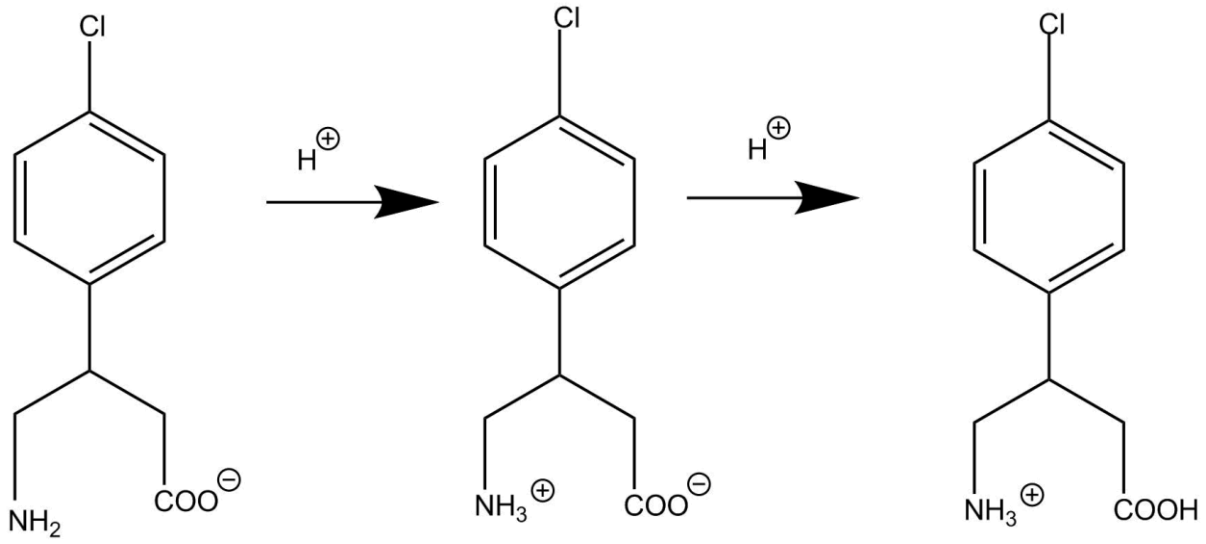

Scheme 4.1 The possible protonation stages of BAC

From the structures of $[BAC^+][OXA^-]\cdot w$, $[BAC^+][POA^-]$, $[BAC^+][2,4ClPOA^-]$ and $[BAC^+][2,4ClPOA^-]\cdot w$, it was observed that the BAC moiety has been protonated on the COO^- functional group. The C=O and O-H bands are present in the spectra and the shift of the bands can be seen as summarised in Table 4.4. The C=O and O-H bands are observed in the wavelength regions of 1710-1680 cm^{-1} and 3300-2400 cm^{-1}, respectively. Furthermore, BAC·SAL·w, 2BAC(4PIC)·w and 2BAC(3,4LUT)·w are in the zwitterionic form; this is seen by the presence of the NH_3^+ and COO^- bands in the 3500-3200 cm^{-1} and 1550-1450 cm^{-1} regions, respectively.

However, the IR spectra for $[BAC^+][2,4ClPOA^-]$ and $[BAC^+][2,4ClPOA^-]\cdot w$ for LAG do not show the expected broad O-H band. The spectra for the basic coformers once again give the same spectra as baclofen which further indicates the difficulty of cocrystallising BAC with basic coformers.

Table 4.4 IR bands observed for the MCCs formed

Functional group	C=O	N-H	O-H	C-O	COO
[BAC$^+$][OXA$^-$]·w SEC	1700	3528	3194	1208	
[BAC$^+$][OXA$^-$]·w LAG	1701	3665	3125	1216	
BAC·SAL·w SEC	-	3252	-	-	1454
BAC·SAL·w LAG	-	3274	-	-	1482
[BAC$^+$][POA$^-$] SEC	1700	3638	3125	1083	
[BAC$^+$][POA$^-$] LAG	1703	-	3049	1060	
[BAC$^+$][2,4ClPOA$^-$] SEC	1660	-	3046	1240	
[BAC$^+$][2,4ClPOA$^-$] LAG	1684	-	-	1173	
[BAC$^+$]2[2,4ClPOA$^-$]·w SEC	1708	-	3123	1160	
[BAC$^+$]2[2,4ClPOA$^-$]·w LAG	1735	-	-	1239	
2BAC(4PIC)·w SEC	-	3540			1471
2BAC(4PIC)·w LAG	-	-			1528
2BAC(3,4LUT)·w SEC	-	3472			1401
2BAC(3,4LUT)·w LAG	-	-			1396

4.4 References

1. Zhang, Y., Fan, D. & Zheng, Y. Comparative study on combined co-pyrolysis/gasification of walnut shell and bituminous coal by conventional and congruent-mass thermogravimetric analysis (TGA) methods. *Bioresour. Technol.* **199**, 382–385 (2016).

2. Batisai, E., Ayamine, A., Kilinkissa, O. E. Y. & Báthori, N. B. Melting point-solubility-structure correlations in multicomponent crystals containing fumaric or adipic acid. *CrystEngComm* **16**, 9992–9998 (2014).

3. Faix, O. Fourier Transform Infrared Spectroscopy. in *Methods in Lignin Chemistry* (eds. Lin, S. Y. & Dence, C. W.) 83–109 (Springer Berlin Heidelberg, 1992).

Chapter 5

Summary and conclusions

The solid state modification of pharmaceuticals via the application of crystal engineering principles is a sustainable way to form new solid forms of a selected active pharmaceutical ingredient (API) without altering its chemical structure. The ultimate aim of the cocrystallisation process is to improve physicochemical or solid state properties of the selected API.

Baclofen (BAC, (R/S)-4-amino-3-(4-chlorophenyl)butanoic acid), a γ amino acid, was the centre of interest of this work because of its recent application in treatment of early-onset alcoholism that is a significant problem in South Africa. Baclofen has low aqueous solubility and thus its efficacy is compromised. From previous research it is known that BAC can form multicomponent crystals (MCCs) with coformers (CFs) of different acid strength and molecular size. The aim of the project was to extend the landscape of the MCCs of BAC (1) by cocrystallising the API with carboxylic acids and also (2) evaluate whether BAC can act as an acid when crystallising with basic CFs.

Cocrystallisations with 37 acidic and 17 basic CFs were carried out by solvent evaporation crystallisation (SEC) and yielded only seven MCCs that contained BAC and the respective CFs, namely oxalic acid ($[BAC^+][OXA^-]\cdot w$), salicylic acid (BAC·SAL·w), phenoxyacetic acid ($[BAC^+][POA^-]$), 2,4-dichlorophenoxyacetic acid ($[BAC^+][2,4ClPOA^-]$ and $[BAC^+][2,4ClPOA^-]\cdot w$), 4-picoline (2BAC(4PIC)·w) and 3,4-lutidine (2BAC(3,4 LUT)·w).

The bulk materials were analysed by thermoanalytical methods (thermogravimetry and differential scanning calorimetry), powder X-ray analysis and Fourier transform infrared spectrometry. Liquid assisted grinding (LAG), as a green chemistry method, was also applied to form the MCCs and the products were analysed similarly to the bulk crystals. The overall conclusion of the bulk property analysis is that (1) the chemical composition of the bulk material agrees well with the single crystal for $[BAC^+][OXA^-]\cdot w$, $[BAC^+][POA^-]$, $[BAC^+][2,4ClPOA^-]$, 2BAC(4PIC)·w and 2BAC(3,4LUT)·w, but (2) discrepancies were noted between the bulk and the single crystal structure for BAC·SAL·w and $[BAC^+][2,4ClPOA^-]\cdot w$; and (3) only in two cases was found to be the LAG a suitable method for cocrystallisation ($[BAC^+][OXA^-]\cdot w$ and $[BAC^+][POA^-]$).

X-ray analysis of the single crystal structures revealed that (1) BAC exists in zwitterionic or cationic form in these crystals, (2) the MCCs represent a large variety of different crystal classes, such as salts, solvates, salt solvates, or cocrystal salt solvates with (3) differing stoichiometry. It was also noted that BAC appeared in many different conformations. The results obtained via knowledge-based conformer generation revealed the six lowest energy conformers of BAC that can be labelled based on the shape of the backbone as linear, C-bend, N-bend, C,N-bend, C-tilt and C-tilt-N-bend. The nine molecules of BAC in the seven MCCs show the following conformational variety: four of them can be classified as C-bend conformer ([BAC^+][OXA^-]·w, BAC·SAL·w, [BAC^+][POA^-] and [BAC^+][2,4ClPOA$^-$]·w), two of the BAC moieties are N-bend (Molecules B in 2BAC(4PIC)·w and 2BAC(3,4LUT)·w), another two are linear (Molecules A in 2BAC(4PIC)·w and 2BAC(3,4LUT)·w), and one can be categorised as C,N-bend conformer ([BAC^+][2,4ClPOA$^-$]). It is interesting to note that the C,N-bend conformer has not been observed in the known crystal structures until now and thus the [BAC^+][2,4ClPOA$^-$] represents a new conformer of BAC found in the solid state.

Comparative crystal packing analysis revealed that the packing arrangement of all the MCCs—with the exception of the oxalate salt—resembles the packing observed in pure hydrophobic α-amino acids, namely the hydrogen bonded layers formed by the polar functional groups of the BAC and the CFs alternating with the hydrophobic aromatic layers. Contrarily, the polar layers formed from the BAC moieties show great variety in their hydrogen bonding pattern.

In conclusion, BAC is a good candidate to form MCCs with acidic or basic CFs, but the predictability of the nature of interactions formed between the BAC moieties or between the BAC and CF molecules are poor and this makes BAC a challenging target when crystal engineering techniques are used.

We believe that the findings of this work are a significant contribution to the field of pharmaceutical research and supramolecular chemistry because the application of baclofen is on the rise for treating addictive disorders.

Appendices

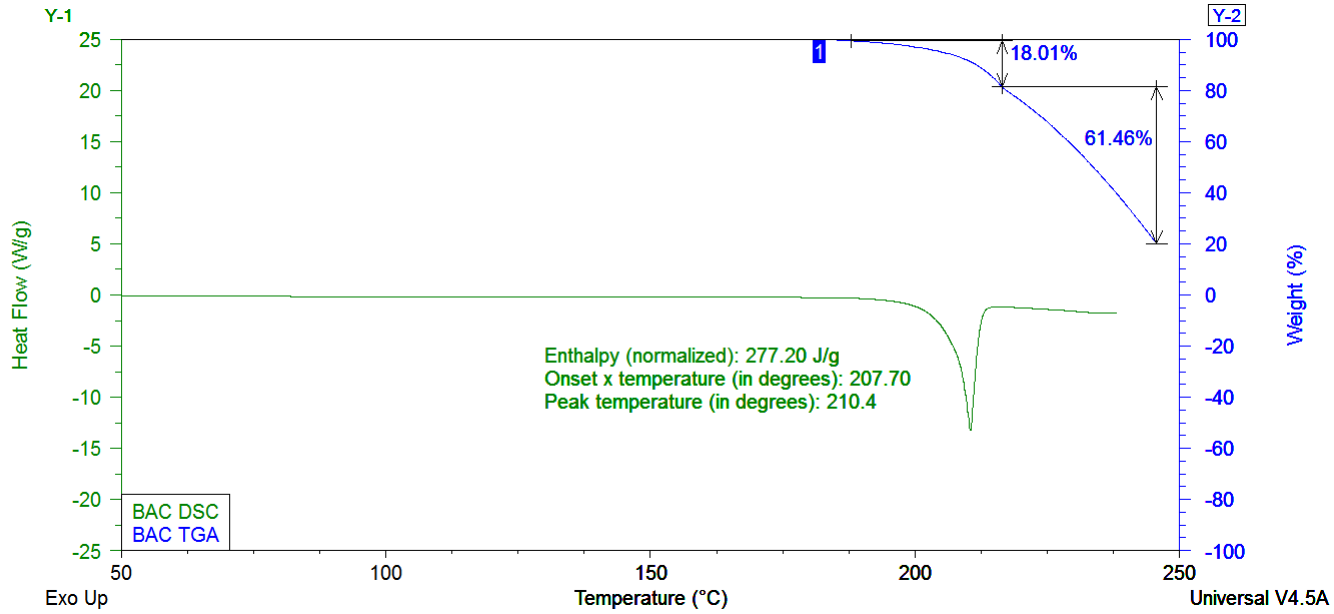

Figure A 1 Thermal analysis of BAC

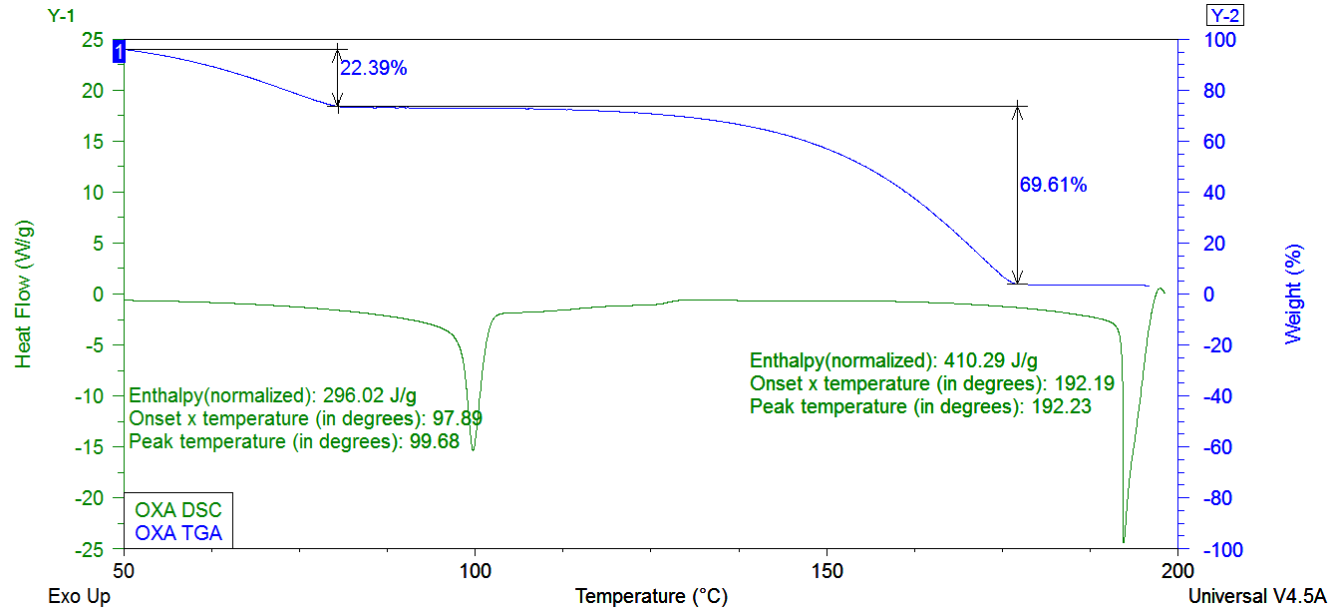

Figure A 2 Thermal analysis of OXA

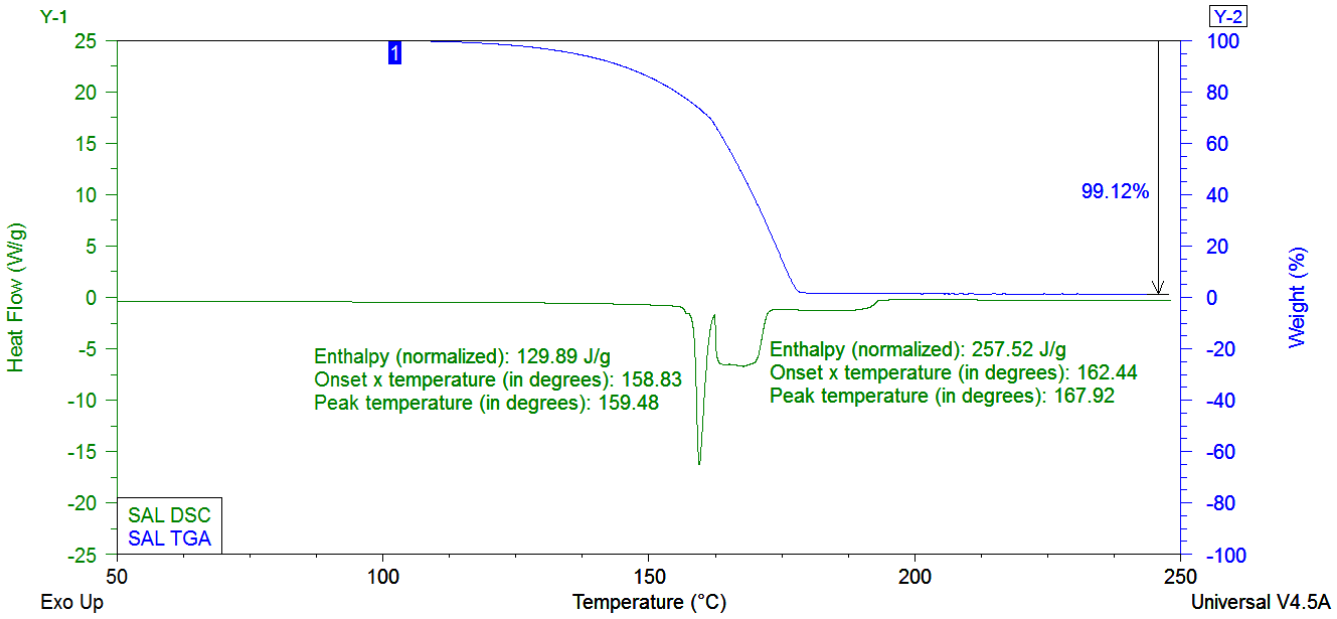

Figure A 3 Thermal analysis of SAL

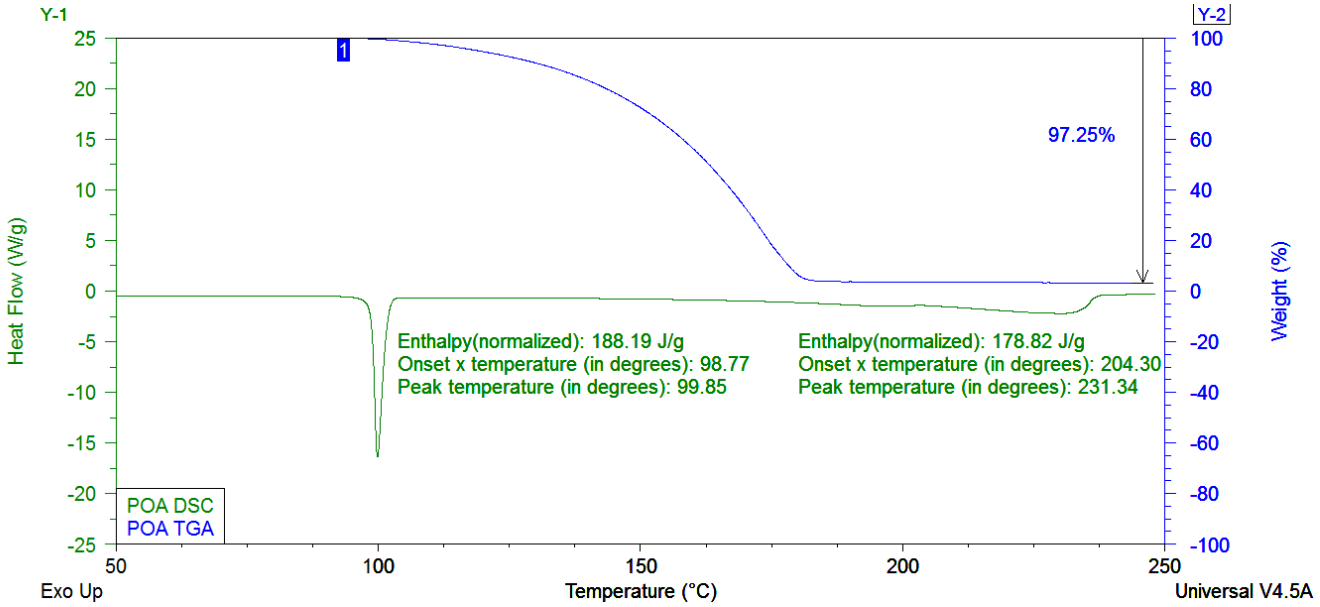

Figure A 4 Thermal analysis of POA

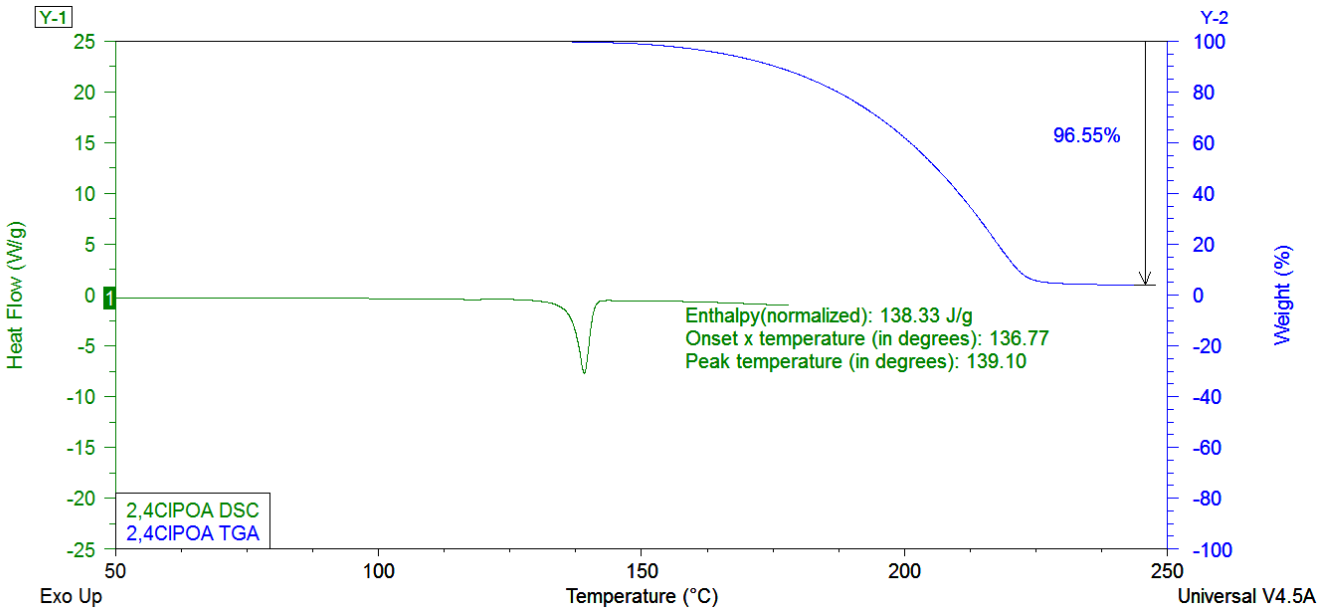

Figure A 5 Thermal analysis of 2,4ClPOA

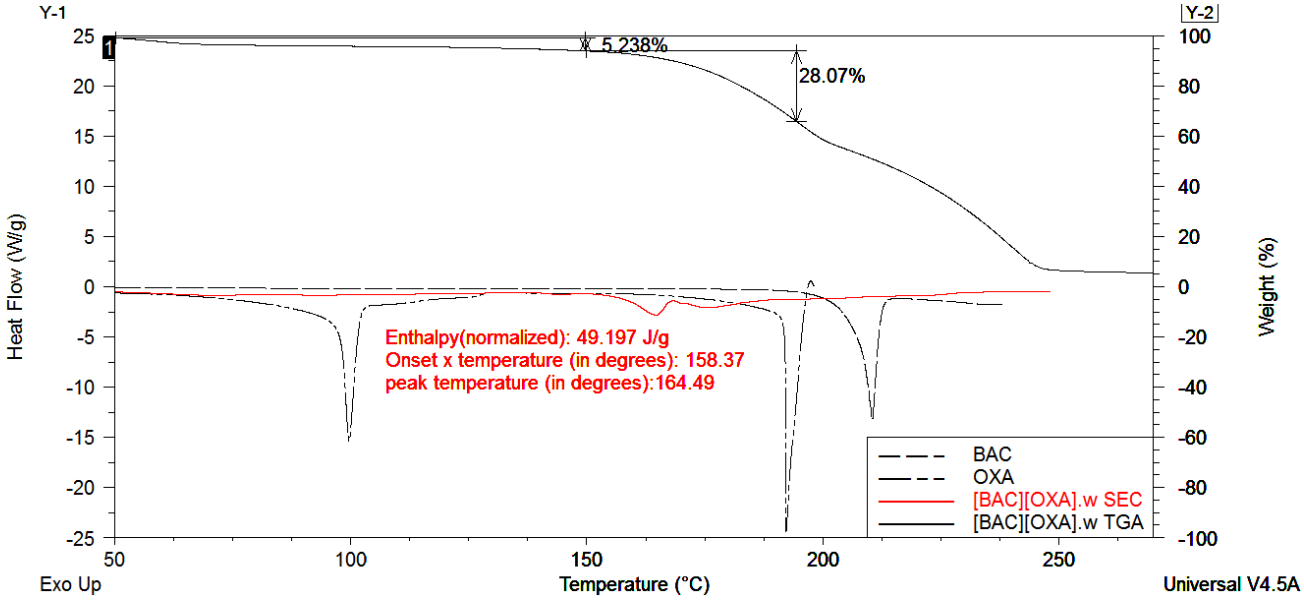

Figure A 6 Thermal analysis of [BAC$^+$][OXA$^-$]·w (bulk of SEC)

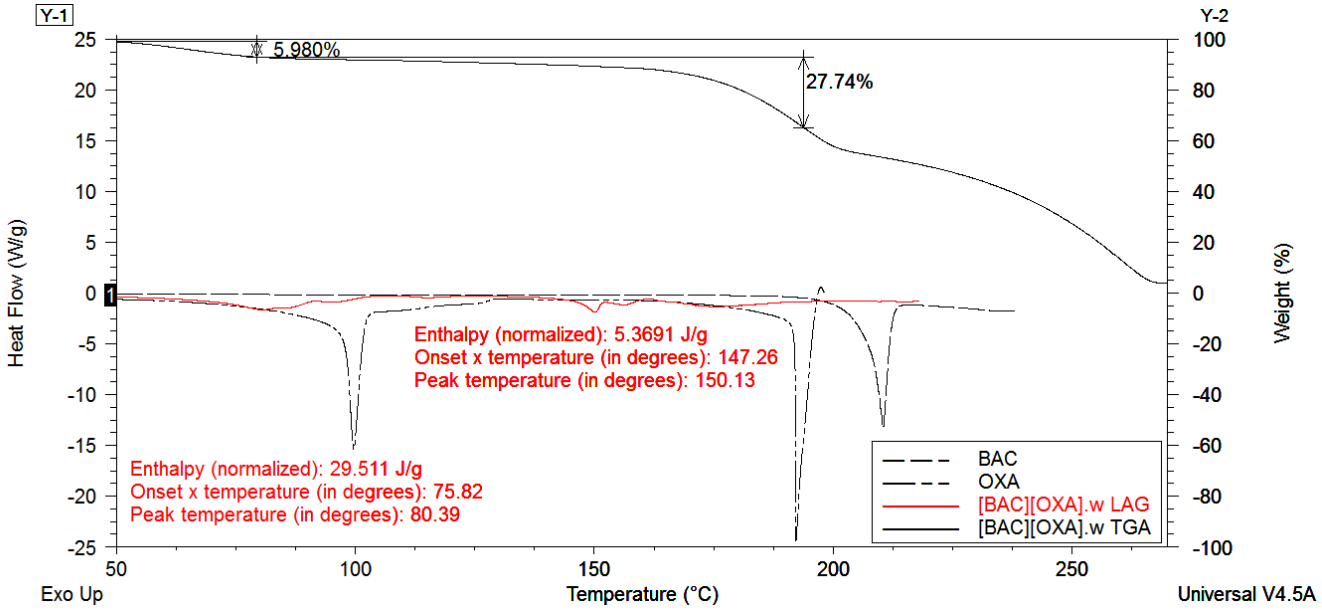

Figure A 7 Thermal analysis of [BAC⁺][OXA⁻]·w obtained by LAG

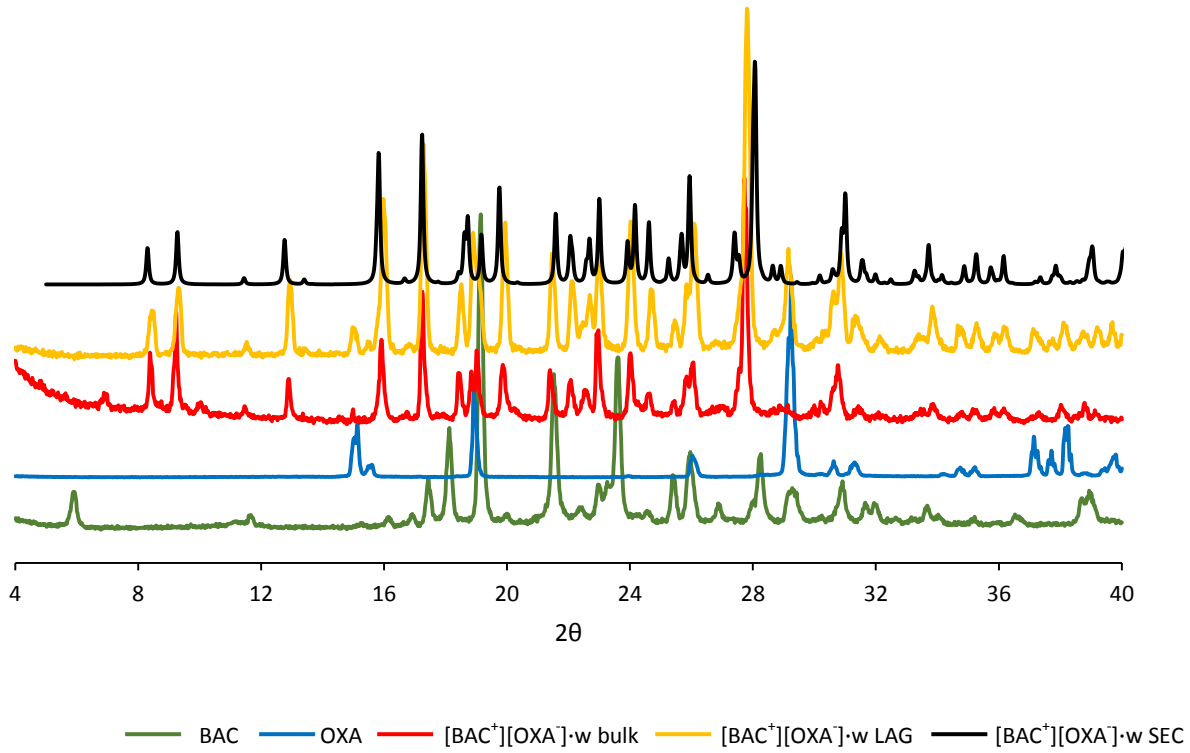

Figure A 8 PXRD analysis of [BAC⁺][OXA⁻]·w

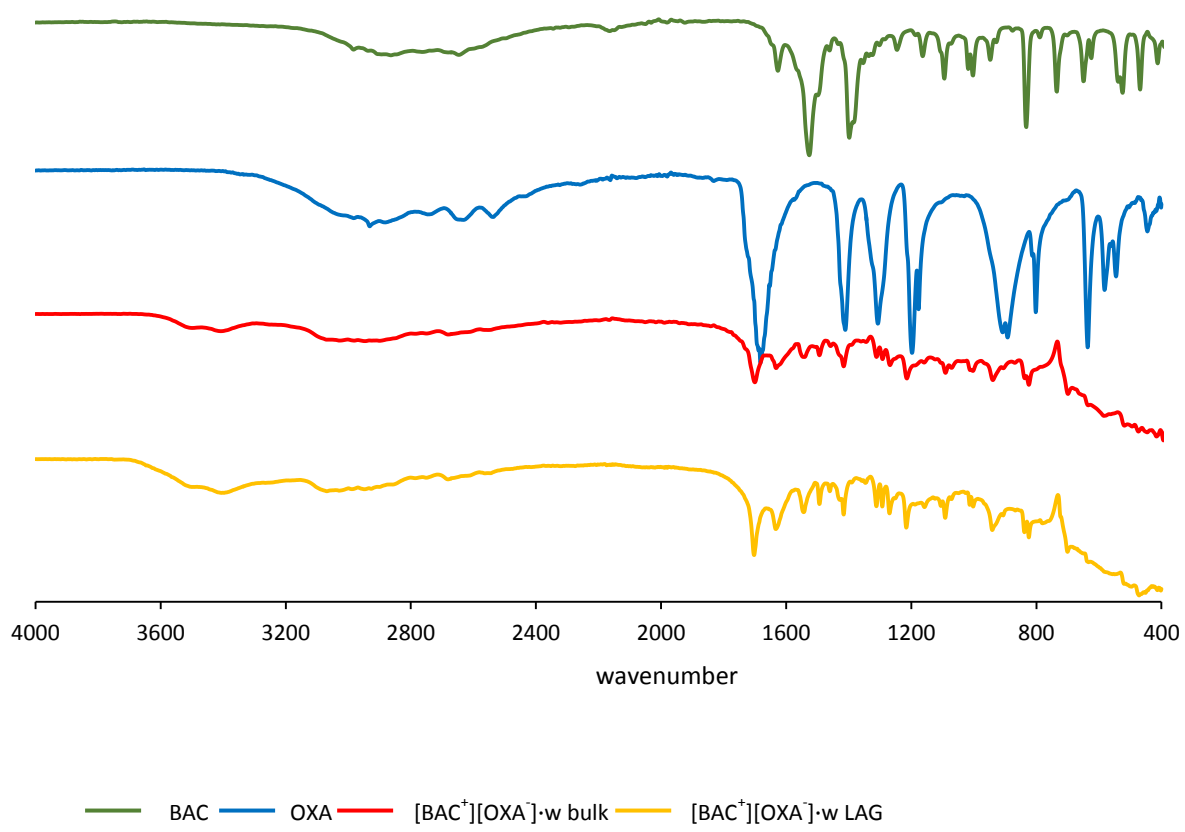

Figure A 9 IR analysis of [BAC⁺][OXA⁻]·w

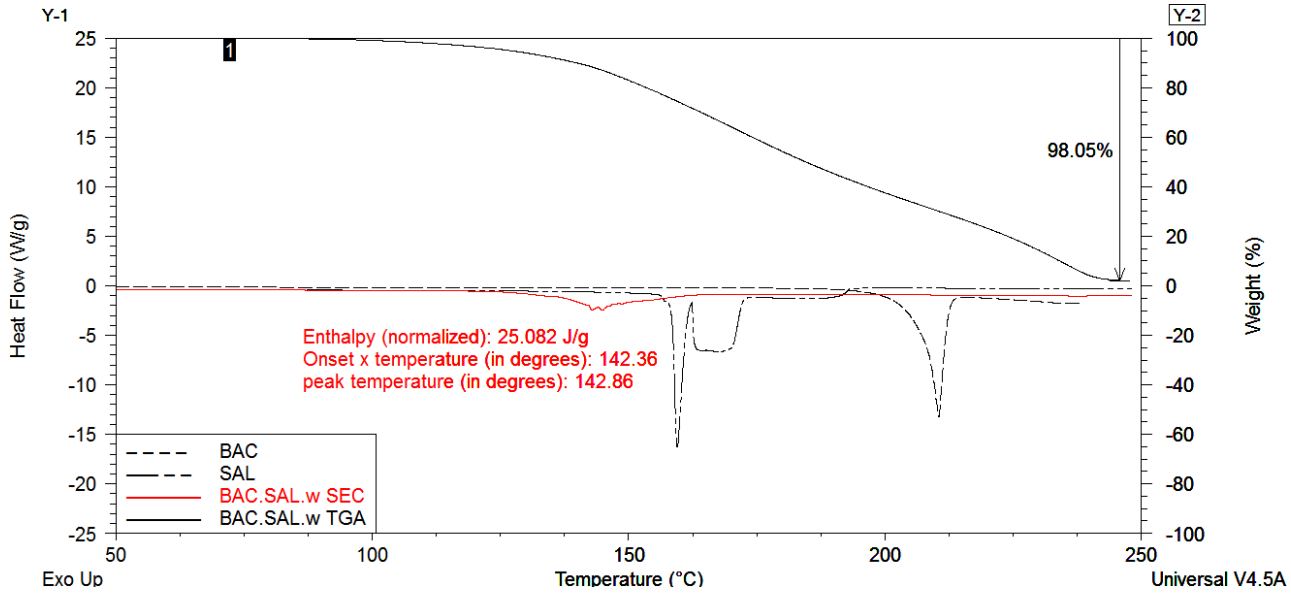

Figure A 10 Thermal analysis of BAC·SAL·w (bulk of SEC)

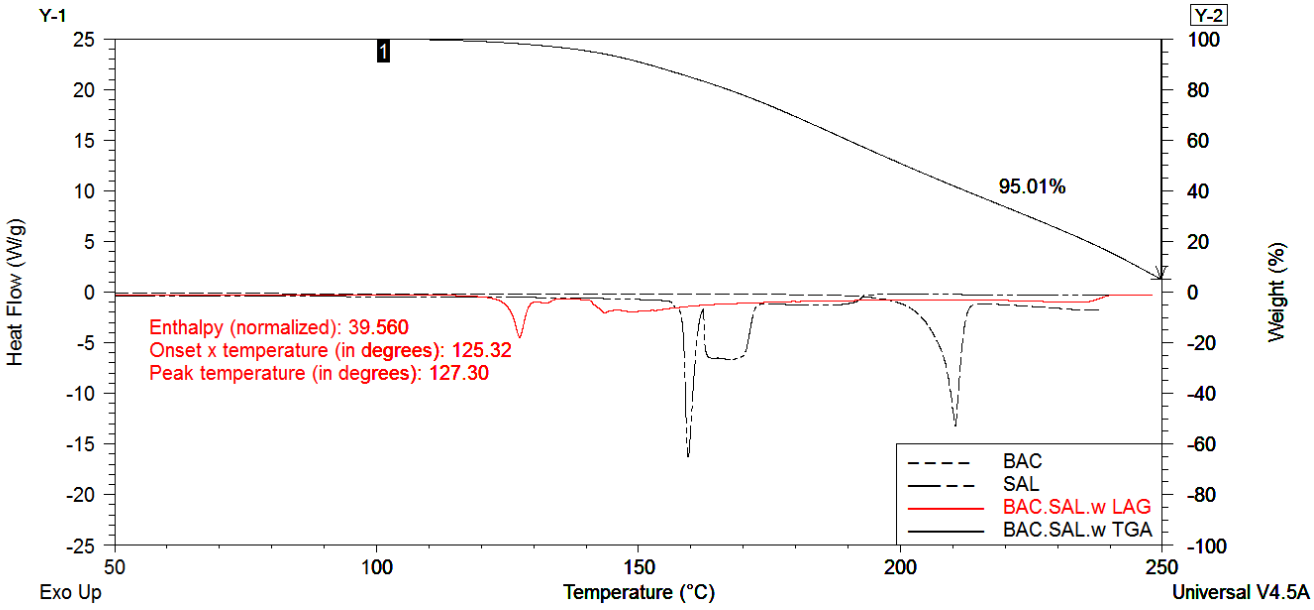

Figure A 11 Thermal analysis of BAC·SAL·w obtained via LAG

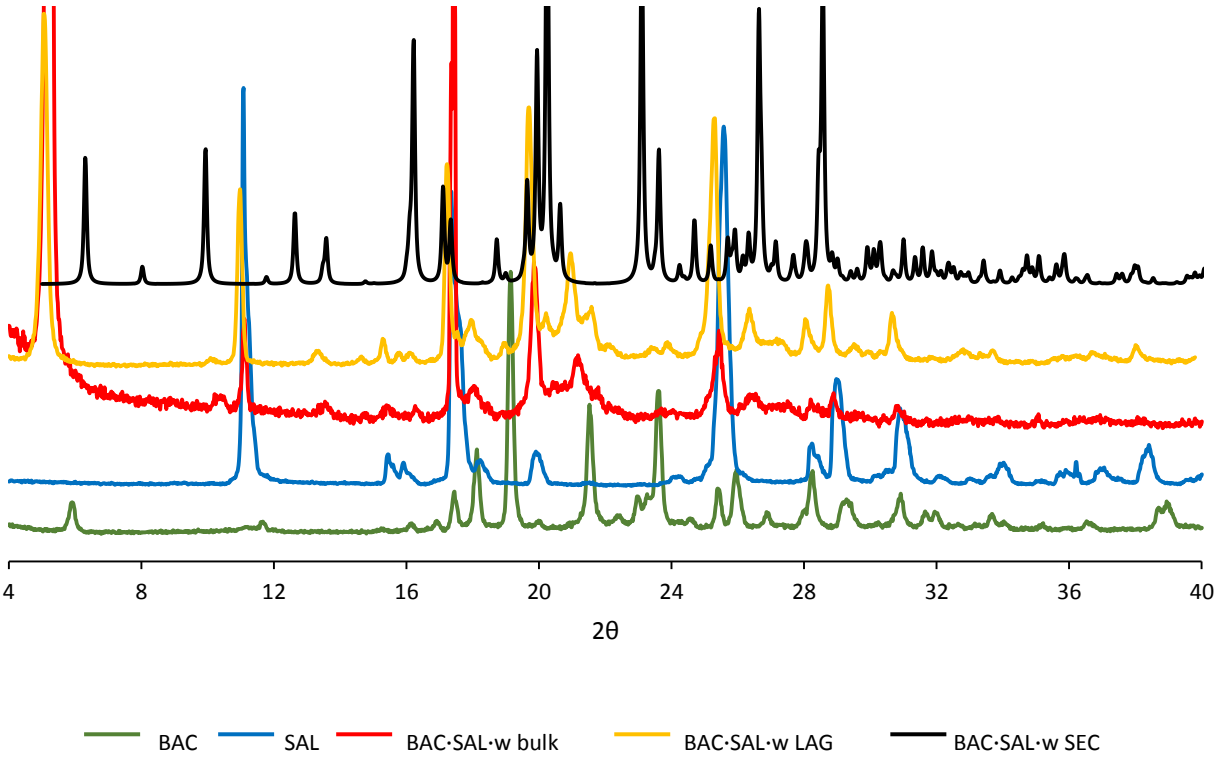

Figure A 12 PXRD analysis of BAC·SAL·w

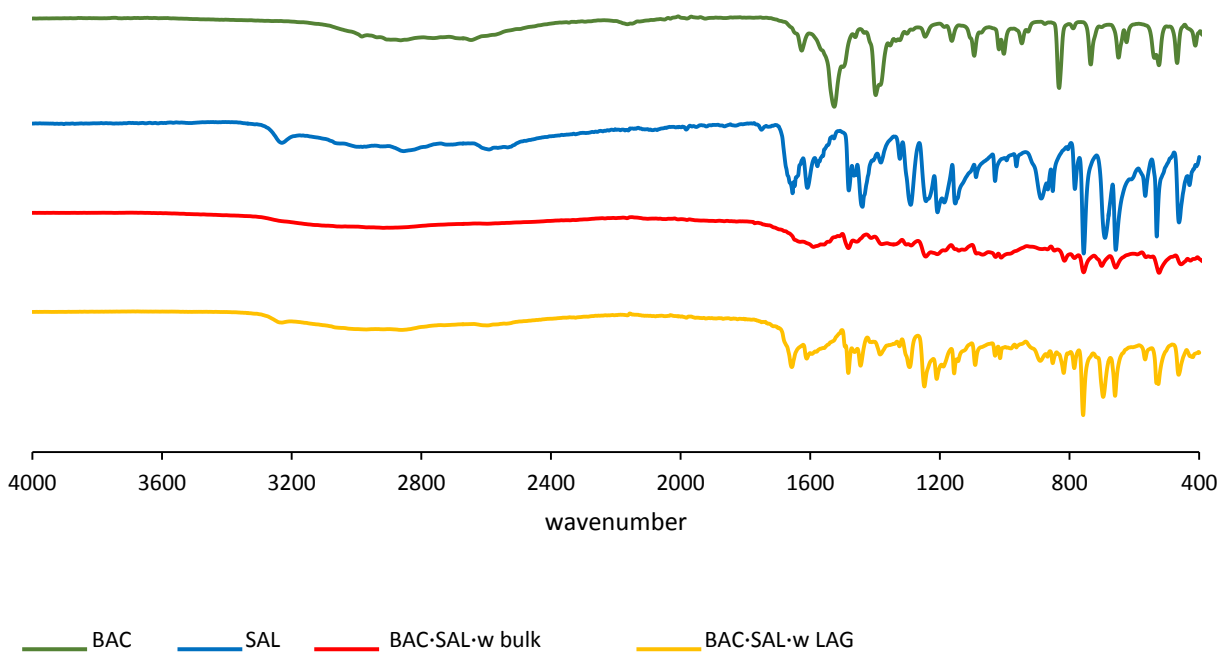

Figure A 13 IR analysis of BAC·SAL·w

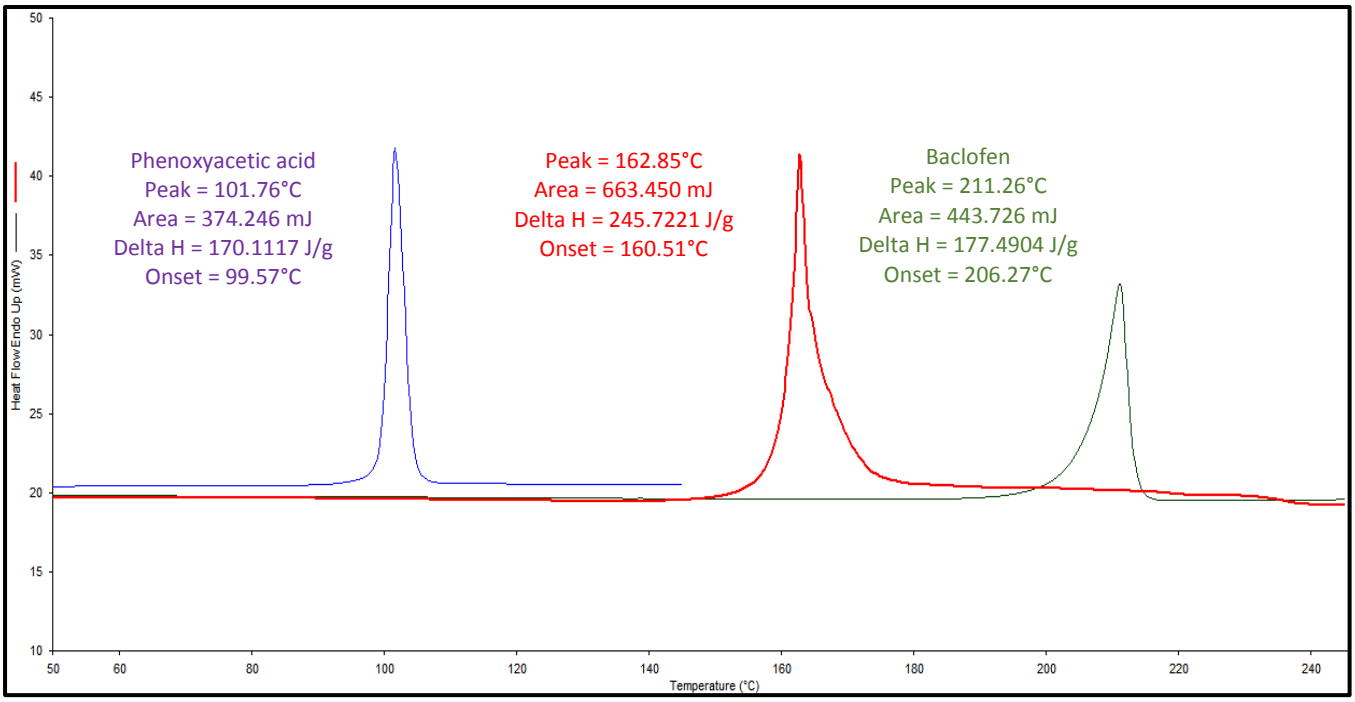

Figure A 14 DSC analysis of [BAC$^+$][POA$^-$] (bulk of SEC)

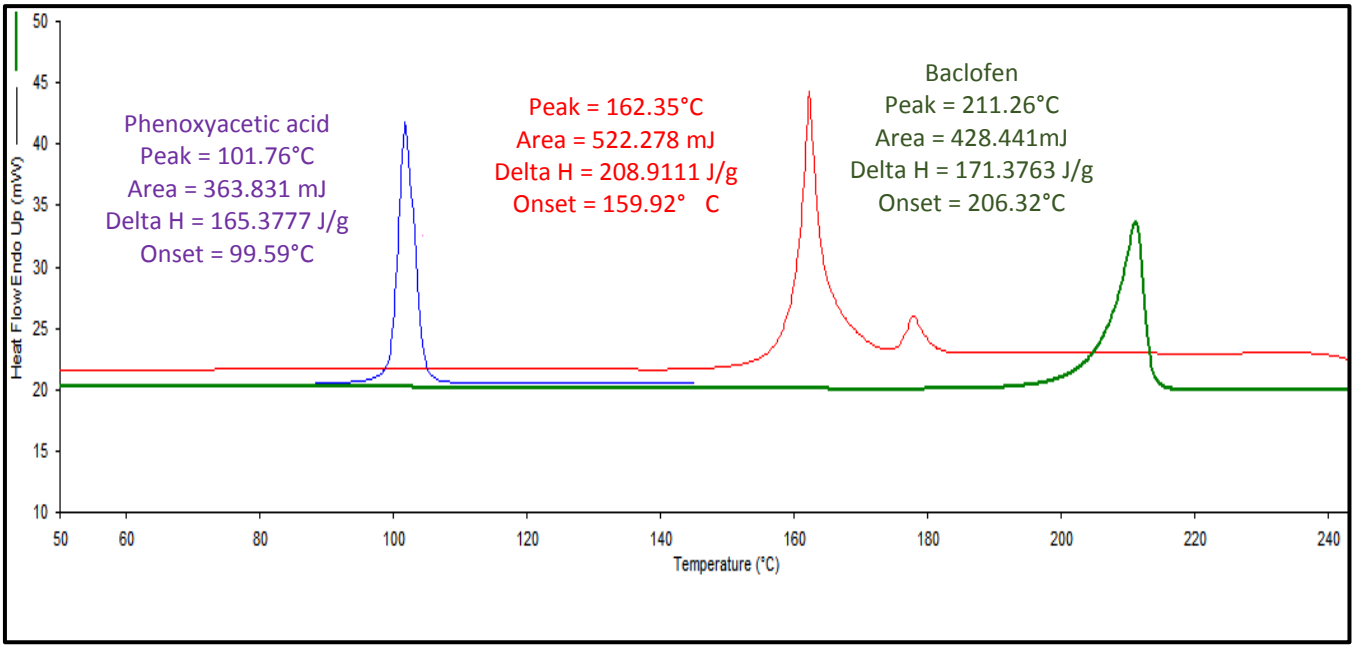

Figure A 15 DSC analysis of [BAC$^+$][POA$^-$] obtained via LAG

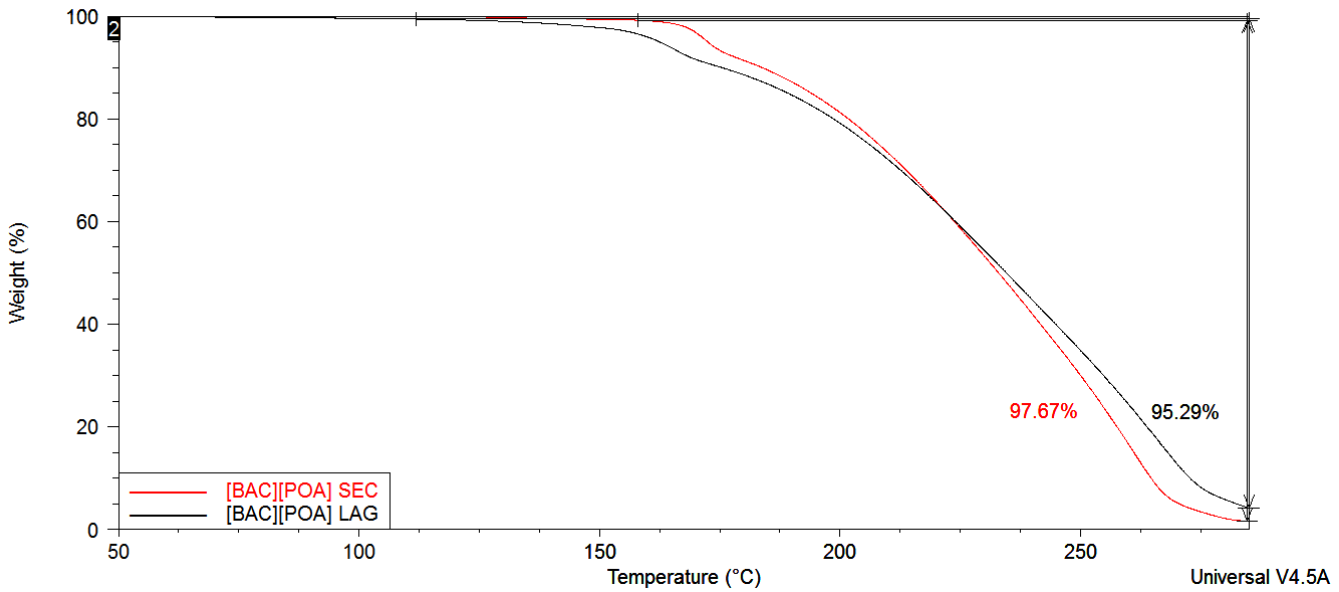

Figure A 16 TGA of [BAC$^+$][POA$^-$] obtained via SEC (bulk) and LAG

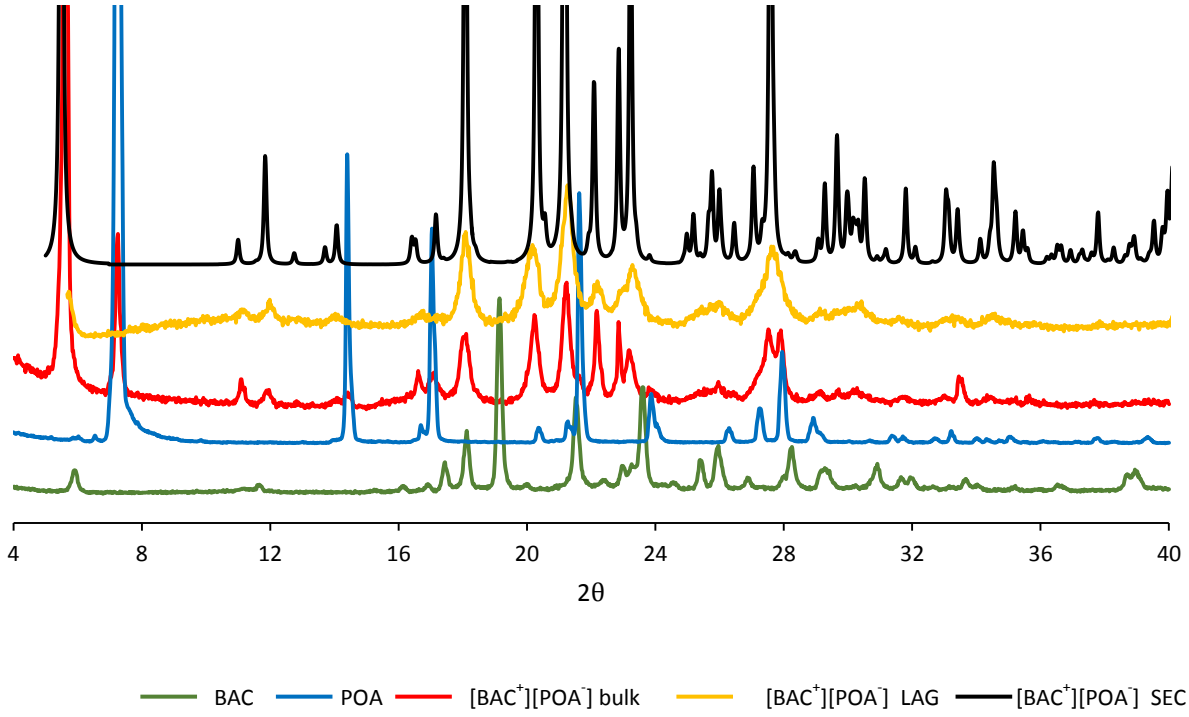

Figure A 17 PXRD of [BAC⁺][POA⁻]

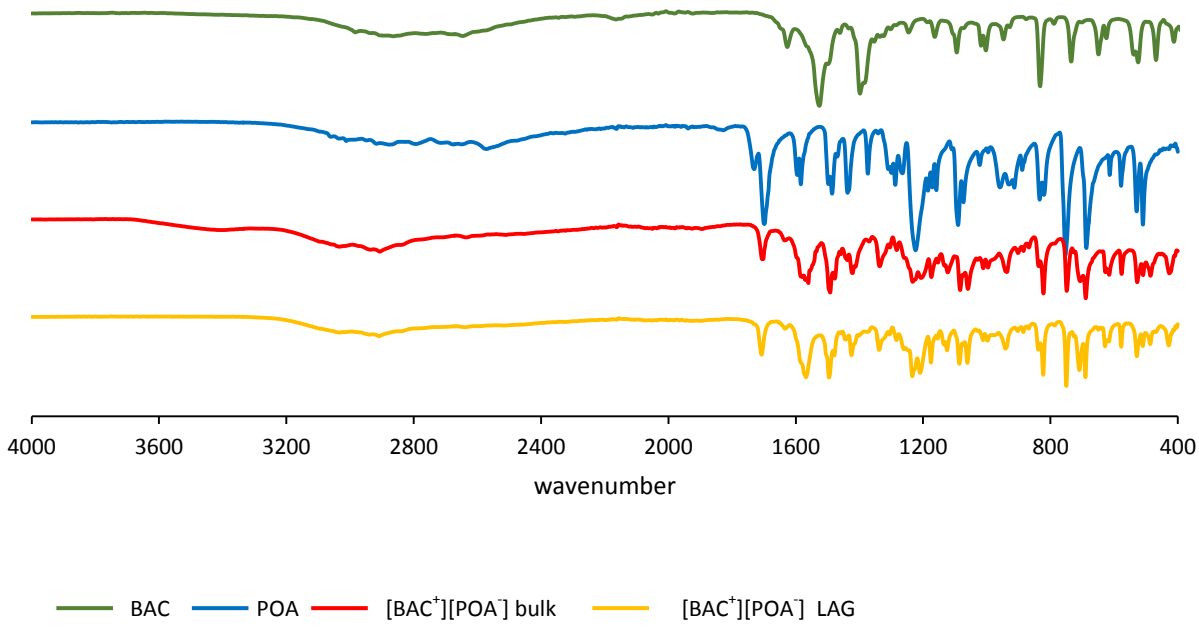

Figure A 18 IR analysis of [BAC⁺][POA⁻]

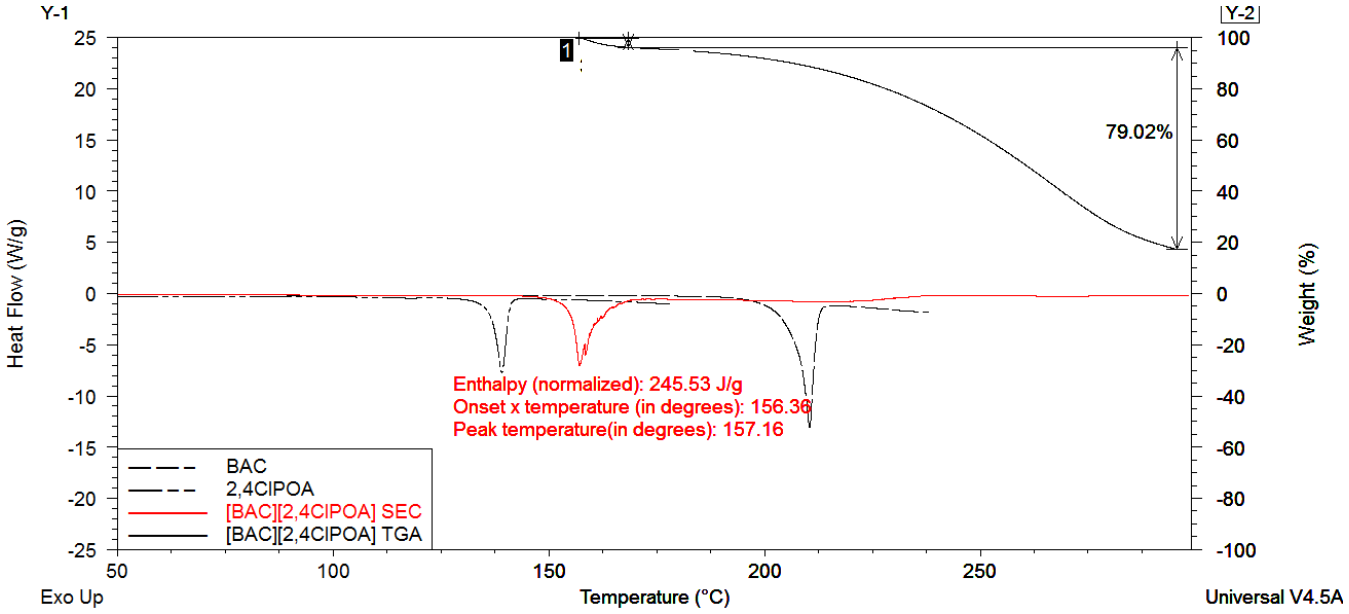

Figure A 19 Thermal analysis of [BAC$^+$][2,4ClPOA$^-$] (bulk of SEC)

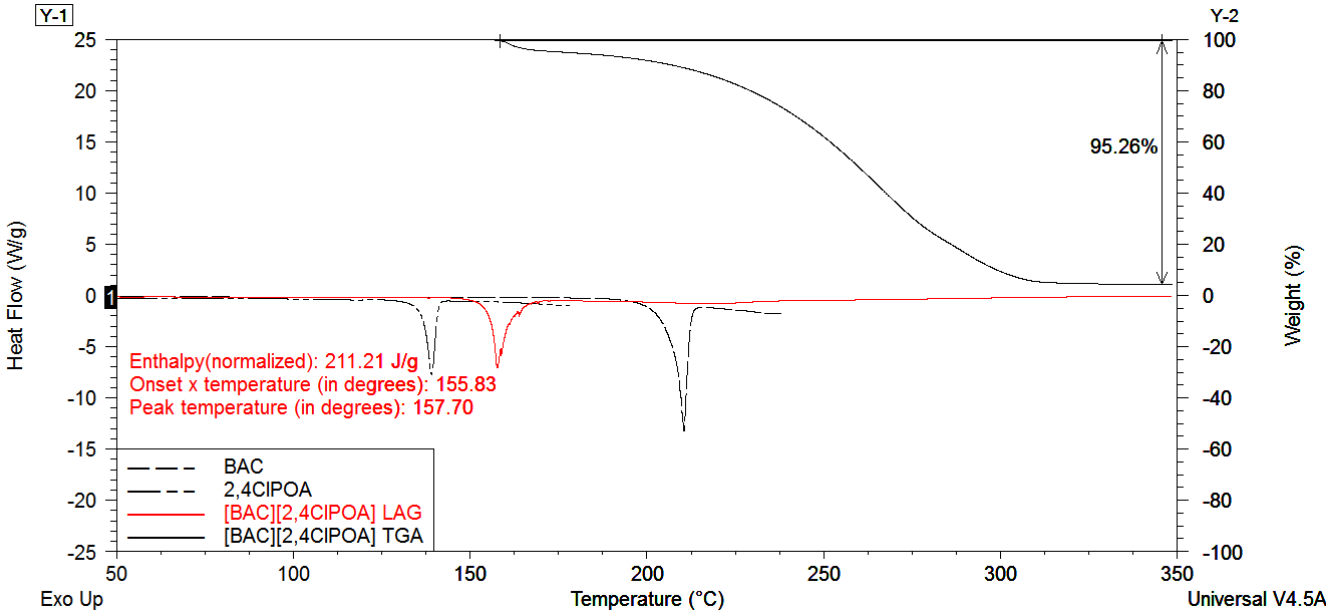

Figure A 20 Thermal analysis of [BAC$^+$][2,4ClPOA$^-$] obtained via LAG

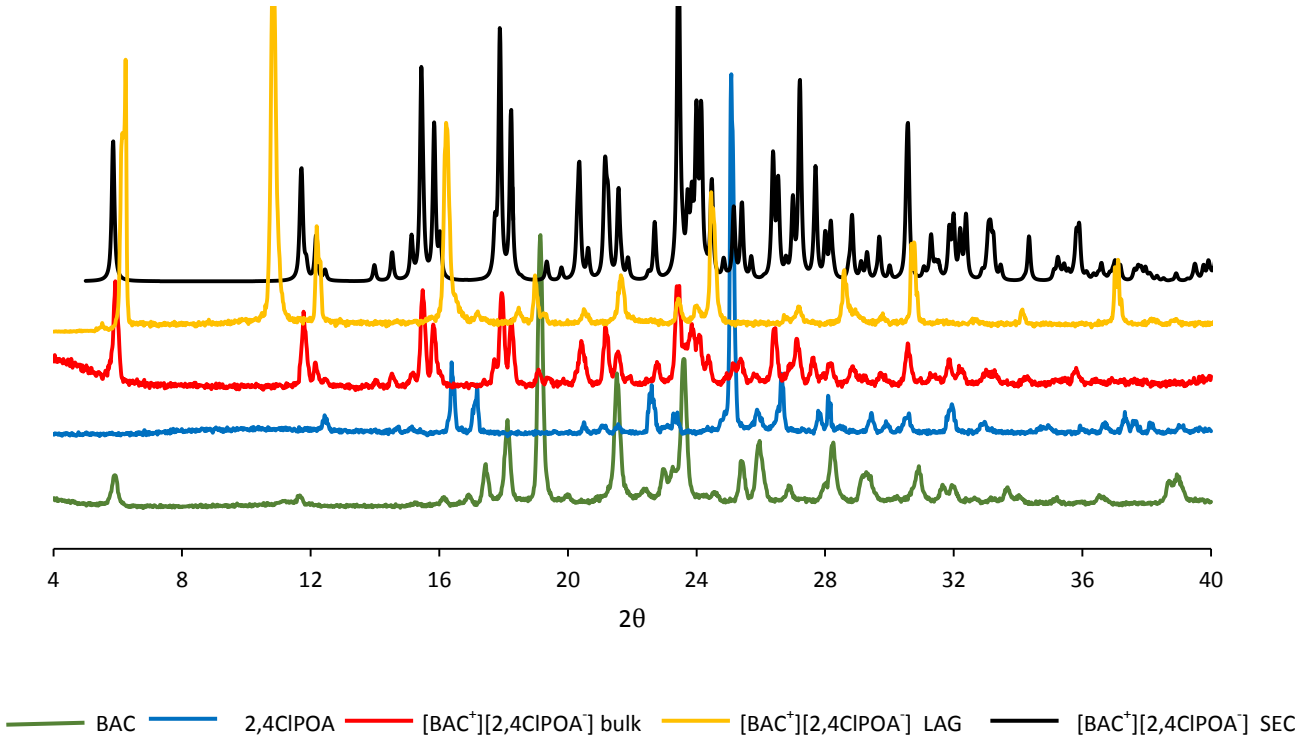

Figure A 21 PXRD of [BAC$^+$][2,4ClPOA$^-$]

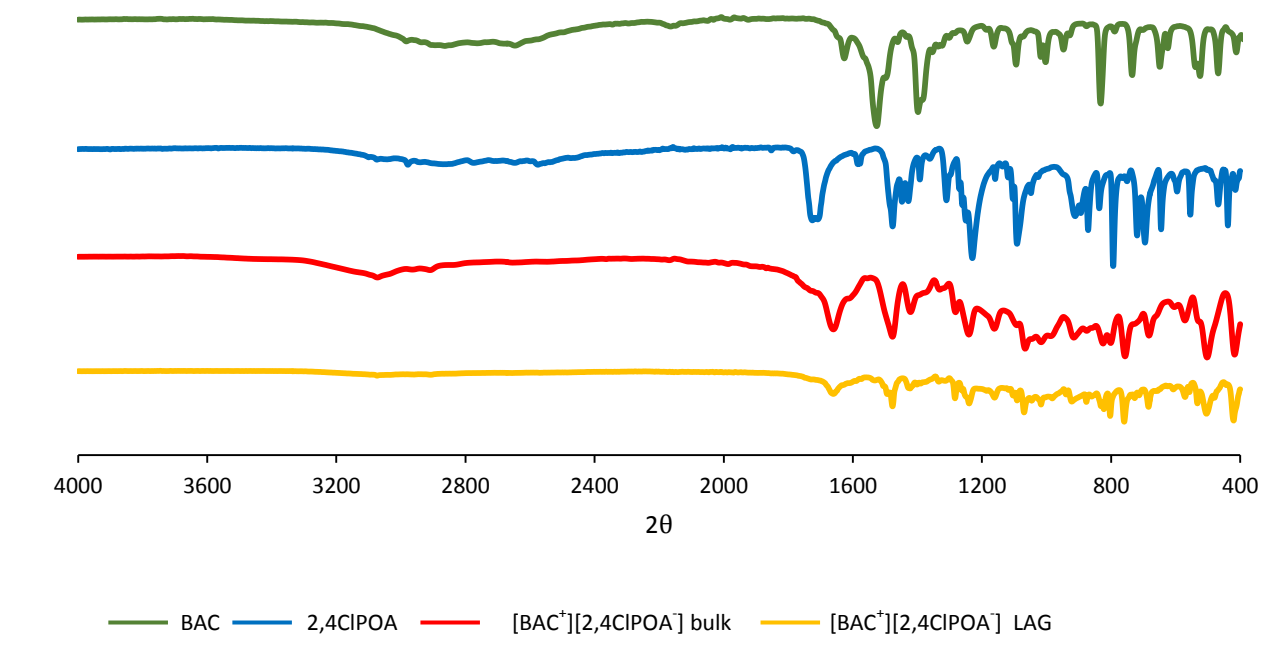

Figure A 22 IR of [BAC$^+$][2,4ClPOA$^-$]

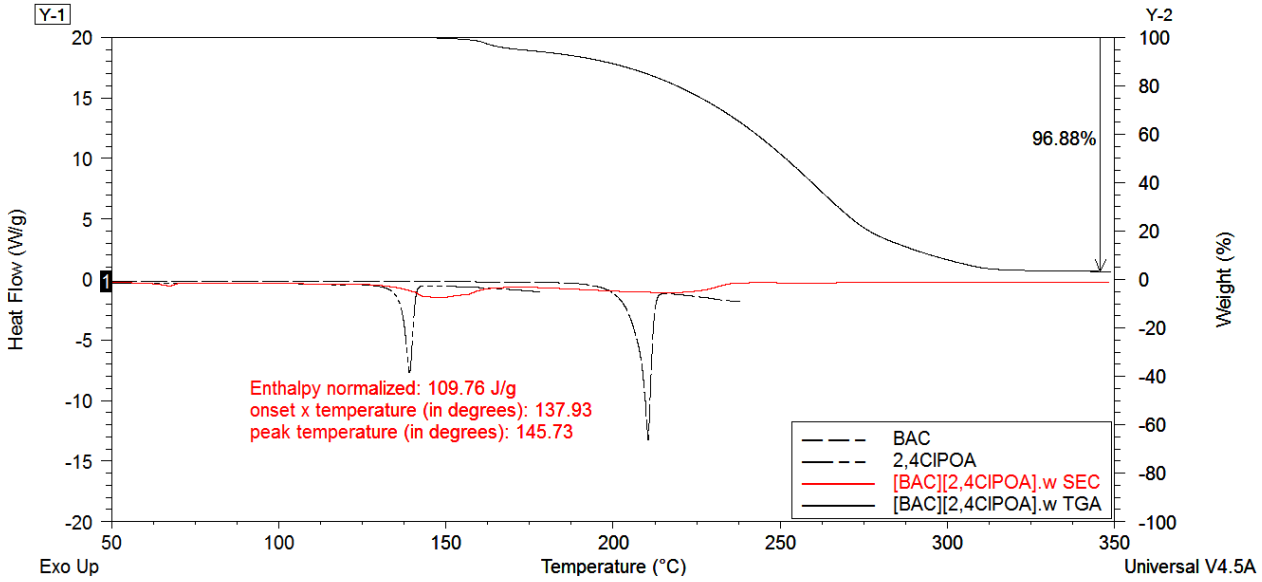

Figure A 23 Thermal analysis of [BAC⁺][2,4ClPOA⁻]·w (bulk of SEC)

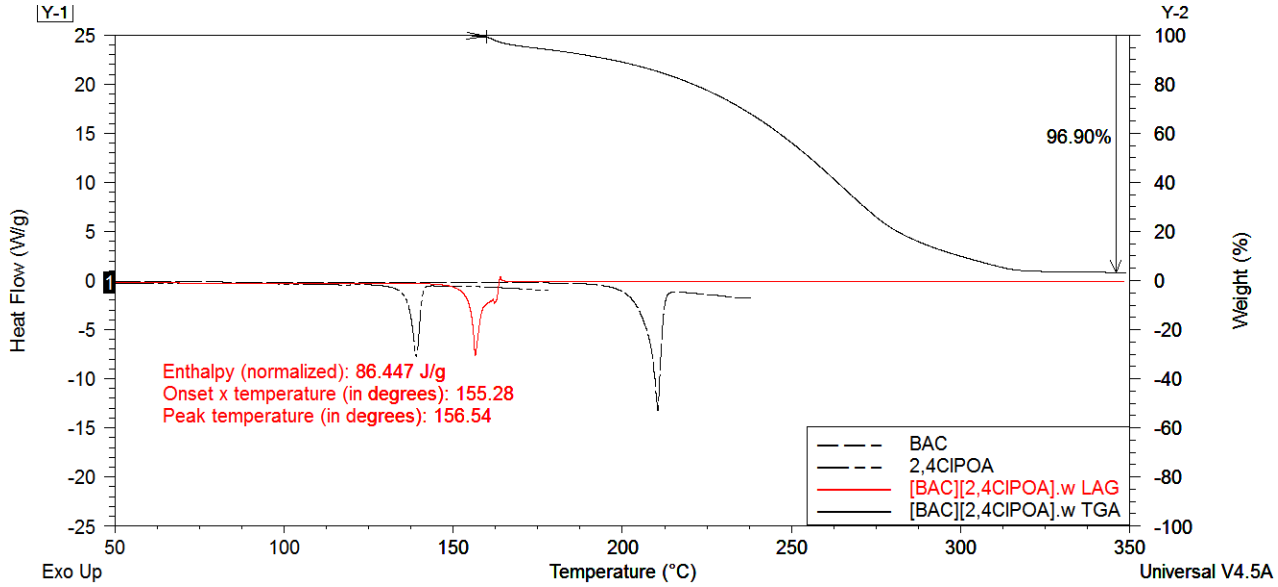

Figure A 24 Thermal analysis of [BAC⁺][2,4ClPOA⁻]·w obtained via LAG

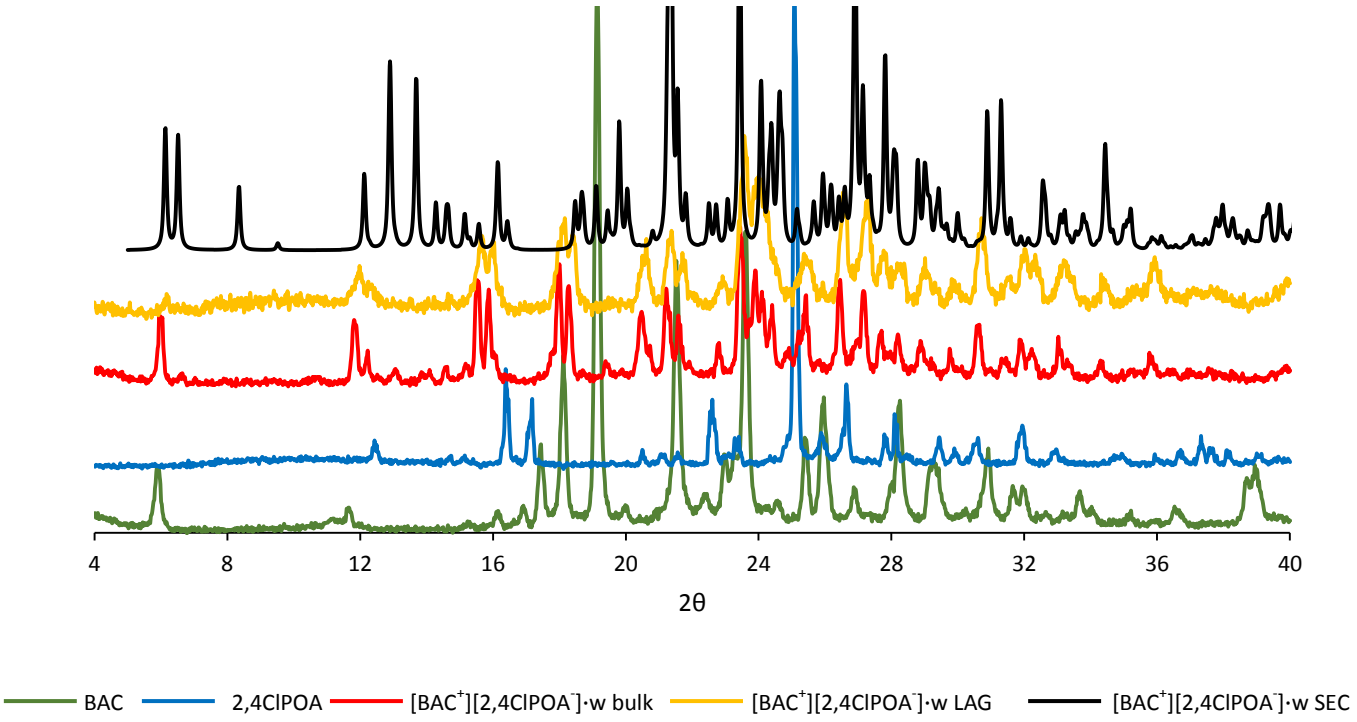

Figure A 25 PXRD analysis of [BAC⁺][2,4ClPOA⁻]·w

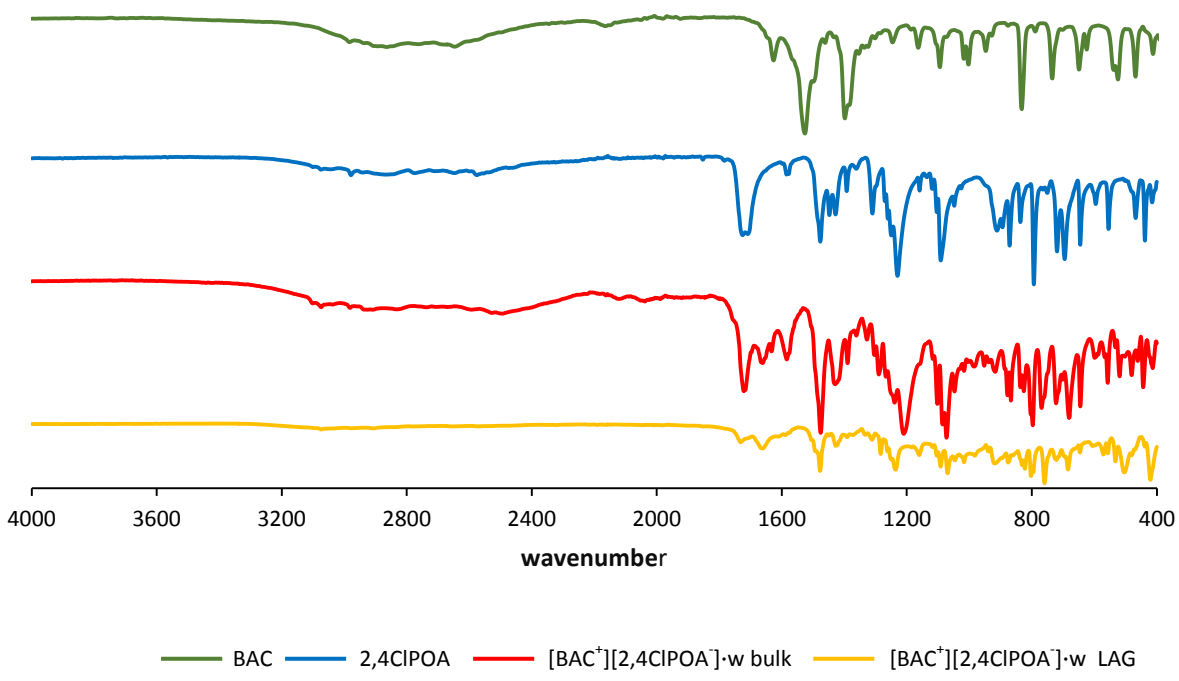

Figure A 26 IR analysis of [BAC⁺][2,4ClPOA⁻]·w

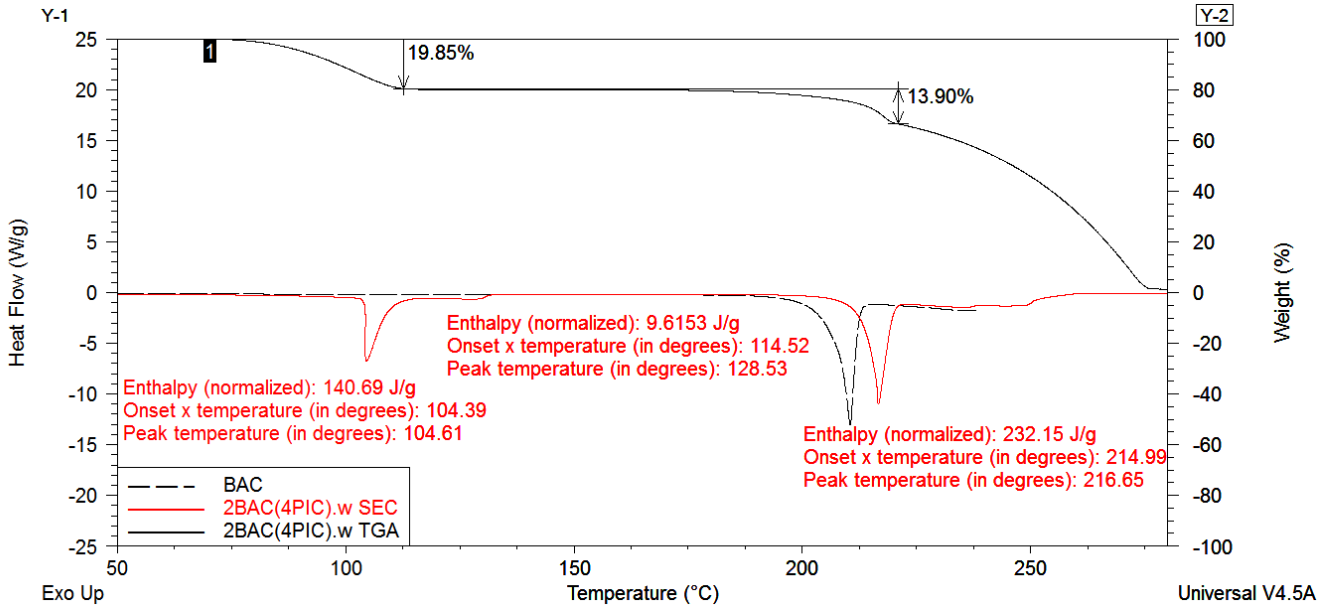

Figure A 27 Thermal analysis of 2BAC(4PIC)·w (bulk of SEC)

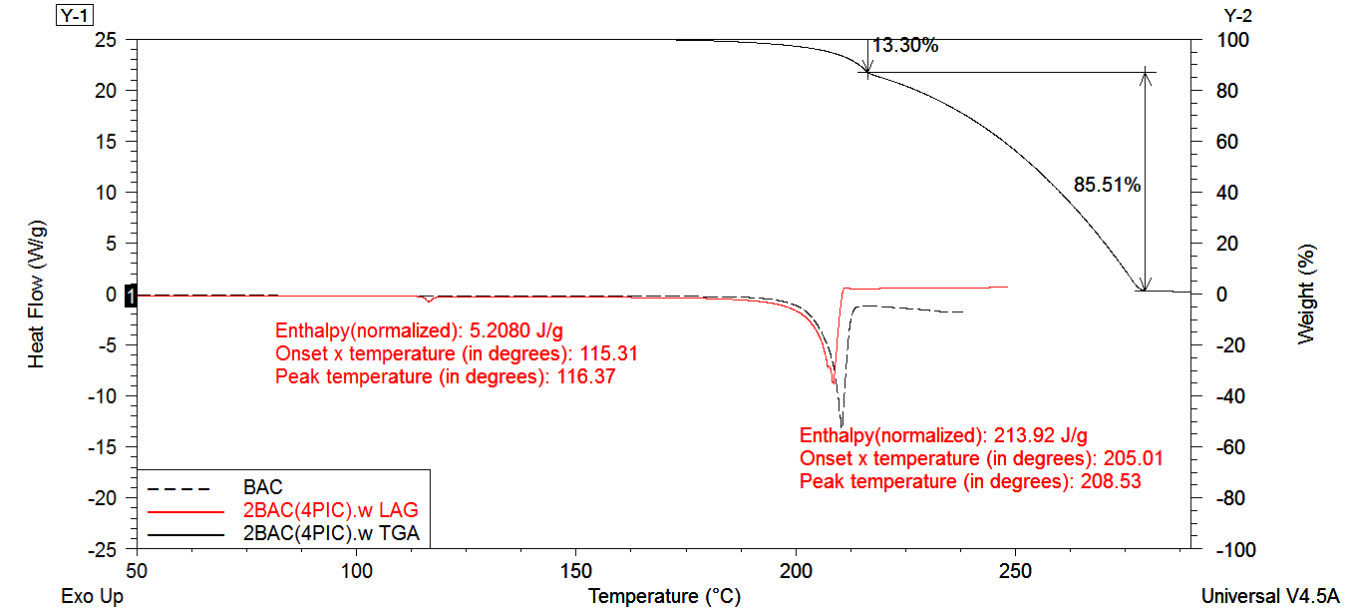

Figure A 28 Thermal analysis of 2BAC(4PIC)·w obtained by LAG

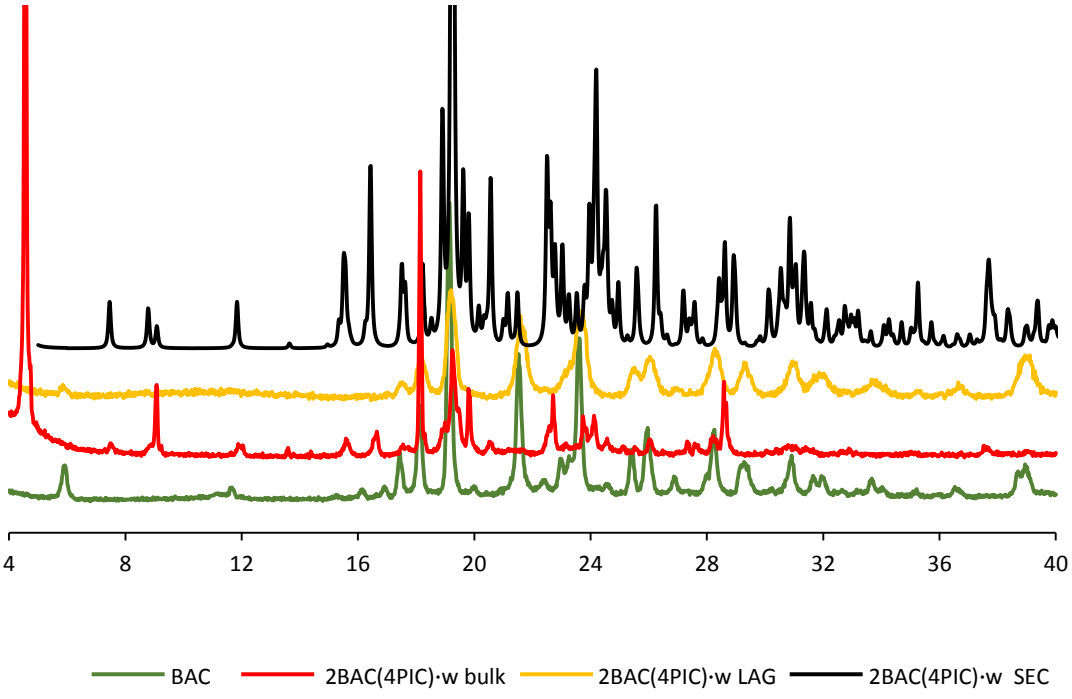

Figure A 29 PXRD of 2BAC(4PIC)·w

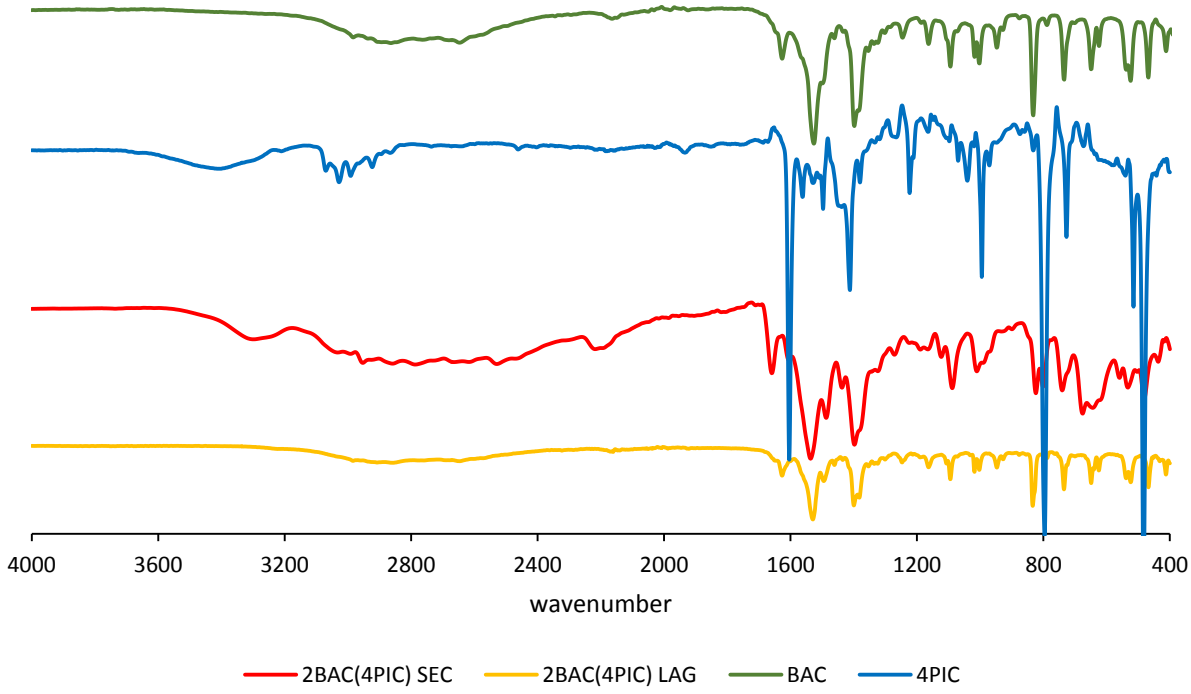

Figure A 30 IR analysis of 2BAC(4PIC)·w

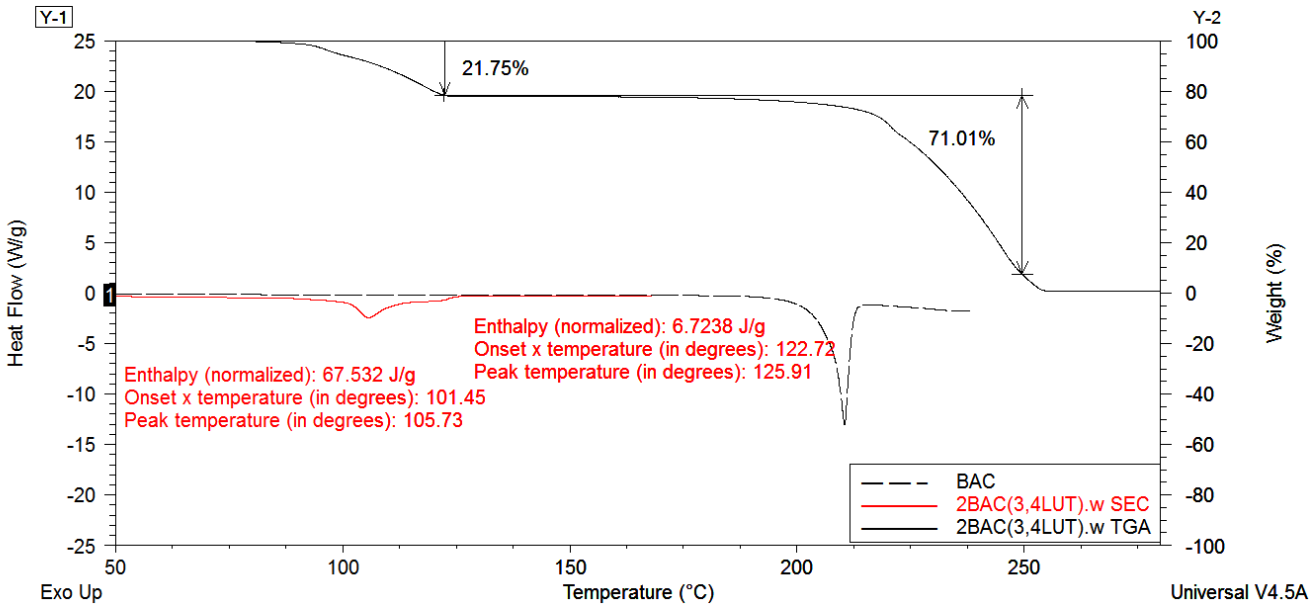

Figure A 31 Thermal analysis of 2BAC(3,4 LUT)·w (bulk of SEC)

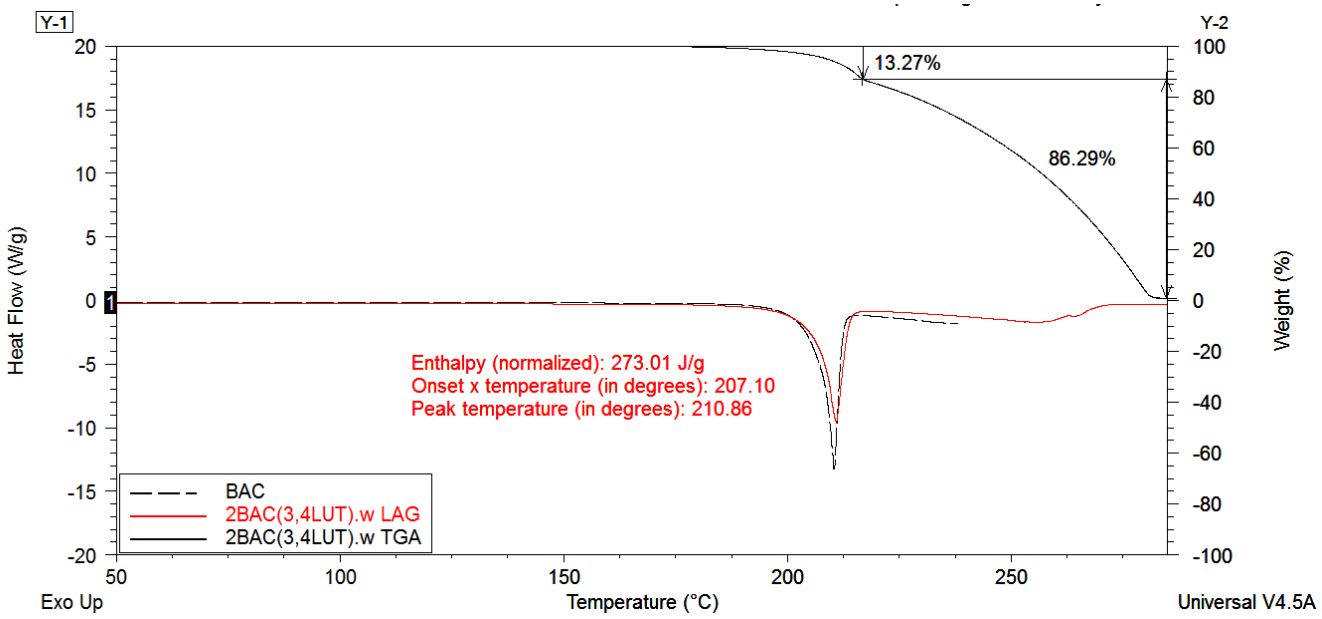

Figure A 32 Thermal analysis of 2BAC(3,4 LUT)·w obtained via LAG

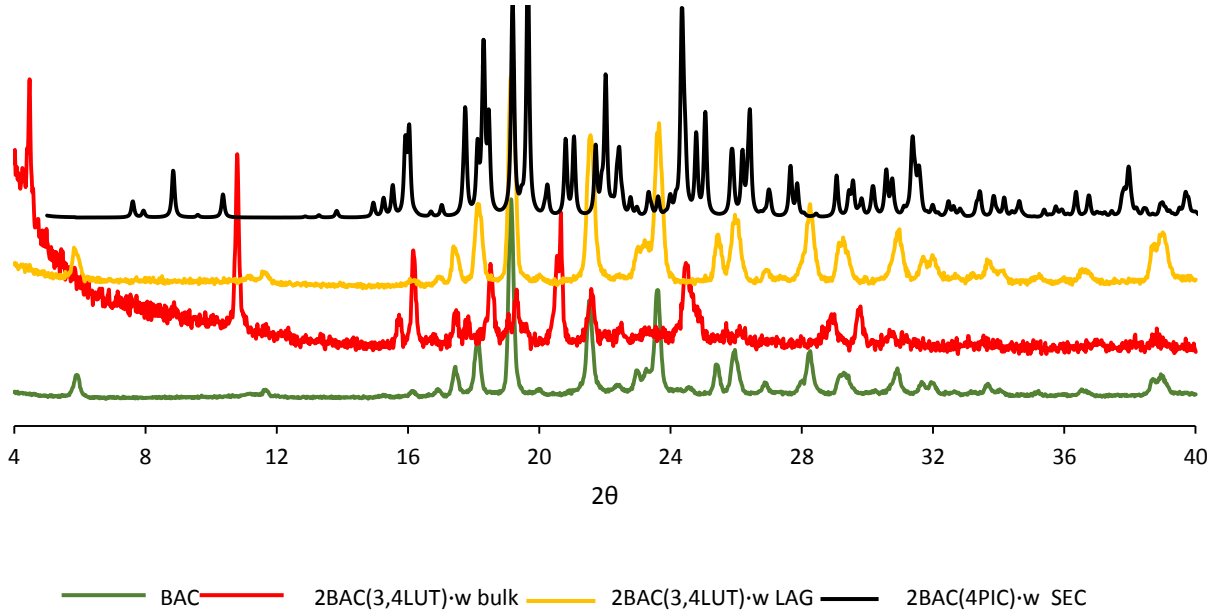

Figure A 33 PXRD analysis of 2BAC(3,4 LUT)·w

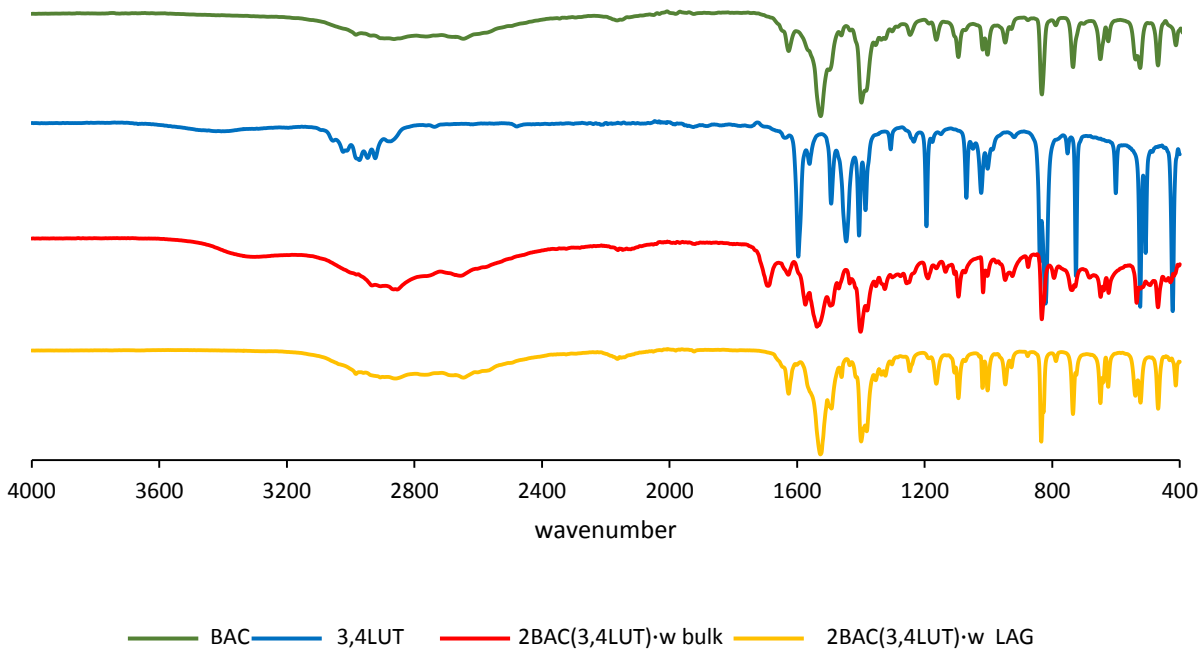

Figure A 34 IR analysis of 2BAC(3,4 LUT)·w